




RESEARCH ARTICLE

The ERA5 global reanalysis: Preliminary extension to 1950

Bill Bell¹  | Hans Hersbach¹  | Adrian Simmons¹ | Paul Berrisford¹ |
Per Dahlgren² | András Horányi¹ | Joaquín Muñoz-Sabater¹  | Julien Nicolas¹ |
Raluca Radu¹ | Dinand Schepers¹ | Cornel Soci¹ | Sebastien Villaume¹ |
Jean-Raymond Bidlot¹ | Leo Haimberger³ | Jack Woollen⁴ |
Carlo Buontempo¹ | Jean-Noël Thépaut¹

¹European Centre for Medium-Range
Weather Forecasts, Reading, UK

²The Norwegian Meteorological Institute,
Oslo, Norway

³Universität Wien, Vienna, Austria

⁴National Center for Environmental
Prediction, NOAA, College Park, MA, US

Correspondence

B. Bell, ECMWF, Shinfield Park, Reading
RG2 9AX, UK.

Email: bill.bell@ecmwf.int

Funding information

The European Union, through the
Copernicus Climate Change Service

Abstract

The extension of the ERA5 reanalysis back to 1950 supplements the previously published segment covering 1979 to the present. It features the assimilation of additional conventional observations, as well as improved use of early satellite data. The number of observations assimilated increases from 53,000 per day in early 1950 to 570,000 per day by the end of 1978. Accordingly, the quality of the reanalysis improves throughout the period, generally joining seamlessly with the segment covering 1979 to the present. The fidelity of the extension is illustrated by the accurate depiction of the North Sea storm of 1953, and the events leading to the first discovery of sudden stratospheric warmings in 1952. Time series of ERA5 global surface temperature anomalies show temperatures to be relatively stable from 1950 until the late 1970s, in agreement with the other contemporary full-input reanalysis covering this period and with independent data sets, although there are significant differences in the accuracy of representing specific regions, Europe being well represented in the early period but Australia less so. The variability of ERA5 precipitation from month to month agrees well with observations for all continents, with correlations above 90% for most of Europe and generally in excess of 70% for North America, Asia and Australia. The evolution of upper air temperatures, humidities and winds shows smoothly varying behaviour, including tropospheric warming and stratospheric cooling, modulated by volcanic eruptions. The Quasi-Biennial Oscillation is well represented throughout. Aspects to be improved upon in future reanalyses include the assimilation of tropical cyclone data, the spin-up of soil moisture and stratospheric humidity, and the representation of surface temperatures over Australia.

KEYWORDS

climate reanalysis, data assimilation, ERA5, ECMWF

This is an open access article under the terms of the Creative Commons Attribution-NonCommercial-NoDerivs License, which permits use and distribution in any medium, provided the original work is properly cited, the use is non-commercial and no modifications or adaptations are made.

© 2021 The Authors. *Quarterly Journal of the Royal Meteorological Society* published by John Wiley & Sons Ltd on behalf of Royal Meteorological Society. This article has been contributed to by US Government employees and their work is in the public domain in the USA.

1 | INTRODUCTION

ERA5 is the fifth generation of atmospheric reanalysis to be produced at the European Centre for Medium-Range Weather Forecasts (ECMWF) and currently covers the period from 1950 to the present. The reanalysis is produced in operational mode, is publicly available 5 days behind real time, and is expected to continue for the next 5–10 years. ERA5 is one component of a suite of climate data products developed and maintained by the European Union's Copernicus Climate Change Service (C3S), hosted at ECMWF (Thépaut *et al.*, 2018).

ERA5 provides hourly estimates of the global atmosphere, land surface and ocean waves at a horizontal resolution of 31 km for the high-resolution (HRES) product, a significant advance with respect to its predecessor ERA-Interim (78 km). An uncertainty estimate is provided by an underlying ten-member ensemble of data assimilations (the EDA product) at half the resolution with 3-hourly output. The main characteristics of ERA5 and comparisons with contemporary reanalyses, focusing on the period 1979–2019 (ERA5^{79→} hereafter), are described in Hersbach *et al.* (2020). This article describes the characteristics of the recently completed segment of ERA5 covering January 1950 to December 1978 (ERA5^{→79}). The article also serves to supplement, and update, Hersbach *et al.* (2020) by placing the trends and diagnostics for the earlier period into the longer-term context provided by the complete ERA5 record.

Reanalyses support a broad range of applications spanning inter-governmental assessments of global climate change (Stocker *et al.*, 2013) at one extreme, to specific and unique use cases requiring accurate representations of local weather at the other. Accordingly, reanalyses aim to provide homogeneity and accuracy in the representation of global and regional climate variables over multi-decadal timescales, as well as accuracy in the representation of synoptic-scale events at sub-daily temporal resolution. For the former class of applications, key aspects of the reanalyses are the representation of the evolution of the mean state of the atmosphere (specifically thermodynamic, dynamical and radiative variables) as well as extremes.

These aspects motivate the extension of reanalyses to cover ever longer periods in order to provide more robust statistics on extremes as well as to provide a longer baseline for the assessment of trends in the mean state. The limits of such extensions are set by the availability of observational data, which determine the fidelity of the reanalysis. One strategy employed in centennial reanalyses (Compo *et al.* (2011), Poli *et al.* (2016), Laloyaux *et al.* (2018)) has been to assimilate surface observations only, available to the middle of the 19th century, in order to ensure homogeneity in the reanalyses, albeit at the expense of accuracy, especially

in the modern satellite era. As a *full-input* reanalysis, ERA5 has been extended back to 1950, prior to which the number of upper air data currently available drops significantly (Hersbach *et al.* (2017)). The availability of upper air observations prior to 1950 continues to improve though, through ongoing coordinated data rescue programmes (Brönnimann *et al.*, 2018b).

An indication of the performance of ERA5 during the period 1950–2020 is provided in Figure 1, which shows the skill of ERA5 re-forecasts, as a proxy for the accuracy of the reanalysis. Results are shown for the forecasts over four regions for which the availability of radiosonde data for all or most of the period gives confidence in the use of the ERA5 analyses to verify the forecasts. The regions are those chosen by Uppala *et al.* (2005) for presenting the skill of pre-1979 ERA-40 forecasts. Analysis quality over the Northern Hemisphere improves steadily as the observing system evolves from the earliest period in the reanalysis. Forecasts for Europe, East Asia and North America are from the outset at least as good as achieved operationally by ECMWF in 1981. The quality of the analysis for the Southern Hemisphere improves dramatically following the first assimilation of data from the TOVS satellite series at the end of 1978, as shown by the forecast skill over Australia and New Zealand. More modest improvements occur here in the 1960s and earlier in the 1970s.

This article has three main aims: firstly to describe features of the production (Section 2), observing system and data assimilation configuration (Section 3) during the early period not covered previously in Hersbach *et al.* (2020), including the assimilation of early satellite data and the exploitation of newly reprocessed conventional observations; secondly to give an indication of the quality of the synoptic fields in this early period (Section 4), through the examples of the North Sea storm of February 1953 and the sudden stratospheric warming of February 1952; and thirdly, to update the time series of analysed variables and diagnostics presented in Hersbach *et al.* (2020) to cover 1950–2020 (Section 5). The purpose here is twofold: to provide an initial assessment of the quality and homogeneity of the reanalysis in the early period, and to identify new features of geophysical significance from the longer time series.

All results shown in this article for 2000–2006 are based on ERA5.1 (Simmons *et al.*, 2020). ERA5.1 has generally smaller temperature biases than ERA5 in the lower stratosphere and upper troposphere for this period. It also provides some improvements to the analysis of ozone and the Quasi-Biennial Oscillation (QBO) of tropical stratospheric winds. ERA5.1 is very close to ERA5 in the lower and middle troposphere.

In Section 6, we describe the known issues in ERA5 during 1950–1979 uncovered so far, including the

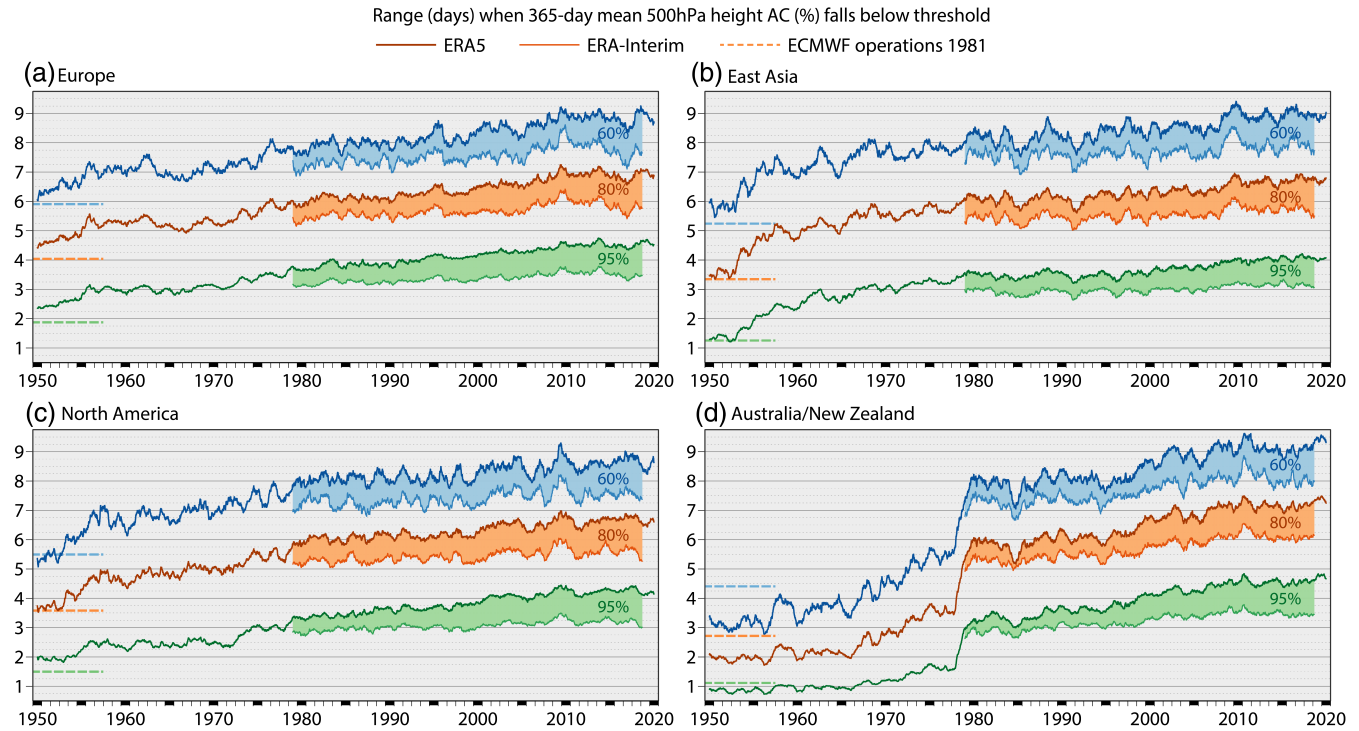


FIGURE 1 Range (days) at which running 365-day mean anomaly correlations of 500 hPa height forecasts at 0000 and 1200 UTC from 1950 to 2020 reaches 95% (green), 80% (orange) and 60% (blue) for (a) Europe, (b) East Asia, (c) North America and (d) Australia/New Zealand. Also shown (dashed) is the average skill of ECMWF operational forecasts for 1981. Heavy lines denote ERA5; thin lines denote ERA-Interim. Shading denotes the difference between ERA5 and ERA-Interim during the period for which both are available (1979–2019)

representation of tropical cyclones and the representation of surface temperatures in the Southern Hemisphere. Concluding remarks and directions for future work form Section 7.

2 | PRODUCTION AND AVAILABILITY OF THE BACK EXTENSION

ERA5⁷⁹ was produced on the ECMWF high-performance computing facility. To accelerate production, the 29-year period was divided into four parallel streams, each with a 1-year overlap to ensure smooth transitions between streams in the troposphere. Each suite ran, on average, at 8 days per day, enabling a production period of 15 months overall. After completion of the initially foreseen 7–8-year production runs, each of the four streams was opportunistically extended to allow for a longer overlap with subsequent streams such that the consolidated final product exhibited smoother transitions for stratospheric humidity. This resulted in two longer streams (from 1950 and 1965) and two shorter streams (from 1959 and 1974), each with different spin-up periods. For example, the seam in early

1965 required less overlap (i.e., extension of the earlier stream) than those which were initially due to be consolidated from January 1958 and January 1972 (and were, in fact, consolidated from July 1959 and January 1974) as the discontinuities in stratospheric humidities were less pronounced in early 1965. In addition, the stream which covered most of the 1970s was extended to the end of 1980. This provided a 2-year overlap (denoted by ERA5^{79–80} hereafter) with ERA5⁷⁹ and permitted an analysis of the effect of the additional observations that were used in ERA5⁷⁹, as well as of a longer spin-up period and a difference in the climatological background error covariances used (see Section 3.6) in ERA5⁷⁹. Several examples of this are described later in this manuscript. Details of the production streams are provided in Table 1 and illustrated in Figure 2, which also shows the climatological background error covariances used as well as major data events (see Section 3).

The consolidated data set is available via the C3S Climate Data Store (CDS, Raoult *et al.* (2017)). The ERA5 online data documentation (available via <https://confluence.ecmwf.int/display/CKB>) provides a detailed description of the various products and a list of all available geophysical parameters.

TABLE 1 Details of the four production streams, comprising both high-resolution (HRES) and ensemble of data assimilations (EDA), that were merged into the consolidated public product from 1950 to 1978

Stream	Used from	Used until	Used for	Started from	Effective spin-up period
1	1950-01	1959-06	9 years 6 months	1949-01	1 year
2	1959-07	1965-02	5 years 8 months	1957-01	2 years 6 months
3	1965-03	1973-12	8 years 10 months	1964-01	1 year 2 months
4	1974-01	1978-12	5 years	1971-01	3 years

Note: The length of each stream varies such that smoother transitions between streams are obtained for stratospheric humidity.

3 | OBSERVATIONS AND DATA ASSIMILATION ASPECTS

3.1 | Overview of the observing system 1950–1979

As detailed in Hersbach *et al.* (2020) (see their figure 2), the ERA5 assimilation system comprises three main components, each ingesting its own set of observations: 4D-Var, assimilating observations sensitive to surface and upper-air atmospheric quantities; Optimal Interpolation (OI) of ocean wave height; and the Land Data Assimilation System (LDAS) for screen variables, soil moisture and snow.

The observing system evolved substantially during the 29 years of ERA5⁷⁹. In January 1950 in 4D-Var, on average, approximately 53,000 observations were actively assimilated per day, originating from conventional sources only (surface and upper air). In December 1978, 570,000 observations were assimilated per day, including 243,000 conventional, 208,000 satellite radiances and 119,000 ozone observations. Ozone and ocean-wave observations,

which in ERA5 originate from satellite instruments, were not available before April 1970 and August 1991, respectively. Therefore, prior to April 1970, the ozone analysis in ERA5⁷⁹ is only indirectly influenced by observations that provide information on upper-air temperature, wind and humidity, while for the entire period of ERA5⁷⁹, ocean-wave products are determined by the near-surface atmospheric forcing. Note, however, that the ocean waves have a two-way coupling back into the atmosphere; that is, the ERA5⁷⁹ wave products are more than just a hindcast.

Time lines per type of observation (or report) and per assimilated geophysical quantity are provided in Figures 3 and 4, respectively. The following subsections describe each of these components in more detail.

3.2 | Conventional observations

ERA5⁷⁹ uses conventional observations prepared initially for ERA-40, spanning September 1957 to December 2001 (ERA-40 BUFR hereafter) and from the operational ECMWF data archive, received through the

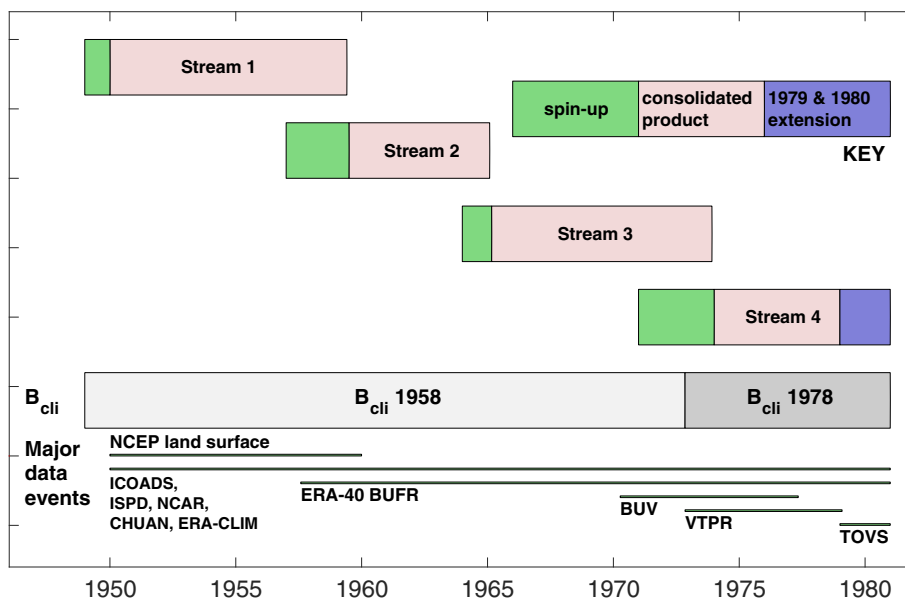


FIGURE 2 Illustration showing the four streams used to produce the final consolidated product (pink) from January 1950–December 1978, complete with the spin-up periods (green) and the extension to the end of 1980 for stream 4 (blue). Also shown are the periods spanned by the two forms of the climatological component of the background error covariances (B_{cli}). Major data events are also shown

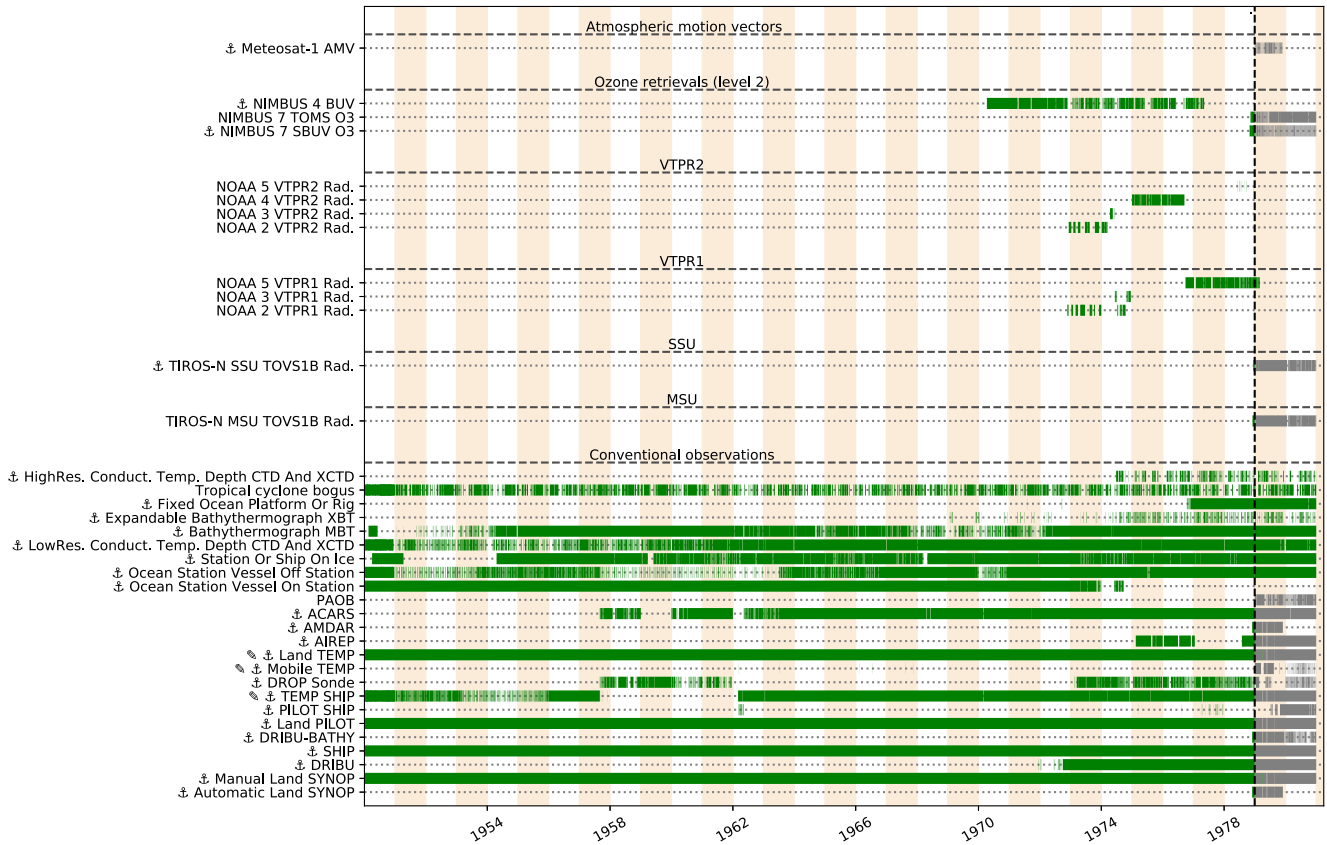


FIGURE 3 Timelines of observations assimilated in the 4D-Var component of ERA5^{→79} and ERA5^{79→80} during the period 1950–1980. Grey bars indicate the observations used in both ERA5^{79→80} and ERA5^{→79}; green bars indicate observations that were used in ERA5^{→79} or only in ERA5^{79→80}. Bars are extended beyond January 1, 1979 only for those observations already in ERA5^{→79}; that is, the bars past January 1, 1979 are not fully representative of ERA5^{79→80}. A pencil symbol preceding an observation type indicates that a prescribed bias correction is applied to at least one assimilated variable (or and/or channel for satellite observations) provided by that observation type. Similarly, an anchor symbol indicates that at least one variable or channel provided by the observation type is used to anchor the analysis; that is, it is assimilated without applying a bias correction

TABLE 2 Overview of the sources of conventional reports as presented to ERA5^{→79} (plus ERA5^{79→80}) and observables that were actively used in the 4D-Var and LDAS components

Data set	4D-Var surface	4D-Var upper air	LDAS	Ref.
ERA-40 BUFR	Ps, U10/V10, Rh2m	T, U/V, Q	T2m, Rh2m, Sd	Uppala <i>et al.</i> (2005)
NCEP land surface			T2m	Simmons <i>et al.</i> (2021)
ISPDv3.2.6	Ps			Cram <i>et al.</i> (2015)
ICOADS2.5.1	Ps, U10/V10			Woodruff <i>et al.</i> (2011)
NCAR UADB-2		T, U/V		NCAR (2014)
CHUAN v1.7		T, U/V		Stickler <i>et al.</i> (2010)
ERA-CLIM v2.1		T, U/V		Brönnimann <i>et al.</i> (2018a)

Note: From this list, ERA5^{→79} only used observations from ERA-40 BUFR. Here Ps represents surface pressure, U10/V10 10-m wind components, T2m 2 m temperature. Rh2m 2 m relative humidity, Sd snow depth and T, U/V, Q upper-air temperature, wind components and specific humidity, respectively.

GTS, afterwards. For ERA5^{→79}, additional observations from other sources were included. Not only did these provide measurements for the otherwise data-void period

prior to September 1957; they also add extra observations post-1957 that are not present in the ERA-40 BUFR data stream.

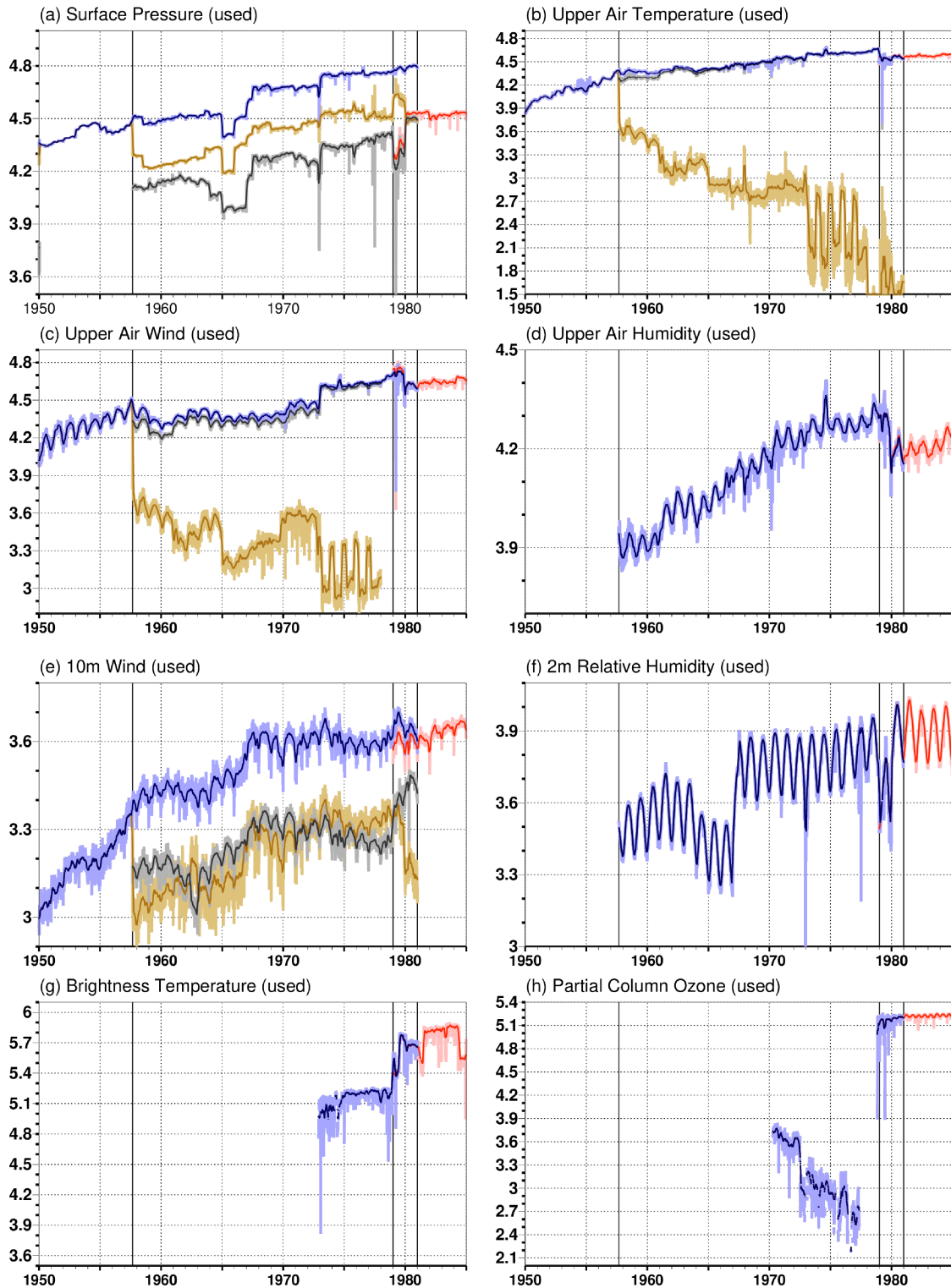


FIGURE 4 Number of daily actively assimilated observations (weak colours) and 30-day means (strong colours), both on log₁₀ scale, for ERA5^{79->} (red), ERA5^{79->} plus ERA5⁷⁹⁻⁸⁰ from non ERA-40 BUFR (ochre), ERA-40 BUFR (grey) and all sources combined (blue) for the eight observables for which observations are assimilated in 4D-Var in the period from 1950 to 1985. Vertical lines indicate (in chronological order) the start of ERA-40 input data (September 1, 1957), the start of the ERA5^{79->} period (January 1, 1979) and the end date of ERA5⁷⁹⁻⁸⁰ (December 31, 1980). Each 0.3 tick on the vertical axis corresponds to a factor of 2, and minor ticks (0.1) to a difference of 26%

The additional sources include surface pressure observations from the International Surface Pressure Data-bank (ISPD, version 3.2.6) and the International Comprehensive Ocean-Atmosphere Data Set (ICOADS, version 2.5.1), as well as marine wind reports from ICOADS. These observations were also assimilated in ERA-20C (Poli *et al.*, 2016) and CERA-20C (Laloyaux *et al.*, 2018). In addition, ERA5^{→79} ingests observations from the NCAR Upper Air Data Base (UADB-2, version 2.0, and additions from versions 2.1 and 2.4), the Comprehensive Historical Upper-Air Network (CHUAN v1.7, Stickler *et al.* (2010)), as well as upper-air observations digitized within the ERA-CLIM and ERA-CLIM2 projects (ERA-CLIM Version 2.1, Brönnimann *et al.* (2018a); Stickler *et al.* (2014)). With the exception of a newer version for the ERA-CLIM archive, this is very similar to the data presented to the experimental ERA-PreSAT reanalysis (Hersbach *et al.*, 2017). The difference here is that, for the first time, ERA5^{→79} assimilates observations from all sources while previous ECMWF reanalyses reaching back to at least 1950 did not ingest any ERA-40 BUFR observations. In addition, surface screen level observations from an NCEP archive going back to 1930 were used in the LDAS, as discussed further in Section 3.3.

An overview of all ingested sources is provided in Table 2, which includes information on the variables actively assimilated in each component of the ERA5 system. Although ISPD provides exclusively pressure observations (at the surface and mean sea level), ERA-40 BUFR and ICOADS provide many more observed variables than are actively assimilated. For ICOADS, a list is provided in Woodruff *et al.* (2011) and Hersbach *et al.* (2015b). The additional upper-air sources also provide information on humidity (specific, relative humidity or dewpoint depression). These were not used in ERA5^{→79}, partly because of suspected systematic biases (Grant *et al.*, 2009) and partly for technical reasons. Upper-air humidity observations from ERA-40 BUFR are not used above 300 hPa until December 1978, and some of them are used up to 100 hPa afterwards, depending on the sonde type.

The mixing of observations from various historical archives unavoidably leads to the presence of duplicates. Duplicates are also known to exist within particular archives. Often these are very difficult to separate as some observations are very close to the original paper records, whereas others have been post-processed. This can involve, for example: conversion and interpolation from native vertical coordinates to standard pressure levels; the application of undocumented bias corrections: reporting only part of the observation (e.g., wind only rather than wind, temperature and humidity); rounding of latitude and longitude, and inconsistencies in time

stamps, station names and classification (e.g., PILOT versus TEMP).

Although the Integrated Forecasting System (IFS) provides rules for duplicate removal in 4D-Var, for ERA5^{→79} a special effort was made. Duplicate removal was performed on any reports that were observed within a certain difference in latitude and longitude (0.3° for upper air, 0.03° for surface observations) and observing time (90 and 15 min for upper air and surface observations, respectively). For upper-air soundings, priority is given to the reports that contain information on the most variables, with humidity at highest priority, followed by temperature and, lastly, wind. In principle this follows the preference of TEMP over PILOT (wind only). However, due to the heterogeneous character of the historical archives, some reports classified as PILOT also contain temperature while some TEMP do not contain temperature. If this is not sufficient, a ranking is made on source. As explained in Hersbach *et al.* (2017), the CHUAN v1.7 data set consists of a raw ('r') and corrected ('c') sub-set, the latter being usually a post-processed and bias-corrected version of the former. Since in ERA5^{→79} prescribed bias corrections are explicitly applied (discussed below), preference is given to 'r' when the duplicate is 'c'. If this is not the case, a further ranking is made on source. Preference is given to the most recently digitized reports from ERA-CLIM, followed by ERA-40 BUFR, and lastly NCAR UADB-2 version 2.0. In cases where, for any reason, a decision cannot be made on the basis of the rules described above, the report with the highest number of observations is selected; when this is equal, the first is selected. For surface observations, the selection tree is much simpler: ERA-40 BUFR data are preferred since they typically contain the most complete reports in terms of geophysical variables. When both observations are ERA-40 BUFR, the first is selected, and when neither are ERA-40 BUFR, the second.

In the screen analyses of the LDAS (see section 2.3 of Hersbach *et al.* (2020) for details), duplicates are removed as well. For all observations with identical locations, the observation closest to the central time of their 6-hourly assimilation window is selected. In addition, the OI analyses have a limit of 50 observations (scanned within a radius of 1,000 km for 2 m temperature and 2 m relative humidity and 250 km for snow depth) which can influence the analysis at each model grid point. Details are provided in section 9 of part II of ECMWF (2016b).

Blacklist rules exclude the usage of observations that are known to be of either poor quality or currently unsuitable for usage in the assimilation system. These typically act on station names and domains (e.g., no 10 m wind over land, only 2 m relative humidity over land and during daytime in 4D-Var, no humidity above 300 or 100 hPa depending on the sonde type). In addition, there is

a first-guess check that disregards observations for which the magnitude of the first-guess departure (model first guess equivalent relative to the observed value) exceeds a predefined multiple (α) of the quadrature addition of the background and observation errors. In 4D-Var, this limit is quite relaxed for conventional observations ($\alpha = 18$), which is enabled by the robust Hüber norm-based variational quality control (Tavolato and Isaksen, 2015) that assigns efficiently low weights to large outliers. As discussed below, IBTrACS observations are an exception. In the LDAS, which does not use Hüber, $\alpha = 3$ for 2 m temperature and humidity and $\alpha = 5$ for snow depth. Since here both observation and first-guess errors are fixed, this leads to 7.5 K for 2 m temperature, 33.5% for 2 m relative humidity and 0.25 m for snow depth.

In ERA5^{79→}, observation errors are constant. In ERA5^{→79}, the evolution of these over time could, in principle, have been taken into account to reflect improvements in instrumentation. For this, the method of Desroziers *et al.* (2005) could have been followed based on low-resolution test runs (scouts) conducted in an iterative fashion to allow for the method to converge. This is quite an elaborate task, especially to account for the evolution of observation errors over the 29-year period. Due to time constraints, it was decided not to deviate from ERA5^{79→}. The specification of observation errors is given in Table 3. More details on observation errors in the 4D-Var component can be found in section 2.6 of part I of the IFS online documentation (ECMWF, 2016b) and in chapter 9 of part II for the LDAS component.

Like ERA5^{79→}, surface pressure observations benefit from variational bias correction (VarBC). The bias model involves a one-parameter (mean bias) adjustment, which is evolved over time for each station identifier, source (ERA-40 BUFR, ISPDv3.2.6, etc.), type of report and station height, independently. A distinction is also made between surface and mean sea level pressure. The weight of the background term for bias parameters is 120 times that of the weight of all observations combined in the corresponding bias group in a 12-hourly assimilation window, which means that VarBC responds with an e-folding time of about 60 days to abrupt changes in observation bias. Although the station identifier is an effective way of stratifying land stations, it has its limitations over sea. Some identifiers such as 'SHIP' are very common, holding observations that can have quite diverse bias characteristics and yet are grouped together. Unfortunately, initially a mistake was made for the bias correction for non-ERA-40 BUFR data. In cases where a station also appeared in the ERA-40 BUFR data set, it was grouped in the corresponding ERA-40 BUFR bias group, whilst otherwise, inadvertently, no bias correction was applied. This was rectified halfway through the production runs. Consequently, from

January 1, 1950 to April 28, 1955, no bias correction was applied to any surface pressure observations (no ERA-40 BUFR data were available), while for July 1, 1959 to May 13, 1961, March 1, 1965 to March 18, 1968 and January 1, 1974 to June 19, 1974, only a small fraction (typically around 2%) of non-ERA-40 BUFR data had not been bias corrected. After completion of ERA5^{→79}, some affected periods were rerun for short periods in which this bug had been resolved. From that, it emerged that it did have a noticeable systematic negative effect on departure statistics and quality of re-forecasts.

For radiosonde temperature, the off-line method of prescribed bias corrections, as described in Hersbach *et al.* (2020), is used in ERA5^{→79}. In ERA5^{79→}, estimates are based on a comparison between neighbouring stations where possible (RICH; Haimberger *et al.* (2012)), whilst an additional solar-elevation-dependent correction is also applied (RISE). In ERA5^{→79}, there are some slight differences: it makes use of an updated set of bias corrections (RICHv1.72) and no solar-elevation-dependent adjustments were applied, since they were deemed too uncertain without constraints from satellite data. Besides reaching back further in time (1905) than the version used in ERA5^{79→} (v1.51), more radiosonde observations could be adjusted in v1.72, particularly in the lower stratosphere of the Southern Hemisphere and tropics, leading to a stronger mean downward adjustment in those regions. As a result, there is a small though systematic difference in the temperature adjustments between both segments of ERA5.

The evolution of the number of observations assimilated in the 4D-Var component of ERA5^{→79} is presented in Figure 4a–h, including satellite radiance observations (Figure 4g) and ozone observations from BUV (Figure 4h). Here, a distinction is made between observations from all sources (blue), ERA-40 BUFR (grey for ERA5^{→79}, red for ERA5^{79→}) and observations from other sources (ochre). A similar plot for all available observations (used plus not used) is provided in Supplementary Figure S1.

For surface pressure (panel a), the combined ISPD and ICOADS holdings contain about twice as many observations as ERA-40 BUFR. Most of the ERA-40 BUFR observations are assimilated, while about half of the non-ERA-40 BUFR observations are rejected. As a result, ERA5^{79→80} uses about twice as many surface pressure observations around 1979 as ERA5^{79→} does. These originate partly from areas that were already well (Eastern United States, Western Europe, and Japan) or reasonably (Argentina) observed in ERA5^{79→} and partly from regions that were poorly observed in ERA5^{79→} (Western United States over the Rocky Mountains, parts of China, Southern Africa). This is illustrated in Supplementary Figure S2, which provides coverage plots of actively used

TABLE 3 (Top) Prescribed observation errors for upper-air temperature, wind and humidity as used in ERA5^{79→79}

Upper-air pressure hPa	TEMP/PILOT			Aircraft	
	Temperature K	Wind m/s	Humidity %	Temperature K	Wind m/s
10	1.66	2.70			
20	1.34	2.07			
30	1.28	1.89			
70	1.28	1.89			
100	1.09	1.98	(18)	0.98	2.29
150	0.80	2.16	(18)	0.90	2.40
200	0.77	2.25	(18)	0.81	2.44
250	0.73	2.25	(18)	0.72	2.40
300	0.64	2.34	18	0.72	2.36
400	0.57	2.25	17	0.73	2.32
500	0.61	1.89	15	0.75	2.23
700	0.70	1.71	13	0.77	2.11
1,000	0.89	1.62	11	1.05	2.04
Land surface			4D-Var, LDAS		
Type of report			Observation error		
any		Ps	0.52 hPa, increasing with height, 4D-Var only		
any		Rh2m	LDAS: 10%; 4D-Var: 10% average, daytime only		
any		T2m	2.0 K, LDAS only		
any		Sd	0.04 m, LDAS only		
Marine surface			4D-Var only		
Type of report			Observation error		
DRIBU		Ps	0.47 hPa		
IBTrACS		Ps	0.78 hPa		
other		Ps	0.73 hPa		
DRIBU		U10/V10	1.33 m/s		
other		U10/V10	1.50 m/s		

Note: For heights other than listed, the observation error is a linear interpolation between the values at the listed pressures, while it is constant from 10 hPa upwards. Upper-air humidity is assimilated as a non-linearly transformed variable Hólm *et al.* (2002), and effective mean observation errors are listed for relative humidity. No upper-air humidity is assimilated before August 1957, up to 300 hPa before December 1978 and up to 100 hPa afterwards for some sonde types. (Middle/Bottom) Prescribed observation errors for surface pressure (Ps), 2 m relative humidity (Rh2m), 2 m temperature (T2m), snow depth (Sd) and 10 m wind components (U10/V10) as used in ERA5. For 2 m relative humidity as used in 4D-Var, the mean observation error is listed, as it is a function of temperature.

observations of ERA5^{79–80} and ERA5^{79→} for January 1979 and January 1980. Both the number of mean sea level pressure and pressure observations at station height are larger in ERA5^{79–80}. The amount of the latter type has increased dramatically. For January 1979, ERA5^{79→} used about 10,000 of such observations, versus 505,000 for

ERA5^{79–80}. In January 1980, the difference is smaller (565,000 versus 989,000). In addition, in ERA5^{79–80}, observations are available more frequently. The sudden increase of observations for ERA5^{79→} in January 1980 typically originates from areas that were already covered by ISPD and ICOADS but not in the ERA-40 BUFR collections.

Nevertheless, data volume in these regions is larger still for ERA5^{79–80}. Around January 1980, no significant increase is observed for the number of pressure observations from ISPD and ICOADS. From these reflections, it is clear that such observations provide an important addition to the available observing system of the time. The departure statistics for surface pressure is much improved for ERA5^{79–80}. For January 1979/1980, this is 1.53/1.68 hPa versus 1.84/1.90 hPa for ERA5^{79→}. There are several reasons for this: the additional observations may be of higher quality and their ingestion improves the analysis and improves the comparison with observations just prior to their assimilation. Three factors contribute to the step change in assimilated surface pressure (a) and upper-air wind observations (c) in early 1973: The increase in the number of surface pressure observations available from the non-ERA-40 BUFR data sets (Supplementary Figure S1); the change in B_{cli} in November 1972, and the introduction of VTPR.

For upper-air temperature and wind (panels b and c), the transition around 1979 is much smoother regarding data usage. In 1973, there is a sharp transition in available data counts from the various data sources (Supplementary Figure S1b, c). For several years prior to that transition, data counts for the new upper-air data sets are about 60% higher than for the ERA-40 BUFR holdings. Afterwards, the latter have higher counts and in effect there is no noticeable transition for the sum of the data sets. This illustrates the value of the new upper-air data sets. Most emphasis had been given to earlier periods for which larger data gaps were known to exist. In 1978, the numbers of these data set sharply decline for upper-air temperature and disappear for upper-air wind, leading to a drop in the total number of available observations. That drop does not appear in the used observations (Figure 4), which indicates a large amount of duplicates just prior to that drop. The assimilation system typically gives preference to ERA-40 BUFR data, most likely because they are more complete. The added value of the new data holdings becomes increasingly important, though, further back in time. For humidity (panels d and f), there is, by design, a smooth transition in 1979 since, as for ERA5^{79→}, these observations all originate from ERA-40 BUFR. There is no obvious jump in data counts around September 1957 for any of the variables when the ERA-40 BUFR data holdings start. This is a healthy sign. Prior to this date most of the new holdings are used, while afterwards the duplicate removal results in the usage of either these or the ERA-40 BUFR holdings such that active data counts do not increase instantly.

For 10 m marine surface wind (e), data counts are slightly higher (by about 10–20%) in ERA5^{79–80}. These do

not originate from particular areas that were not available from the ERA-40 BUFR holdings (not shown).

Panel g refers to all satellite radiances: VTPR during the period from November 1972 to February 1979, and a fourfold increase in radiance data volumes assimilated following the introduction of the TOVS instruments from January 1979 onwards. Panel h refers to BUV ozone observations.

3.3 | Land surface observations prior to September 1957

Although the ERA-20C and CERA-20C centennial reanalyses benefited from several sources, none of these provided observations of surface air temperature and humidity over land for use in the LDAS component, and these reanalyses did not contain a LDAS component. ERA5^{79→} did have access to such observations from ERA-40 holdings, but these began only at the end of August 1957. It was not possible to remedy this for humidity, but synoptic temperature data held by NCEP were provided in a form that could be readily adapted for ingest by ERA5^{79→}. The original data sources are specified by Simmons *et al.* (2021). These data were analysed in the first production stream, which was used for products issued for the period from 1950 to the middle of 1959.

Observational coverage in the ERA5 LDAS component has been discussed by Simmons *et al.* (2021), and an example for February 1956 is presented later, in Figure 20. Coverage varies considerably by region. Data counts for North America are broadly similar from 1950 to 1966, after which there is a jump in data numbers that can be seen in the global numbers for surface pressure, 10 m wind and 2 m relative humidity presented in Figure 4. The same is true for Europe, following a rise in data numbers at the beginning of 1952. Observation coverage over much of Asia is also relatively good, but there are few observations for China prior to August 1956, and there is a gap inherited from ERA-40 in holdings from China, India as well as Brazil, Canada and a number of smaller countries for 1965 and 1966. The additional NCEP data set provides relatively few observations for South America and Africa. Coverage over Australia is very poor for spells prior to 1977, another inheritance from ERA-40, but the NCEP data have a reasonable number of observations between July 1951 and December 1957.

3.4 | The usage of IBTrACS observations

ERA5^{79→} had access to 6-hourly tropical cyclone best track pressure reports from the International Best Track Archive

for Climate Stewardship (IBTrACS, Knapp *et al.* (2010)), which contains a rich data set of tropical cyclone (bogus) observations. For technical reasons, these had not been assimilated in ERA5^{79→}. These reports, which are contained in ISPD v3.2.6, were also assimilated in two previous centennial reanalyses produced by ECMWF, viz. ERA-20C and CERA-20C, in which only surface observations were assimilated. However, strict quality control led to the rejection of many of these observations, with the result that many tropical cyclones were not well represented. In addition, in CERA-20C (Laloyaux *et al.* (2018), Kosaka (2018)), it was found that bypassing the first-guess check and retuning observation errors for Best Track observations did not give satisfactory results as it degraded the fit to other observations. In the latest 20CRv3 reanalysis Slivinski *et al.* (2019), by-passing of quality control was successful, and the usage of an observations error of 2.5 hPa gave satisfactory results. Despite the previous results from CERA-20C, a similar setup was tested in ERA5. Both the first-guess check and the Hüber norm were switched off, which means that the same weight was given to these observations, regardless of the first-guess departures. Initial tests in ERA5^{79→} scout runs looked promising, after which it was decided to enforce the usage of these observations.

Later, during production, it was discovered that occasionally the resulting analysis produced cyclones which were too deep, rather than too shallow, as found previously in CERA-20C. The reason for this discrepancy was twofold: (a) inadvertently, too much weight was given to these observations in the ERA5^{79→} data assimilation system: observation errors of 0.78 hPa were assigned, rather than a more optimal choice of 2.0 or 2.5 hPa, and (b) the data assimilation system was not provided with the information that these observations represent a minimum in the pressure field. As a result, the analysis fit at an observation location is usually good, but often the assimilation system places the minimum pressure away from the observations and this minimum is then typically deeper. Therefore, the compromised quality of the tropical cyclone analyses in ERA5^{79→} is not related to the quality of the pressure estimates from the IBTrACS, but a result of the sub-optimal method used to assimilate them. It continues to prove challenging to extract detailed information from sparse and rudimentary surface pressure observations alone.

An example of a well-behaved case is presented in the top panels of Figure 5 for Hurricane Charlie. Both the ERA5 analysis at the observation location and the minimum pressure are close to the IBTrACS observations. An example where the ERA5 analysis is far too deep is given in the lower panels for Typhoon Doris. Here, on May 11, 1950, the ERA5 analysis at the observation location (blue curve)

underestimates the IBTrACS observation (black curve). However, the assimilation system has displaced the minimum, which results in a tropical cyclone that is actually far too deep (by about 60 hPa, red curve) rather than too shallow.

For the 41,763 IBTrACS observations that were assimilated in ERA5^{79→}, the average standard deviation of the analysis departure is 5.4 hPa, while it is 9.0 hPa for the minimum pressure closest to the observation. In ERA5^{79→}, where IBTrACS were not assimilated, for the 81,760 observations from 1979 to the end of 2010, this is 15.6 and 13.2 hPa, respectively. Therefore, based on these numbers alone, the way in which the IBTrACS were assimilated looks promising. Full density plots between all IBTrACS observations and minimum ERA5 pressure, provided in Figure 6, give a different picture. The encouraging statistics arise mainly from the density-rich less-extreme cases. For deeper tropical cyclones, the minimum ERA5^{79→} pressure often undershoots, sometimes severely. The worst case is a minimum of 840 hPa. It emerges (not shown) that the undershoot is more frequent in the early period of ERA5^{79→}.

For ERA5^{79→}, which did not assimilate IBTrACS, tropical cyclones are clearly too shallow. From this, it follows that the sub-optimal assimilation of these observations not only leads to an overestimation of the intensity of tropical cyclones in ERA5^{79→} but also results in a discontinuous behaviour in comparison with the ERA5 segment from 1979 onward. For example, although for ERA5^{79→} the cumulative distribution function match (thin grey line) is closer to the diagonal (though slightly overshooting) than it is for ERA5^{79→} (which shows a clear underestimation of minimum ERA5 pressure), the behaviour between these two segments is quite different. For these reasons, ERA5^{79→} should not be used for studies on tropical cyclones.

The erroneously strong tropical cyclones also have a distinct impact on the extreme statistics of ocean waves, which will be discussed in Section 6.

3.5 | Satellite observations

3.5.1 | Vertical Temperature Profiling Radiometer (VTPR)

VTPR, a predecessor of the High-Resolution Infrared Radiation Sounder (HIRS) instrument, is a passive infrared sounder carried on four satellites (NOAA-2 through -5) and provided data from November 1972 until February 1979. The instrument is a filter radiometer (McMillin *et al.* (1973)) and includes six temperature sounding channels in the 15 μm CO₂ band, with weighting functions

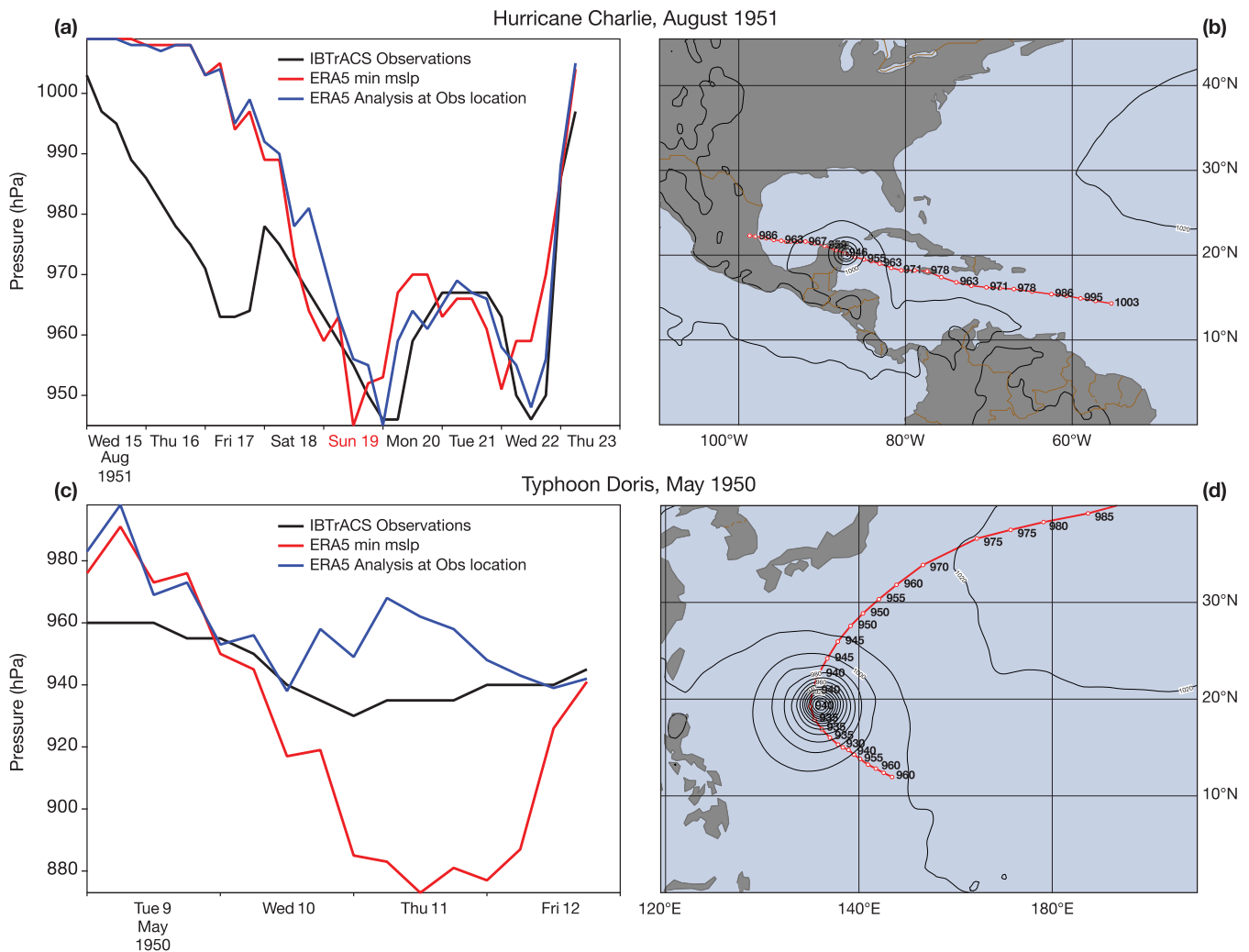


FIGURE 5 Time evolution of the estimated central mean sea level pressure from IBTrACS (black line) and the ERA5 analysis (red line) for (a) Hurricane Charlie and (c) Typhoon Doris. The analysed mslp values at the observation locations are plotted in blue. (b, d) Mean sea level pressure maps showing the position of these cases. The red line shows the path of the hurricane, reconstructed from the 6-hourly IBTrACS observations. Isobars are every 10 hPa

spanning the surface to the upper stratosphere, as well as a water vapour sounding channel centred at 535 cm^{-1} and a window channel centred at 833 cm^{-1} . ERA5⁷⁹ uses a reprocessed VTPR data set (Li *et al.*, 2005) which was assimilated in both ERA-40 (Uppala *et al.*, 2005) and JRA-55 (Kobayashi *et al.*, 2015). Each satellite in the series carries two nominally identical VTPR instruments (VTPR-1 and -2). During 1973, operations switched between the two instruments regularly, although after 1975 the instruments were operated continuously for extended periods.

As for all other radiance data sets assimilated in ERA5, VTPR uses RTTOV-11 (Lupu and Geer, 2015) as the observation operator, and employs time-varying CO_2 concentrations in the radiative transfer calculations. Black-listing, to remove data during periods where the data quality is significantly lower, is based on that developed

for JRA-55 (Kobayashi *et al.*, 2015) supplemented by additional blacklisting periods identified by low-resolution pre-production runs of the ERA5 configuration. The resulting data coverage over the lifetime of the sensor is indicated in Figure 7 for channel 4 of VTPR, and the remaining channels in Supplementary Figures S3–S8. Channels determined to be cloud free are assimilated, using a cloud detection scheme adapted from Krzeminski *et al.* (2009). Observation errors, shown in Table 4, are modified from those estimated in ERA-40 because a posteriori methods for the estimation of observation errors (Desroziers *et al.* (2005)) indicated that smaller observation errors could be used.

Measured spectral pass-bands for the channels of the VTPR instruments are documented (McMillin *et al.*, 1973) and exhibit some variability between nominally identical channels, but the mapping from measured pass-bands to

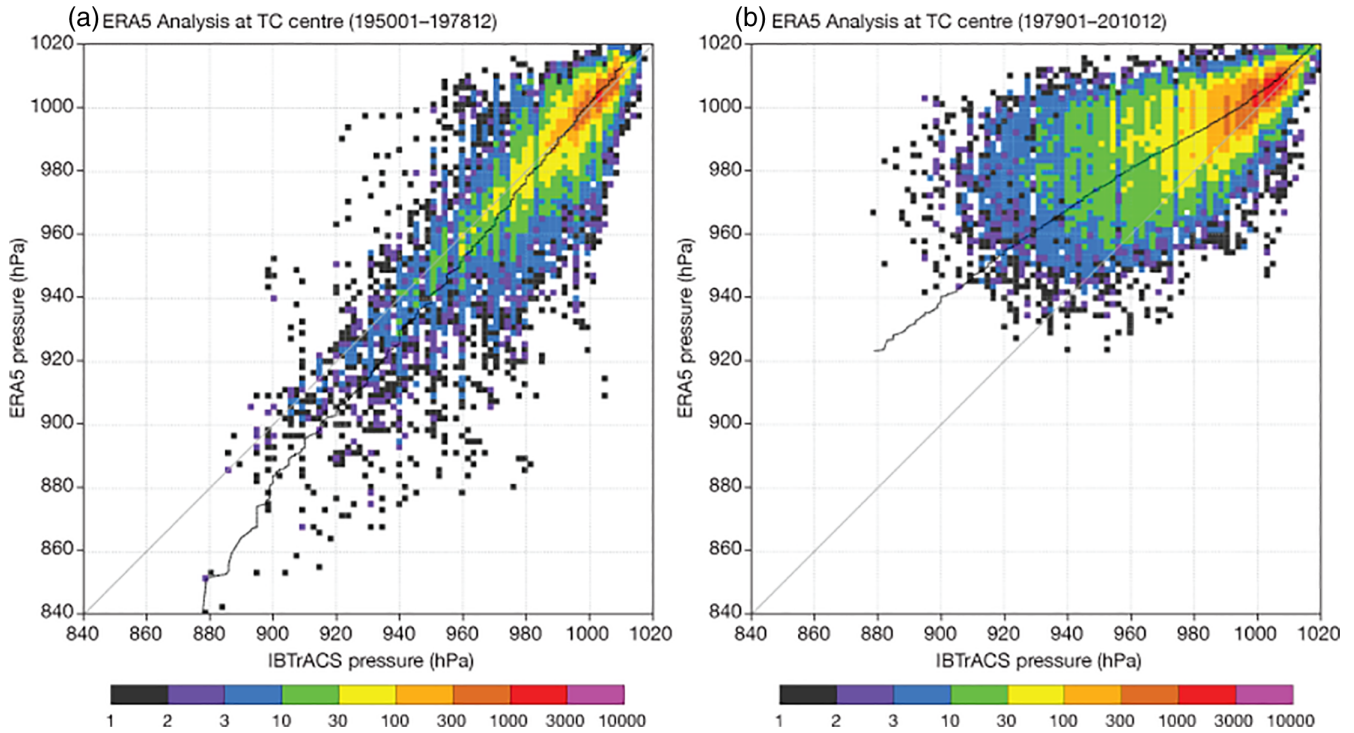
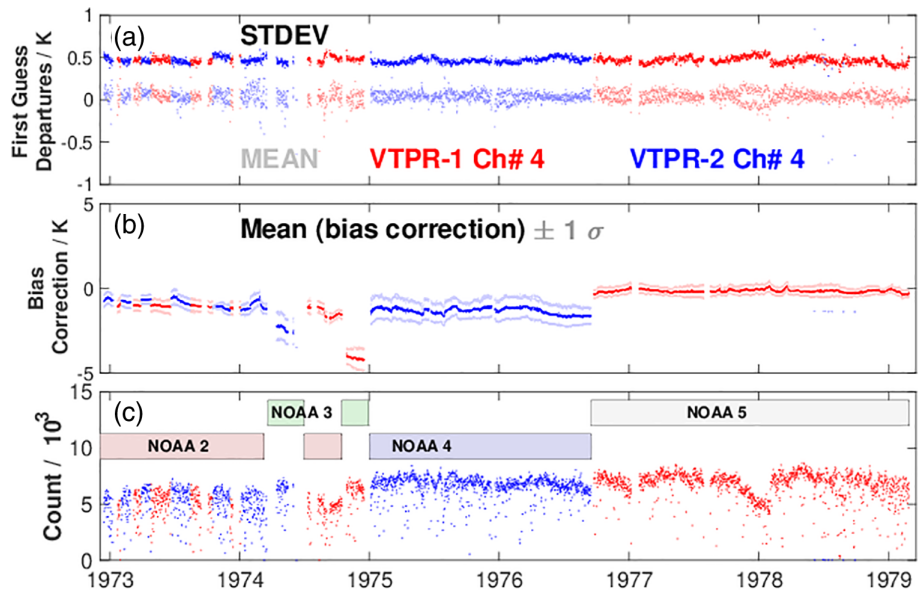


FIGURE 6 Density plot for the comparison between IBTrACS observations and closest minimum of ERA5 pressure for (a) ERA5^{→79} (41,763 observations) and (b) ERA5^{79→} (81,760 observations) until end 2010. IBTrACS were assimilated in ERA5^{→79} but not in ERA5^{79→}. The thin grey line is the cumulative distribution function match between IBTrACS and ERA5 pressure

FIGURE 7 (a) Time series of first-guess departures (mean, faint; standard deviation, bold) for VTPR channel 4 (centred at 708 cm⁻¹ and with a weighting function peaking at 400 hPa) during the lifetime of the series (November 1972 to February 1979), showing statistics for both VTPR-1 (red) and VTPR-2 (blue). (b) The bias correction applied to this channel, showing mean bias correction (bold) and (±) one standard deviation (faint) of the bias correction applied in each cycle. (c) Number of observations assimilated in each cycle, together with the coverage provided by the satellites NOAA-2 to NOAA-5



specific instruments is undocumented and hence ambiguous. RTTOV radiative transfer coefficients for all measured pass-bands are available, and an optimization (mapping coefficients to the eight individual VTPR instruments) was carried out using departure statistics derived from short (14-day) assimilation experiments carried out with each of the 32 possible permutations of coefficient sets with instruments. The mapping was based on minimum

first-guess departure variances, together with estimates of the mean biases produced by each coefficient set. The mappings are indicated in Supplementary Table ST1.

In pre-production testing using low-resolution (T319) versions of ERA5, the assimilation of VTPR significantly improved analysis and forecast accuracy in the data-sparse Southern Hemisphere. The standard deviation of short-range forecast fits to surface pressure/2 m relative

TABLE 4 Prescribed observation errors for VTPR in both ERA-40 and ERA5

Channel number	Channel centre /cm ⁻¹	Observation errors (K)		Land		Ocean
		CY41r2/ ERA-40	ERA5	<i>h</i> < 2,000 m	<i>h</i> ≥ 2,000 m	
1	668.5	2.00	1.00	•	•	•
2	677.5	1.00	0.80	•	•	•
3	695.0	0.80	0.50	•	•	•
4	708.0	0.70	0.50			•
5	725.0	0.60	0.60			•
6	747.0	0.60	0.60			•
7	535.0	2.00	2.00	•		•
8	833.0	1.00	1.00	○	○	○

Note: Also shown are the channel selections over land (including high land, with surface elevation higher than 2,000 m) and ocean. Black dots (•) indicate a channel is actively assimilated; open circles (○) indicate a channel is monitored. All channels are blacklisted at the edge of the swath (field of view numbers 1 and 23) as well as over the Caspian Sea, defined by the latitude range 36–48° N and longitude range 46–55° E.

humidity/10 m zonal wind component observations in the Southern Hemisphere was improved by 30%/18%/10%, respectively (Figure 8). For radiosonde temperatures (Supplementary Figure S9), fits were improved by 8–20% from the surface up to the mid-stratosphere in the Southern Hemisphere. Impacts were smaller in the Northern Hemisphere. Comparison with the improvements made during the ERA5 production runs is inexact, as there is no control experiment with no VTPR data, but a rough indication of the improvements realised in the production runs during the VTPR mission can be estimated by taking average standard deviations for first-guess departures over the 6 years following the introduction of VTPR with the same statistics for the preceding 6 years. Standard deviations for surface pressure/2 m relative humidity/10 m zonal wind components were reduced by 33%/7%/6%, respectively. Figure 9 shows the change in first-guess departure statistics for the Southern Hemisphere (south of 20° S) land-based surface pressure observations during the period 1950–2020. Statistics for the period January 1950–December 1978 are from ERA5^{→79}, while those from January 1979–December 2019 are from ERA5^{79→}. A step change (i.e., an improvement) in the departure statistics is evident at the time when VTPR is introduced. Although the number of surface pressure observations is increasing steadily during the period from mid-1967 to late 1978 (by a factor of approximately two), the step change in departure statistics upon the introduction of VTPR and the simultaneous change in the climatological component of the background error covariance in November 1972 (see Section 3.6) is more pronounced than the increase in surface pressure observation numbers at this point, and indicates the improvement in surface pressure background fields is most likely a consequence of introducing VTPR. The fraction of surface pressure observations assimilated

also increases at this time, consistent with the effects of introducing VTPR in pre-production testing.

3.5.2 | Backscatter ultra-violet spectrometer (BUV)

BUV is a nadir-scanning optical spectrometer on board the Nimbus-4 satellite launched in a sun-synchronous polar orbit on April 8, 1970. The instrument was designed to provide the total atmospheric content of ozone and vertical ozone structure in the atmosphere by measuring, during daylight, the intensity of the Earth's backscattered radiance and incoming solar irradiance. Although the BUV instrument was operational from April 10, 1970 until May 6, 1977, it provided complete coverage only until July 1972, after which time the spatial distribution of data became increasingly sparse owing to the partial failure of the solar power array on Nimbus-4 (Johnson *et al.* (2012)).

The reprocessed SBUV ozone data set version 8.6 (McPeters *et al.* (2013)), provided by NASA, contains BUV ozone vertical profiles which have been assimilated in ERA5. However, these data are not assimilated in the Ensemble of Data Assimilations (EDA, see Section 3.6).

3.6 | Data assimilation aspects

ERA5^{→79} uses the same hybrid incremental 4D-Var system as used in the ECMWF operational NWP model (IFS cycle 41r2) from March to November 2016 and in ERA5^{79→} as well as a separate Land Data Assimilation System (LDAS), as used in ERA5^{79→} and described in Hersbach *et al.* (2020). Summarising the key features: a ten-member Ensemble of Data Assimilations (EDA, at

FIGURE 8 Results from pre-production testing of VTPR data showing the change in (a) analysis and (b) first-guess departure standard deviations for SYNOP data in the Southern Hemisphere, normalised relative to a control experiment which assimilated no VTPR data. Experiments use the following static part of the B matrix (details in Section 3.6): (black) B_{cli}^{41R2} ; (orange) B_{cli}^{79} ; and (green) B_{cli}^{78} as used in production. These experiments covered the period January–September 1975

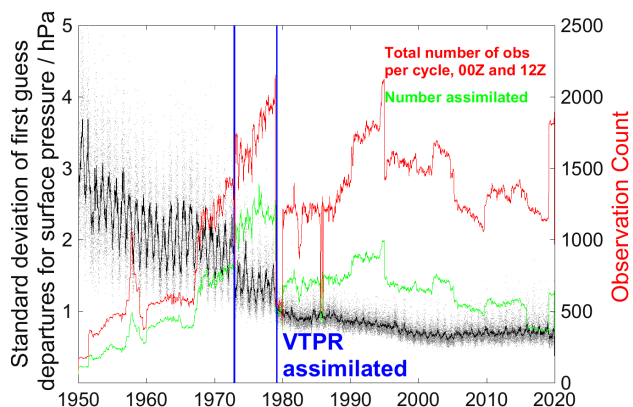
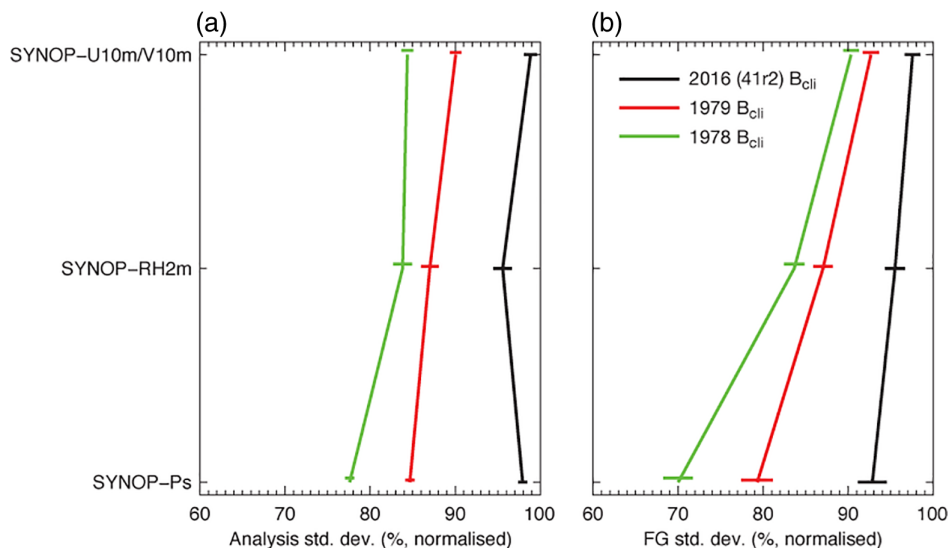


FIGURE 9 The evolution of the standard deviation of first-guess departures for land-based SYNOP observations of surface pressure from both BUFR and ISPD sources, in the Southern Hemisphere south of 20° S, showing values per cycle (00Z and 12Z, grey, faint) and 30-day running means (black) as well as 30-day running means of total observation counts (red) and the number of observations assimilated (green). Also shown (bounded by blue vertical lines) is the period during which VTPR data were assimilated

63 km resolution) is used to estimate flow-dependent background error covariances (Bonavita *et al.*, 2016) for the high-resolution component (HRES, at 31 km). In each of the ten members, other than the control member, observations, model tendencies, sea surface temperature (SST) and sea ice concentration (SIC) are perturbed to produce an ensemble of analyses and associated short forecasts. To compensate for sampling errors resulting from the relatively small ensemble size, the dynamically evolving EDA-based component is combined with a static component (B_{cli}). As the observing system evolves, so the background errors evolve, reducing in magnitude (of the variances) and characteristic length scales as

the observing system constrains the analysis ever more accurately.

In the initial production runs of ERA5^{79→}, two distinct versions of B_{cli} were employed, covering the period from January 1979 to December 1999 (1979- B_{cli}) and from January 2000 onwards (41r2- B_{cli}). Subsequently, an updated version of ERA5 (ERA5.1, Simmons *et al.* (2020)) was released in which the use of 1979- B_{cli} was continued through the period from January 2000 to December 2006 in order to reduce temperature biases in the lower stratosphere. In ERA5^{→79}, a further two versions of B_{cli} were used, covering the period prior to the assimilation of satellite sounding data (January 1950 to November 1972, 1958- B_{cli}) and the period covering the VTPR mission (November 1972 to December 1978, 1978- B_{cli}). The extension of ERA5^{→79} to the end of 1980 also used 1978- B_{cli} . These were estimated from dedicated runs of the EDA spanning 4 months in each of two seasons in 1958 and 1978, respectively, in order to represent the seasonality in background errors. The resulting B_{cli} used for ERA5 are illustrated in Figure 10, which shows the vertical profiles of global average standard deviations and horizontal length scales for temperature and relative humidity for the highest-resolution minimisations (T255, 79 km). As expected, the background error standard deviations for temperature and humidity show a monotonic decrease in magnitude with time, typically reducing by a factor of 2–3 from 1958- B_{cli} to 41r2- B_{cli} . For the horizontal length scales, the reduction is generally around a factor of two for temperature and less for humidity. Background errors for vorticity and divergence (Supplementary Figure S10) show qualitatively similar behaviour.

Figure 11 shows the evolution of the first-guess departure standard deviations for upper-air and surface observations in both ERA5^{→79} and ERA5^{79→} during the

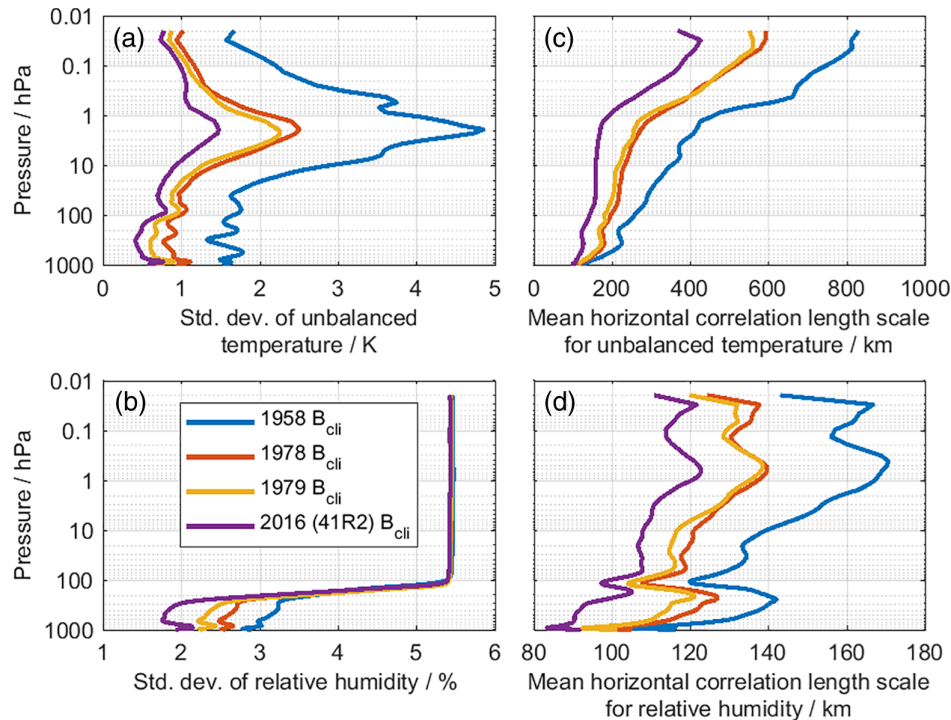


FIGURE 10 Global mean standard deviations of (a) unbalanced temperature and (b) relative humidity for the four distinct (1958, 1978, 1979 and 2016) static components (B_{cli}) of the background error covariances for the highest-resolution inner-loop minimisations (T255, 79 km) used for ERA5. Also shown are the mean horizontal correlation length scales for (c) unbalanced temperature and (d) relative humidity

period 1950–1985. As expected, the standard deviations generally reduce in magnitude throughout ERA5^{→79}, modulated by significant inter-annual variability. The curves for ERA5^{→79} merge well with those for ERA5^{79→}, while for surface pressure and 10 m wind these are significantly lower than those for ERA5^{79→} in the overlap period (as also highlighted in Section 3.2), as a result of the additional observations assimilated in ERA5^{→79}. Also encouraging are the downward step changes for upper-air temperature statistics (at 400 and 850 hPa) associated with the initial assimilation of satellite data from VTPR (1973) and the TOVS instruments (1979). There are several anomalies though, the most significant of which are the 10% increase in the standard deviations for surface pressure from 1965 to 1967, associated with a temporary lack of coverage in some areas (most notably China) as well as a longer-term anomaly from 1965 to 1974. This anomaly is not a particular feature of the specific stream (stream 3) as the same anomaly is observed in the spin-up period for stream 4 (not shown). The gradual increase in the standard deviations for upper-air temperatures in the layer centred at 50 hPa from the late 1960s until the late 1970s remains unexplained.

The EDA spread (Figure 12) and the mean analysis increments (Figure 13) also provide useful diagnostics to check the consistency of ERA5^{→79} in the context of the entire ERA5 record. Figure 12 shows the reduction in the EDA spread for temperature, zonal winds, humidity and ozone during 1950–2020. The spread in temperature in the troposphere reduces from typical values of around

1 K in 1950, to 0.5 K in 1979, to 0.2–0.3 K in 2020. The steady reductions during the period are punctuated by step changes, most notably for temperature and zonal wind, in 1957, 1972, 1979 and 2006. These changes are associated with significant improvements in the observing system: the introduction of ERA-40 BUFR upper-air temperatures, humidities and winds from September 1957 and the general improvement of the radiosonde network in the Southern Hemisphere in advance of the International Geophysical Year in 1958; the introduction of VTPR observations from November 1972; the introduction of sounding data (HIRS, MSU and SSU) from the TOVS satellites in late 1978, and; the introduction of large numbers of radio occultation observations from 2006. For specific humidity, in addition to the steady reduction in spread, periods of accelerated improvements follow the introduction of VTPR, TOVS and ATOVS satellite data in 1972, 1978 and 1998, respectively.

Figure 13 shows that, in the troposphere, mean analysis increments for temperature show good consistency during 1950–2020, with magnitudes typically below 0.1 K. For the mid-troposphere (300–700 hPa), they are considerably smaller, at less than ~ 0.03 K. Similarly for the mid-lower stratosphere, the mean increments are below 0.1 K and consistent throughout the record.

In the range 3–10 hPa, ERA5^{→79} analysis increments for temperature are notably smaller for the period from 1973 to 1978 than for the periods before or after. The magnitude of the increments above 10 hPa is markedly larger in ERA5^{79→}, especially during 1979–1984, and

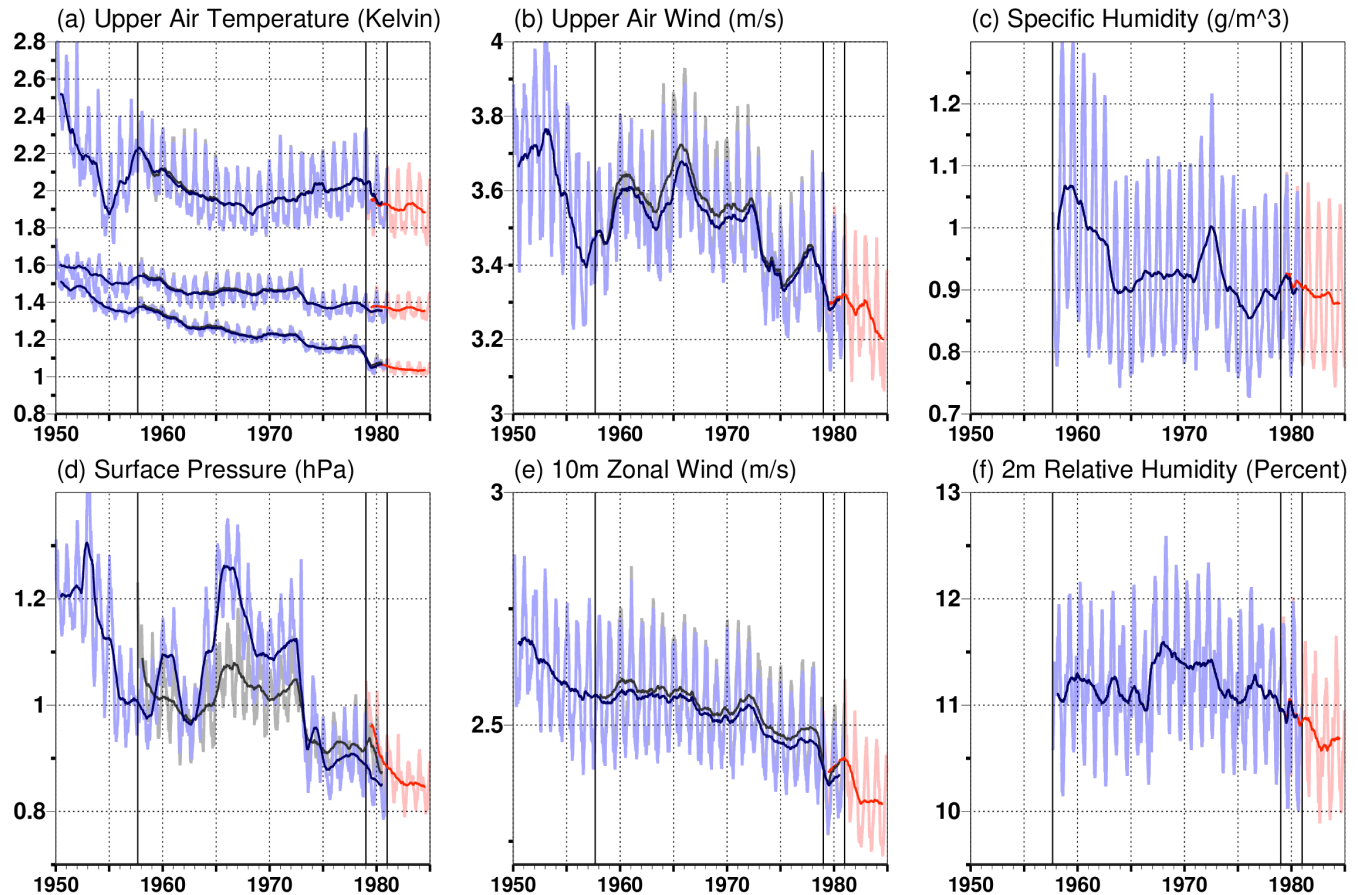


FIGURE 11 Thirty-day mean (weak colours) of the standard deviation of first-guess departures and 360-day mean (strong colours), for used data in ERA5 (red) and ERA5 back extension from all data sources (blue) and BUFR data only (grey) for (a) upper-air temperature from radiosondes (from top to bottom in the panel) within ± 25 hPa of 50, 850 and 400 hPa; (b) upper-air zonal wind from radiosondes, dropsondes and PILOTS; (c) upper-air humidity from radiosondes and dropsondes; (d) surface pressure from SYNOP, buoys, ships and METAR; (e) 10 m zonal wind over sea from various in situ sources; and (f) 2 m relative humidity from SYNOP. The statistics for (a, b) are number-weighted averages of the standard deviation over pressure bands of 50 hPa throughout the vertical, without making corrections for any pressure-dependent biases

exhibits a dipole structure, with negative increments up to about 5 hPa and positive increments above this level. It is likely that the form of the mean increments at these levels post-2006, when GNSS-RO observations are providing high-accuracy observational constraints on the analysis, represent more optimal corrections at each analysis cycle, and reflect model bias at these levels.

For 1973–1978, the most significant constraint at these levels is provided by channel 1 of VTPR, which has a broad weighting function peaking in the range 2–20 hPa (Li *et al.*, 2005). VTPR channel 1 is bias corrected using variational bias correction, which corrects the observations to the analysis. This is consistent with the near-zero mean increments at the levels spanned by VTPR channel 1 for 1973–1978. After 1979, SSU channel 3, peaking between 1 and 10 hPa, is assimilated without variational bias correction in order to anchor the stratospheric temperature analysis. The resulting analysis increments,

from early 1979 onwards, are more aligned with those evident post-2006, although not perfectly. As there was less confidence in the radiometric performance and radiative transfer modelling for VTPR (compared with SSU), it was decided to apply variational bias corrections to VTPR channel 1 in ERA5⁷⁹. The features evident above 3 hPa for the period 1973–1978 are primarily influenced by the form of the background error covariances at this level and reflect the transitions in November 1972 (1958- \mathbf{B}_{cli} to 1978- \mathbf{B}_{cli}) and in January 1979 (1978- \mathbf{B}_{cli} to 1979- \mathbf{B}_{cli}). As a note, the analysis increments for temperature above 10 hPa in ERA5^{79–80} (not shown) are very similar to those seen in ERA5⁷⁹ during 1973–1978, highlighting the important role of the change in \mathbf{B}_{cli} in January 1979 in producing the large increments in ERA5⁷⁹ mentioned above.

For temperature, the dominant feature in the troposphere is the positive increment throughout the ERA5 record of magnitude ~ 0.06 K in the range 100–300 hPa,

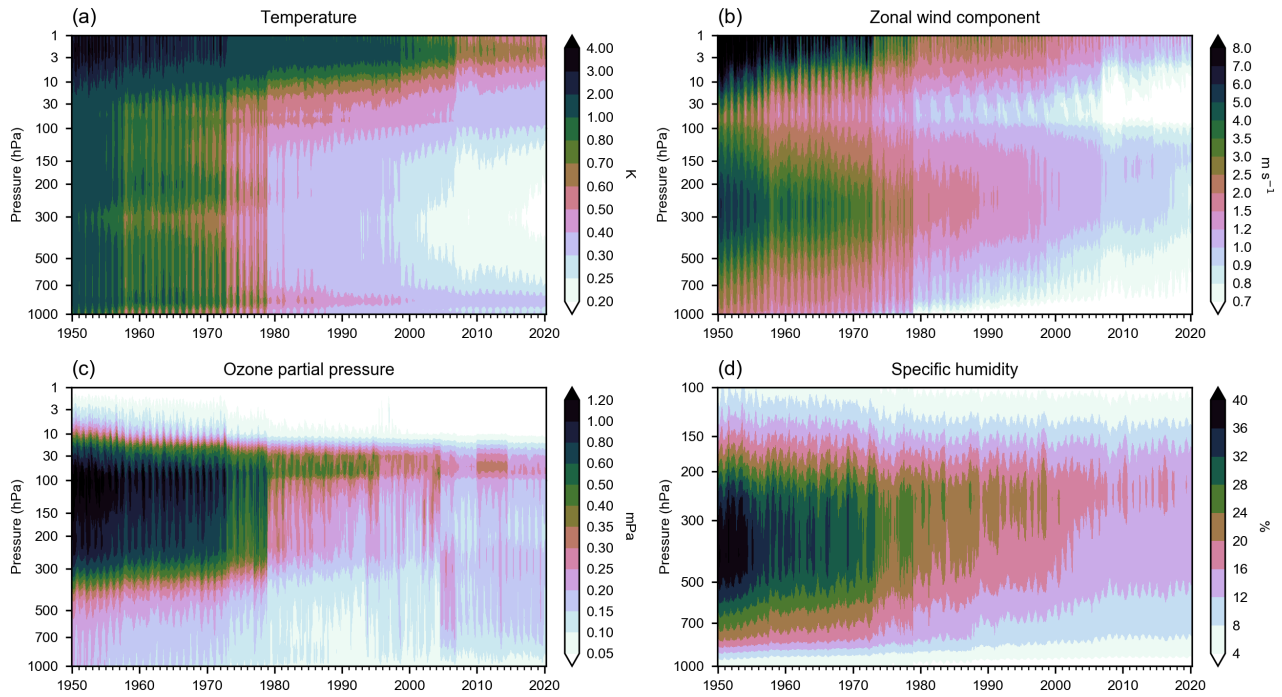


FIGURE 12 EDA spread versus pressure and time during the ERA5 record from 1950 to 2020 for (a) temperature, (b) zonal wind, (c) ozone partial pressure and (d) specific humidity

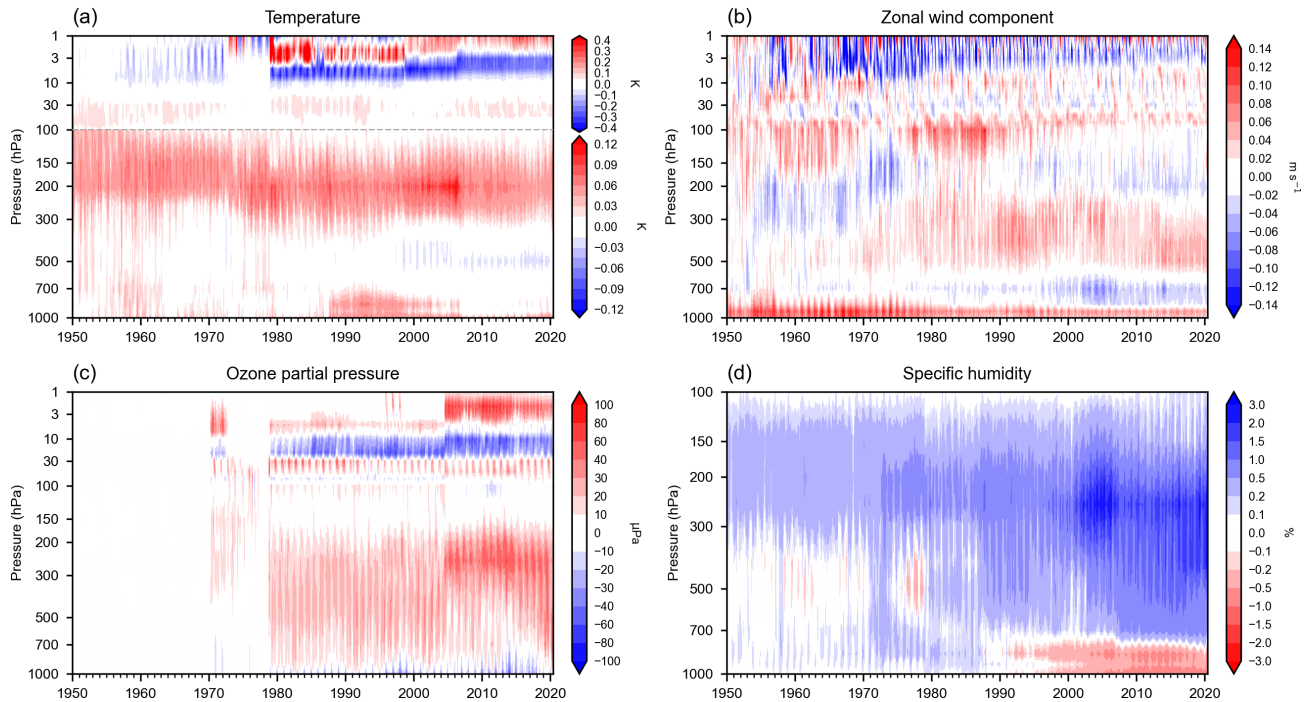


FIGURE 13 Mean analysis increments versus pressure and time during the ERA5 record from 1950 to 2020 for (a) temperature, (b) zonal wind, (c) ozone partial pressure and (d) specific humidity

consistent with the DA system correcting a forecast model cooling tendency in the upper troposphere.

For zonal wind, although the magnitudes of the increments are similar throughout the atmosphere, at typically

less than 0.1 m/s, the picture is less coherent during ERA5^{→79} compared with ERA5^{79→}. The introduction of VTPR observations appears to bring the profile of wind increments during 1972–1978 into better agreement with

those for ERA5^{79→}. This is also the case for humidity increments at levels between 200 and 300 hPa and below 700 hPa, where the transition from ERA5^{→79} to ERA5^{79→} is relatively smooth. In the mid-troposphere, from 300 to 700 hPa, the picture is more complex, with a seemingly anomalous period of drying increments from 1974–1978 at levels between 300 and 700 hPa.

For ozone, significant increments are evident from April 1970 to July 1972 at levels between 3 and 300 hPa, corresponding to the period when BUV observations were assimilated in large numbers (see Figure 4 and the discussion in Section 3.5.2). The form of the increments during this brief period is similar to those obtained in the last decade, when ozone was well observed. After July 1972, when the numbers of assimilated BUV observations drops by a factor of four, analysis increments at levels 3–30 hPa are smaller. Only when ozone-sensitive observations from SBUV and HIRS are introduced, from early 1979 onwards, do the stratospheric ozone increments return to the form of those observed in recent years.

3.7 | Forcings and boundary conditions

The ERA5 radiation forcing terms are largely based on the World Climate Research Programme (WCRP) initiative CMIP5 as described in (Hersbach *et al.*, 2015a) and, for example, take account of the contribution of volcanic eruptions to stratospheric sulphate aerosol.

The data sets and methods used to prescribe sea surface temperature (SST) and sea ice concentration (SIC) in the full ERA5 are described in detail in Hersbach *et al.* (2020) and Hirahara *et al.* (2016) and will only be briefly summarised here. For ERA5^{→79}, SIC and SST are based on two different releases of the Hadley Centre Sea Ice and Sea Surface Temperature data set version 2 (HadISST2): HadISST2.0 is used for SIC, whereas HadISST2.1 (Titchner and Rayner, 2014) is used for SST. In HadISST2.0, the SIC component is similar to that used in the earlier version of the data set, HadISST1.1 (Rayner *et al.*, 2003), and thus similar to that used in ERA-40. The original products are provided on a $0.25^\circ \times 0.25^\circ$ latitude–longitude grid as monthly means for the 1950–1960 period and as 5-day means (pentads) from January 1961 onwards.

Comparisons of time series of spatial averages of SST from ERA5 with those from various other data sets have been reported by Simmons *et al.* (2021). There is general agreement among data sets as to the rate of warming since the mid-1970s, but uncertainty as to the amount of warming over the preceding 10 years or so. The HadISST2.1 data set used in ERA5 during these 10 years behaves similarly to the COBE SST used in the JRA-55 reanalysis (Kobayashi *et al.*, 2015), and both are much closer to the HadSST3

data set than to the newer HadSST4 data set (Kennedy *et al.*, 2019), which has a larger temperature increase from the 1960s to the 1970s. Otherwise, there is relatively little difference in low-frequency variability between these and other data sets covering the period from 1950 onwards.

Time series of total sea ice area (SIA) for the Arctic and Antarctic regions are shown in Figure 14 and compared with those from other data sets, including 20CRv3 (Slivinski *et al.*, 2019) and three versions of the HadISST data set (v1.1, v2.1 and v2.2). In the Arctic, the five data sets bear great similarity in their depiction of the long-term trend and interannual variability of SIA. This is particularly true in March (Figure 14a), despite SIA being consistently and markedly higher in HadISST2.1 and HadISST2.2. The differences between data sets are much more prominent in the Antarctic, especially prior to the mid-1970s, revealing different approaches to the estimation of SIC values in the absence of direct satellite observations. HadISST2.1, HadISST2.2 and 20CRv3 exhibit unrealistically large SIA values in the 1950s and 1960s relative to the post-1979 period ($\sim 100\%$ larger in February, and $\sim 30\%$ larger in September, in the 1950s than in the 1980s). In a reanalysis, such sea ice changes can lead to artificial trends in some atmospheric fields such as precipitation and surface temperature. In contrast, ERA5 and HadISST1.1 exhibit values that are much more in line with those observed during the satellite era. The resemblance of 20CRv3 with HadISST2.1 and HadISST2.2 in the evolution of Antarctic SIA since 1950 can be explained by the use of HadISST2.3 in the former (Slivinski *et al.*, 2019).

4 | REPRESENTATION OF SYNOPTICS

4.1 | North Sea storm of February 1953

On January 31 and February 1, 1953, a combination of high spring tides and an intense storm in the North Sea caused a storm tide which swept south-eastwards along the east coast of the UK, reaching the coastline of the Netherlands in the early hours of February 1, causing widespread breaches of sea defences (Prichard (2013)). The associated flooding resulted in over 2,500 deaths, 1,800 of which were recorded in the Netherlands. Subsequently, in the following decades, sea defences were significantly fortified on the North Sea coastlines of the UK and the Netherlands, including the construction of the Thames Barrier east of London, and the Delta Works system of dams and barriers in the Netherlands.

The ERA5 analyses (Figure 15) show a region, on the western flank of the depression, of significant wave heights

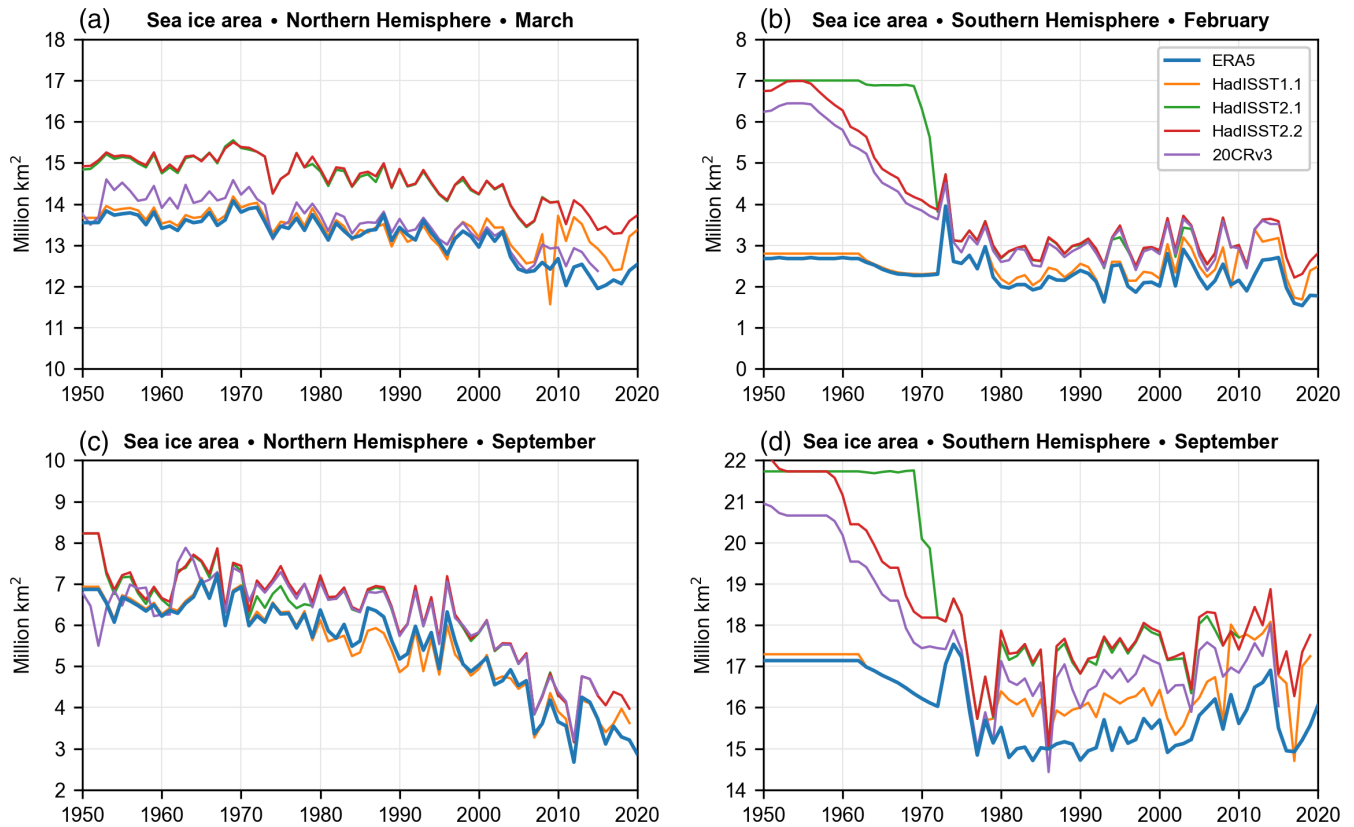


FIGURE 14 Time series of monthly mean total sea ice area for the Northern Hemisphere (NH; left panels) and Southern Hemisphere (SH; right panels) during 1950–2020 from ERA5 (thick blue line) and four other data sets: HadISST v1.1 (orange), HadISST v2.1 (green), HadISST v2.2 (red) and 20CRv3 (purple). The time series are shown for the month of year corresponding to the annual maximum and minimum total sea ice area in each hemisphere (March and September in NH, September and February in SH)

in excess of 10 m which travels around the northern coastline of the UK and south-eastwards in the North Sea towards the coastline of the Netherlands. ERA5 as well as CERA-20C (not shown) capture the large-scale evolution of the storm well. Indeed, the manual surface pressure analysis of the time from the Met Office (shown in Figure 15) also depicts the location, extent and minimum pressure of the storm well, as a result of the well-observed surface pressure and wind fields in this part of Europe in 1953. The advantage of the higher temporal and spatial resolutions in ERA5 becomes more evident when inspecting the evolution of wind gust analysed by ERA5 and CERA-20C (Figure 16), which shows that ERA5 generally reproduces the timing and intensity of wind gust, relative to observations (MetOffice (1954)), better than CERA-20C throughout January 31.

The bottom panel of Figure 16 shows the evolution of 10 m wind speed at Vlissingen (wind gust data are not available for stations on the coastline of the Netherlands during this period) in both reanalyses as well as hourly observations obtained from an automated weather station. ERA5 appears to underestimate the 10 m wind speeds throughout January 31, more so than CERA-20C. After

the peak winds (21Z on January 31 to 06Z on February 1), ERA5 represents the evolution of observed 10 m winds well for the subsequent 36 hours. This example illustrates that ERA5 is able to provide more realistic synoptic detail compared with that achieved in previous ECMWF reanalyses in this early pre-satellite period, at least for events in the well-observed European sector.

4.2 | Sudden stratospheric warming, February 1952

Two major stratospheric phenomena, sudden warmings and the QBO, were discovered from radiosonde observations made in the 1950s. ERA5's representation of the QBO from that decade onwards is discussed later, in Section 5.5.

The discovery of the stratospheric sudden warming phenomenon, for which ERA5 provides hemispheric context, was made by Scherhag (1952) by studying radiosonde ascents from Tempelhof Airport, Berlin, many of which were assimilated by ERA5. Hourly analyses of temperature at 30 hPa over Tempelhof and the corresponding observations are shown in the left-hand

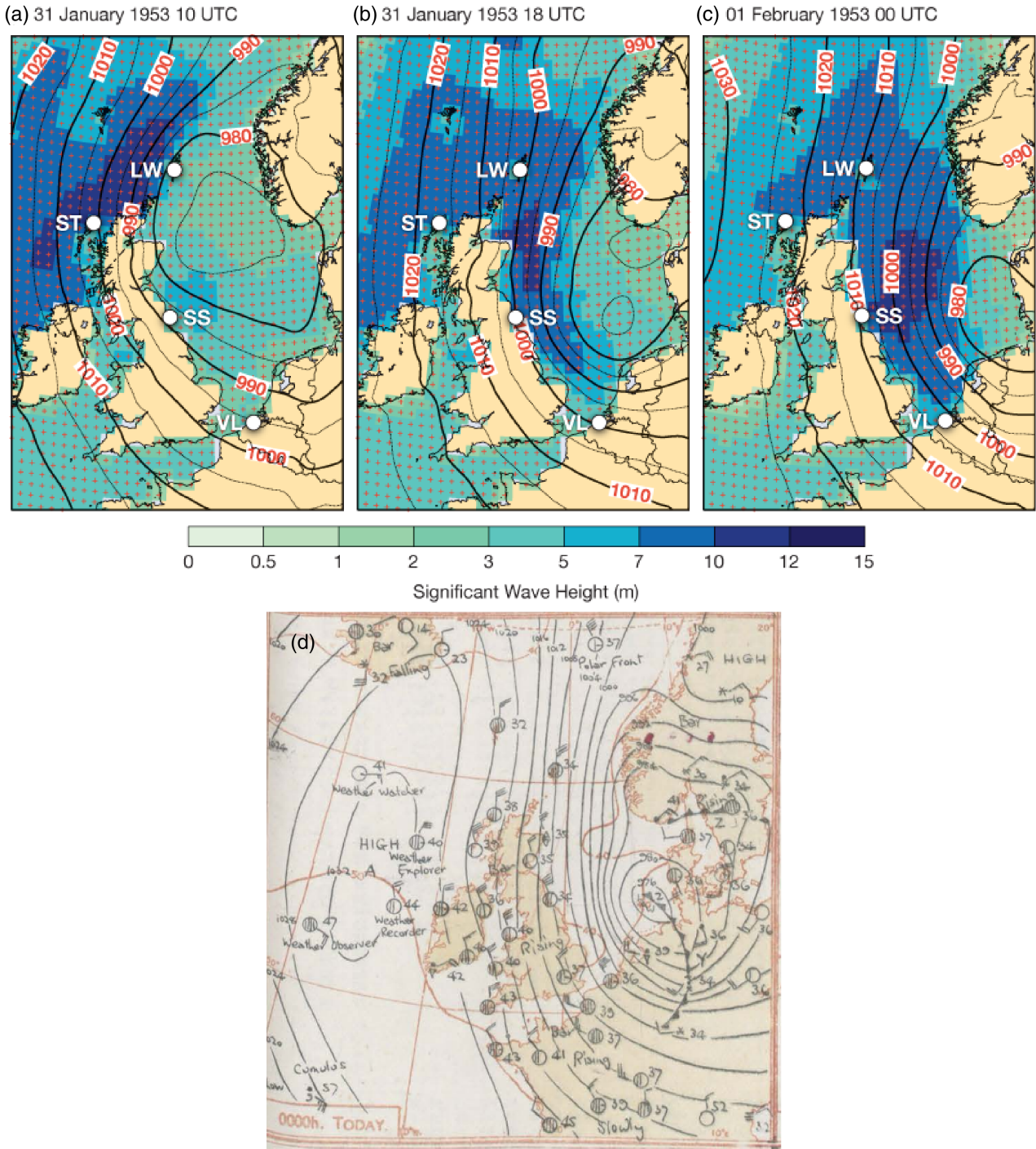


FIGURE 15 ERA5 analysis of mean sea level pressure (contours, in steps of 5 hPa) and significant wave height (colours, m) for the 1953 North Sea flood on January 31, 1953 at (a) 1000 UTC and (b) 1800 UTC and (c) on 1 February at 0000 UTC. Red pluses indicate the ERA5 native grid. (d) The February 1, 00Z Met Office mean sea level pressure analysis of the time, from the Met Office Daily Weather Report

panel of Figure 17 for January to March 1952. It was the rapid rises in temperature observed in late January and more especially late February that led Scherhag to refer to “explosive” stratospheric warming and to dub such behaviour the “Berlin Phenomenon”. Accounts refer to larger warming still at 10 hPa, but the ERA5 observational database has few observations at this level,

indicating a potential benefit from further data recovery. The temperature of -32°C measured at 30 hPa at 0900 UTC on February 28 is the highest temperature of any of the 5,510 values assimilated for this level in ERA5 in the period from January to March 1952. The coldest such temperature was -78°C recorded by the U.S. Air Base at Thule in north-western Greenland at 1500 UTC

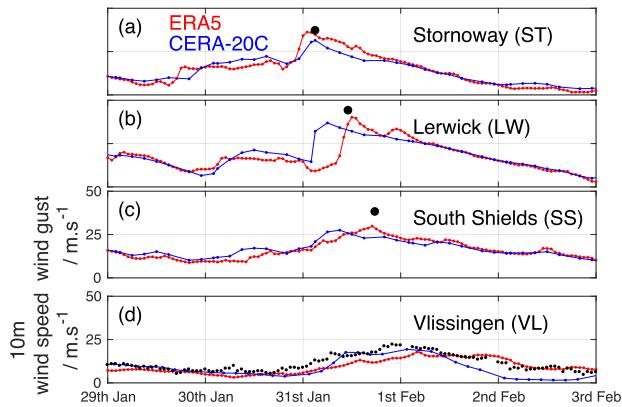


FIGURE 16 Evolution of ERA5 (red, hourly) and CERA-20C (blue, 3-hourly) analyses of 10 m wind gust (in m/s) at (a) Stornoway, (b) Lerwick and (c) South Shields from 00Z on January 29, 1953 until 00Z on February 3, 1953. Also shown (black dots) are the maximum observed wind gusts at these locations during the period, recorded in the Met Office Monthly Weather Report of the time (MetOffice (1954)). (d) Analysed 10 m wind speeds (in m/s) at Vlissingen (source: Rijkswaterstaat, the Netherlands), together with 10 m wind speed observations (black dots) from an automated weather station

on January 26, in the core of the polar vortex. Observations over Thule are sparser than those over Berlin, but matched well by the ERA5 analysis. A substantial increase in temperature over Thule in early February is associated with the movement of the polar vortex illustrated below. The Berlin temperatures tend to be underestimated, particularly in February and March. Both the cold lower stratospheric bias of the ERA5 model and underadjusted bias in the radiosonde measurements are possible factors.

What was observed over Berlin and Thule is put in context by Figure 18, which shows maps of 30 hPa temperature and geopotential height. The top two rows show ERA5 analyses at 5-day intervals from February 3 to 28, 1952. The bottom row shows corresponding 5-day forecasts verifying on February 18, 23 and 28. During the first half of February, the core of the cold vortex moves from Greenland to northern Russia and the vortex elongates and weakens. High pressure and relatively high temperatures are

established over Canada and Greenland. The vortex splits in the final week of February. The weaker of the two sub-vortices moves over Southern Europe, and a relatively small patch of anomalously warm air moves over Berlin. The 5-day ERA5 forecasts evidently represent reasonably well the major 5-day changes in circulation and temperature depicted by the analyses. This is notwithstanding errors in detail such as the southward displacement of the warm air that in reality crossed Berlin on February 28, on a track that was sampled by the radiosonde ascents from Tempelhof Airport.

Of the 1,851 30 hPa temperature observations assimilated for February 1952, 1,628 (almost 88%) were from radiosondes launched north of 20° N. The standard deviations of the background and analysis fits to the bias-adjusted temperatures from these radiosondes are 2.3 and 1.5 K, respectively. The background temperature is 0.4 K lower on average than the bias-adjusted observed temperature; the corresponding value for the analysis is 0.2 K.

The ERA5 analyses for the 1950s provide a resource for examining other warmings that occurred early in the observational record. There is scope to extend by a few years catalogues of events from 1958 onwards such as provided by Charlton and Polvani (2007) and Butler *et al.* (2017), and to extend other studies such as carried out under the auspices of the SPARC Reanalysis Intercomparison Project, Ayarzagüena *et al.* (2019) for example. Perhaps most notable is the warming of late January and early February 1957 analysed by Teweles (1958), who with the data and methods at his disposal was able to present and discuss Northern-Hemispheric charts at 100 hPa, and charts and cross-sections over North America up to as high as 15 hPa. In this case, ERA5 depicts a split of an elongated polar vortex into two, beginning in late January. By February 10, separate vortices were located over Canada and south-western Russia and high pressure extended from Iceland over the North Pole to north-eastern Siberia. This development was captured in the 10-day forecast from January 31, albeit with a delay of about 2 days in the split of the vortex. Other candidates for

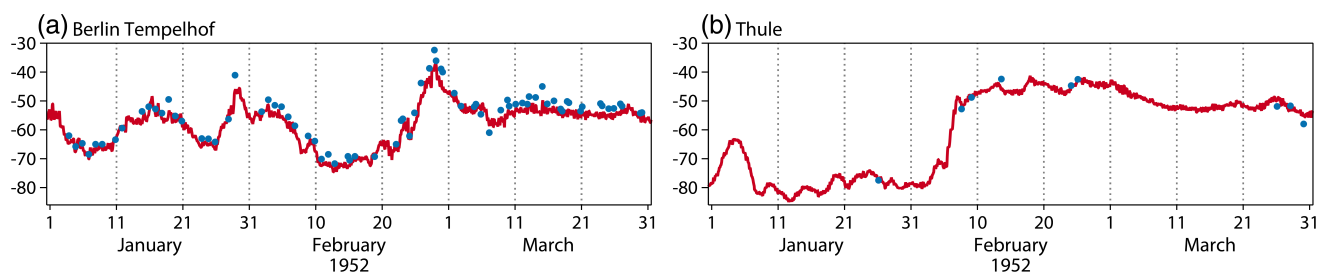
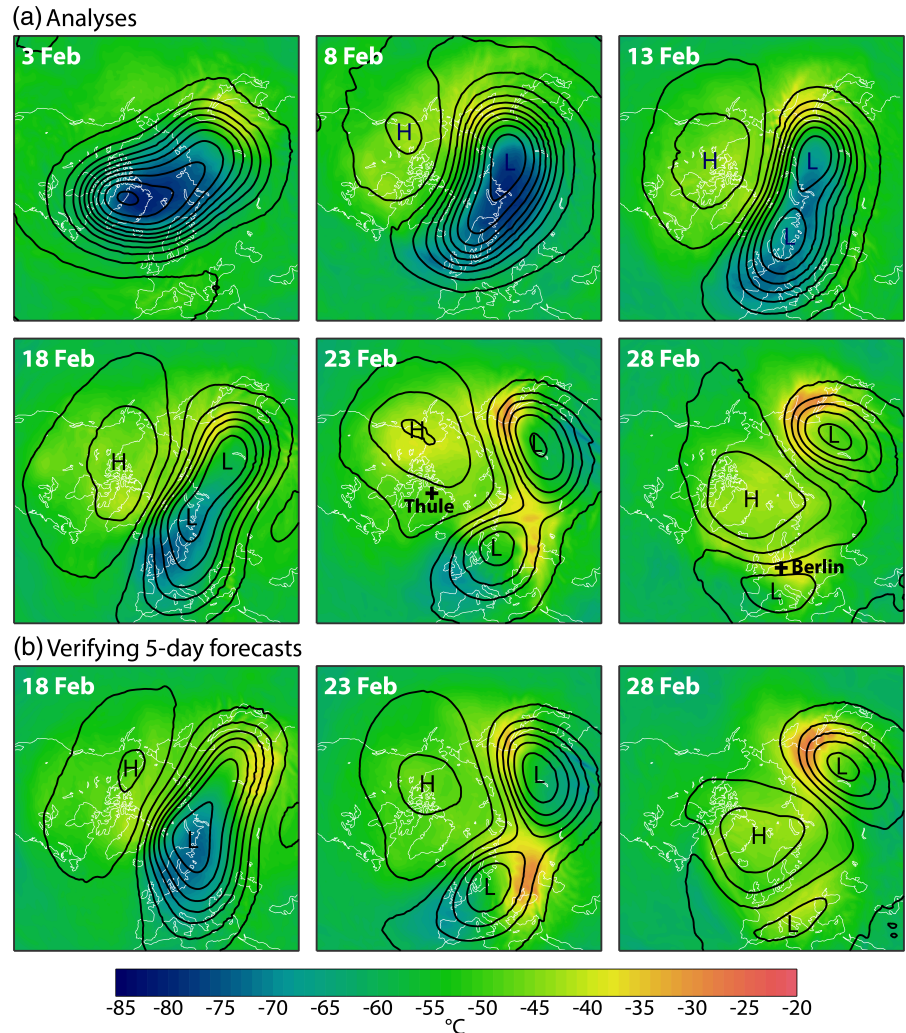


FIGURE 17 ERA5 analyses and radiosonde observations of 30 hPa temperatures (°C) for (a) Berlin Tempelhof and (b) Thule

FIGURE 18 (a) ERA5 analyses of temperature (shading) and geopotential height (contour interval 20 dam) over the Northern Hemisphere at 30 hPa and 1200 UTC, at 5-day intervals from February 3 to 28, 1952. (b) Corresponding 5-day forecasts verifying on February 18, 23 and 28, 1952



further study are a similar split of the vortex in February 1951 and a pronounced southward migration of the vortex over Russia in January 1955.

5 | ERA5 SURFACE AND UPPER-AIR FIELDS

5.1 | Surface air temperatures

An extensive investigation has been made into ERA5's representation of surface air temperature and humidity, temperature and humidity at a nominal height of 2 m above the ground. The principal aim was to assess the reliance that can be placed on ERA5 for routine monitoring of climate variability and change, in particular the use of ERA5 in the climate monitoring bulletins published by the C3S (<https://climate.copernicus.eu/monthly-climate-bulletins>). Results have been documented in full by Simmons *et al.* (2021); some discussion for temperature is given here.

Figure 19a shows time series of global-mean surface air temperature for ERA5 from 1950 to 2020 and JRA-55 from 1958. It also shows corresponding global-mean surface temperatures from the GISTEMP (Lenssen *et al.* (2019)) and HadCRUT5 (Morice *et al.* (2020)) analyses of monthly climatological data, and indicates the spread of the values given by these data sets and additional monthly analyses from Berkeley Earth (Rohde and Hausfather (2020)) and NOAA GlobalTemp (Zhang *et al.* (2019)). Data sets were processed as described by Simmons *et al.* (2017). Comparison with ERA-Interim has been shown by Hersbach *et al.* (2020).

All data sets portray little trend in global-mean temperature from the 1950s to the second half of the 1970s, sustained warming thereafter and superimposed inter-annual variability. The values shown are in particularly good agreement from the early 1970s to the mid 2010s, although this comes in part simply from presenting the data as anomalies relative to 1981–2010. Differences among the monthly data sets in the 1950s and 1960s

12 month running mean surface temperature anomaly (K) relative to 1981–2010

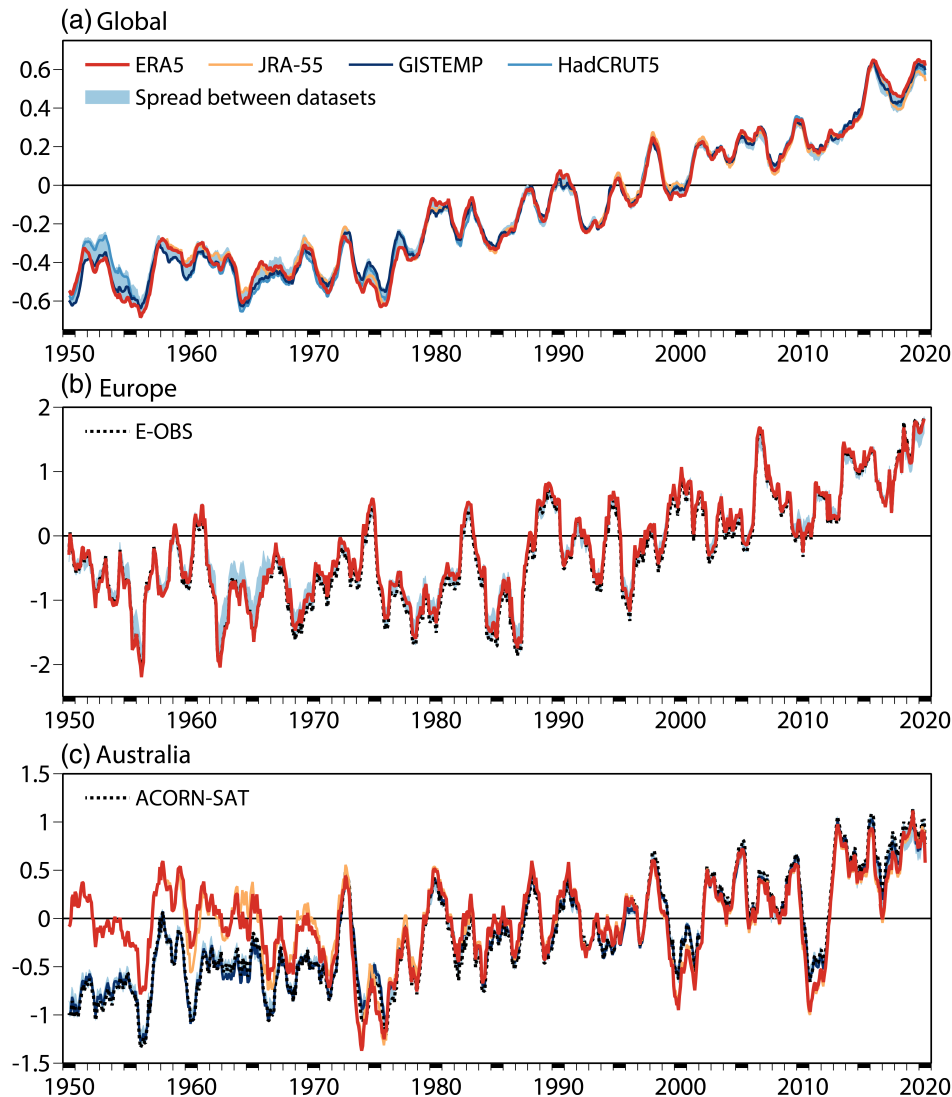


FIGURE 19 Twelve-month running-mean surface temperature anomaly (K) relative to 1981–2010, from 1950 to 2020: (a) global average, for ERA5, JRA-55, HadCRUT5 and GISTEMP, and the spread (pale-blue shading) among these data sets plus Berkeley Earth and NOAAGlobalTemp; (b) European average from ERA5 and E-OBSv21, and the spread (blue shading) between these data sets and the others used in (a); (c) Australian average from ERA5, JRA-55, GISTEMP and ACORN-SAT, and the spread (blue shading) between all data sets other than ERA5 and JRA-55. In (b), the averages for ERA5 and E-OBS are calculated using only grid points for which E-OBS has complete coverage in time. The ERA5 climate for 1981–2010 is used to calculate both the E-OBS and the ERA5 anomalies

stem largely from differences in SST analyses and differences over the Antarctic. There are also differences because the monthly data sets provide a mix of air temperatures over land and SST, whereas the reanalyses provide air temperatures everywhere; implications of this have been discussed by Cowtan *et al.* (2015) for climate modelling and Simmons *et al.* (2017) for reanalysis, among others. Using SST rather than marine air temperature raises ERA5's global-mean surface temperature by 0.05 K on average for 1950–1969. ERA5 temperatures are nevertheless expected to be on the low side in the global mean, by a few hundredths of a Kelvin from 1958 to 1966, and by closer to 0.1 K prior to 1958, because lower numbers of analysed observations over land result in a less effective correction of the cold bias of ERA5's background forecasts.

There is also some increase in spread among data sets after 2015. ERA5 has by a small margin the highest

temperatures relative to 1981–2010 for the latest years, partly due again to its provision of marine air temperature not SST. It does not, however, have the largest least-squares linear trend for 1979–2018. These trends, in K/decade, round to 0.19 for HadCRUT5, 0.18 for ERA5, Berkeley Earth, GISTEMP and JRA-55, and 0.17 for NOAAGlobalTemp. ERA5 does have the largest trend over the shorter 1991–2020 standard climatological reference period. Values in K/decade are 0.24 for ERA5, 0.23 for GISTEMP and HadCRUT5, and 0.21 for Berkeley Earth, JRA-55 and NOAAGlobalTemp in this case.

Figure 19b, c shows time series for Europe, defined as land from 20° W to 40° E and from 35° to 80° N, and Australia, land from 110° to 160° E and from 50° to 10° S. These are the two continental areas with respectively the best and worst long-term agreement among data sets, and for each there is a regional data set based directly on observations in addition to the global data sets: E-OBS

for Europe (Cornes *et al.* (2018), here version 21 at 0.25° resolution) and ACORN-SAT for Australia (Trewin (2013), here country-average version-2 values).

Surface air temperature has increased much more rapidly over Europe than globally over the past 35 years, following a slow decrease from the early 1950s to the mid 1980s. Conditions over Europe are observed and modelled well enough for all data sets to be in good agreement. ERA5 is also in good absolute agreement with E-OBS for these area-averaged temperatures; this is demonstrated in Figure 19b by using the ERA5 climate for 1981–2010 as the reference for defining both the ERA5 and the E-OBS anomalies. There is a little sensitivity to missing data values in E-OBS, as sampling ERA5 to match E-OBS data coverage, as done here, slightly increases recent values and slightly degrades agreement with the values derived without sampling from the other global data sets.

Conversely, results for Australia show pronounced differences between the reanalyses and the data sets based directly on monthly climatic data records. This is most marked prior to 1970, when ERA5 and JRA-55 have significantly higher temperatures relative to 1981–2010 than the other data sets. This appears not to be due simply to the sparse observations of surface air temperature analysed by ERA5 and JRA-55, nor to the way the surface analysis is carried out, as the background forecasts (not shown) from the two reanalyses are in even worse agreement with the other data sets prior to 1970: such surface air observations as are analysed bring the reanalyses somewhat closer to the other data sets, though by no means close enough. Further discussion is given in Section 6.

Although agreement over Australia is generally very much closer after 1970, there are periods in 2000/2001 and 2011/2012 when the reanalyses are distinctly colder than the other data sets, relative to climatology. This holds for ERA-Interim also. It also occurs, though for shorter periods of time, in 1973/1974 and 2016/2017. It will be seen in the following section that this happens when rainfall is above average, commonly linked with La Niña events. One factor is that the values from the reanalyses are averages over synoptic times, whereas the other data sets are based primarily on monthly records of the average of daily maximum and minimum temperatures. The relationship between the two types of average shifts when the underlying surface is moistened by heavy rainfall. Biases in the background forecasts of the reanalyses may also change in such circumstances.

ERA5 is prone to other regional blemishes, in particular where observations are few in number in the early years and analysis increments otherwise are generally large. This is the case, for example, over most of China, where the ERA5 analysis scheme normally reduces a relatively large cold bias of the background forecast. This does not happen

prior to August 1956, however, when ERA5 has access to few observations from the region, and again throughout 1965 and 1966 when no surface air temperature observations at all for the region (and indeed some other regions) are found in ERA5's input database. This is the case also for other types of observation for these years, as can be seen for surface pressure and 2 m relative humidity in Figure 4.

Monthly climatic extremes have temperature anomalies that are typically measured in several degrees, or even ten or more degrees at high latitudes. The representation of such extremes in reanalyses is little affected by the much smaller biases that may mar estimates of trends, but can nevertheless still be sensitive to observational coverage. Figure 20 presents just one example. It shows in panels a to d maps of anomalies in surface temperature for February 1956, chosen as it is from the early part of the reanalysis period and is the month with record cold average conditions over Europe, relative to the climatological normal for the month. Maps are for GISTEMP, HadCRUT5 and the ERA5 background and analysis. Panels e and f show the background and analysis departures for ERA5.

The maps of anomalies are in good agreement where each analysis has access to observations. All show the cold conditions over Europe, peaking over south-western Russia. Although not illustrated here, ERA5 shows that this was associated with anomalous easterly flow, with anticyclonic anomalies centred near Iceland and Novaya Zemlya, and relatively low pressure centred near Italy. Conditions were also colder than normal over much of Siberia, and it was also relatively cold over western North America. Consistent with the anomalous flow pattern, temperatures were not as low as usual for February over the far north of Siberia and over the seas to the north and west. Positive anomalies also occurred over eastern North America, Greenland, north-eastern Africa and the Middle East. Australia was relatively warm in the south and west, and cool in the north and east. The analyses differ in the magnitude of the warm conditions over the North Pacific and North Atlantic, and more substantially over the oceans of the Southern Hemisphere and the data-sparse Antarctic.

There are also differences between ERA5 and the other data sets with regard to the weak anomalies over Argentina and south-western Africa. Figure 20e, f shows that few or no observations in these regions were supplied to ERA5, and the ERA5 analysis carries over positive anomalies from its background forecasts that are indicated by neither GISTEMP nor HadCRUT5. GISTEMP and HadCRUT5 have access to monthly climatological data for some regions where ERA5 does not have access to historical synoptic observations, over South America in particular for this month. ERA5 also lacks observations

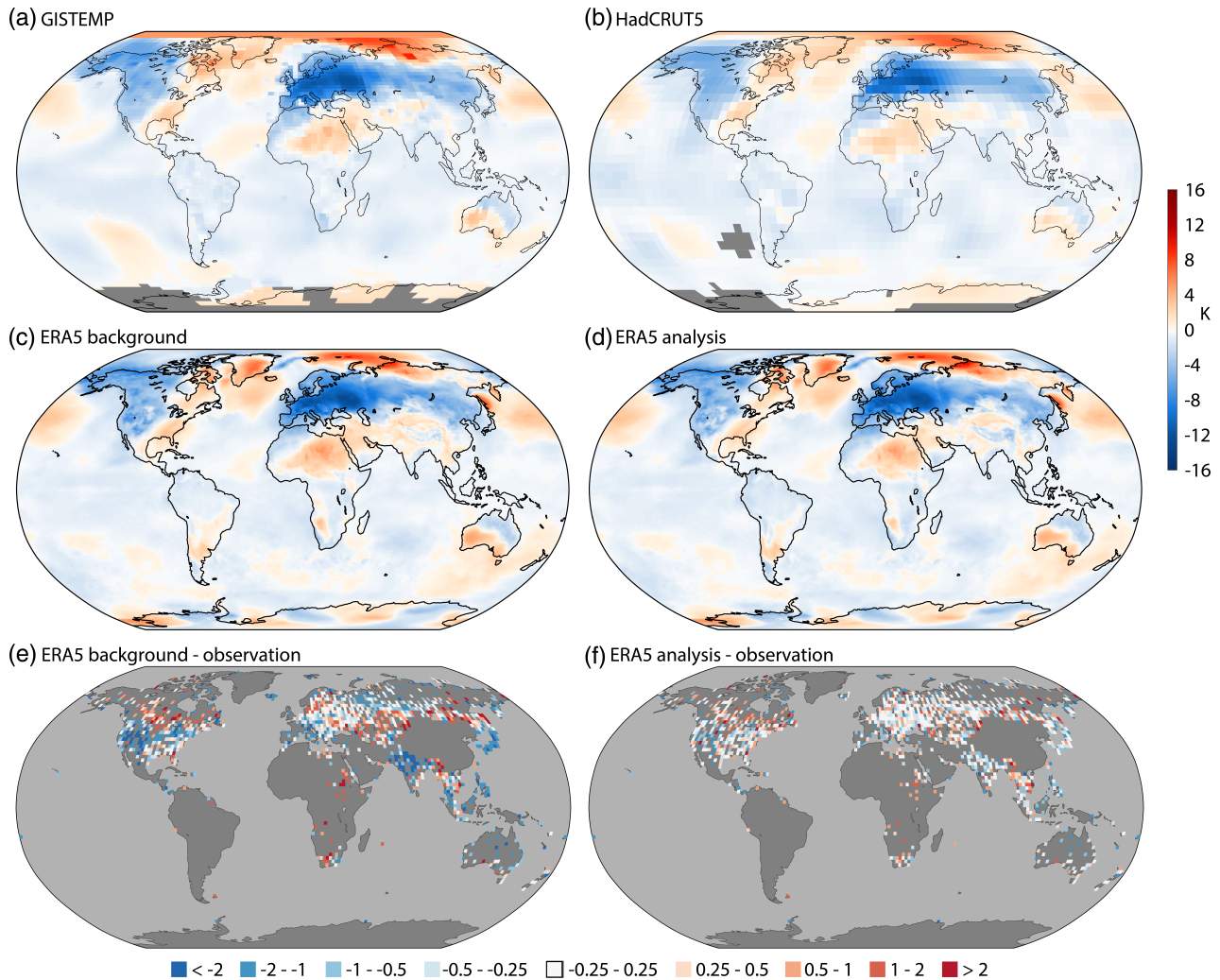


FIGURE 20 Average surface temperature anomalies (K) relative to 1981–2010 for February 1956: (a) GISTEMP, (b) HadCRUT5, (c) ERA5 background and (d) ERA5 analysis. Corresponding average (e) background–observation and (f) analysis–observation differences are shown for ERA5, based on values averaged over $2^\circ \times 2^\circ$ grid boxes that contain at least ten observations during the month. Values for GISTEMP and HadCRUT5 are plotted only for grid squares for which no more than two months are missing in the calculation of the 1981–2010 reference

over China at this time, as noted above, but anomalies there are relatively weak. The spatial extrapolation used by GISTEMP and HadCRUT5 produces a temperature anomaly in the vicinity of the North Pole that agrees poorly with the anomaly from ERA5. ERA5 is also alone in producing relatively low temperatures along the ice edge between Greenland and Svalbard.

Although the maps for the ERA5 background forecasts and analyses look similar at first sight, the analysis scheme for surface air temperature works as intended where observations are plentiful, significantly reducing biases in the background forecasts that reach up to 2 K or higher at some locations. This can be seen by comparing panels e and f over the western United States, northern India, and Japan, for example. The background bias is relatively small over Europe, however. Maps of this type for more recent times are discussed by Simmons *et al.* (2021).

5.2 | Precipitation

No direct measurement of precipitation is assimilated over the period of extension of ERA5 back to 1950, so the analysis of rain-gauge data provided by the Global Precipitation Climatology Centre (GPCC; Becker *et al.* (2013)) provides important independent data against which ERA5 may be judged. Comprehensive discussion of precipitation products is beyond the scope of this article, but by way of example, Figure 21 shows continental-average time series of running 12-month-mean precipitation rate, from ERA5, JRA-55, GPCC and (from 1979 onwards) version 2.3 of GPCP (Adler *et al.* (2003)). The figure extends and amends one (Supplementary Figure S6) presented by Hersbach *et al.* (2020). It extends back to 1950, and amends the earlier figure by replacing values from ERA-Interim by the precipitation rates taken from ERA5 in the forecast range from

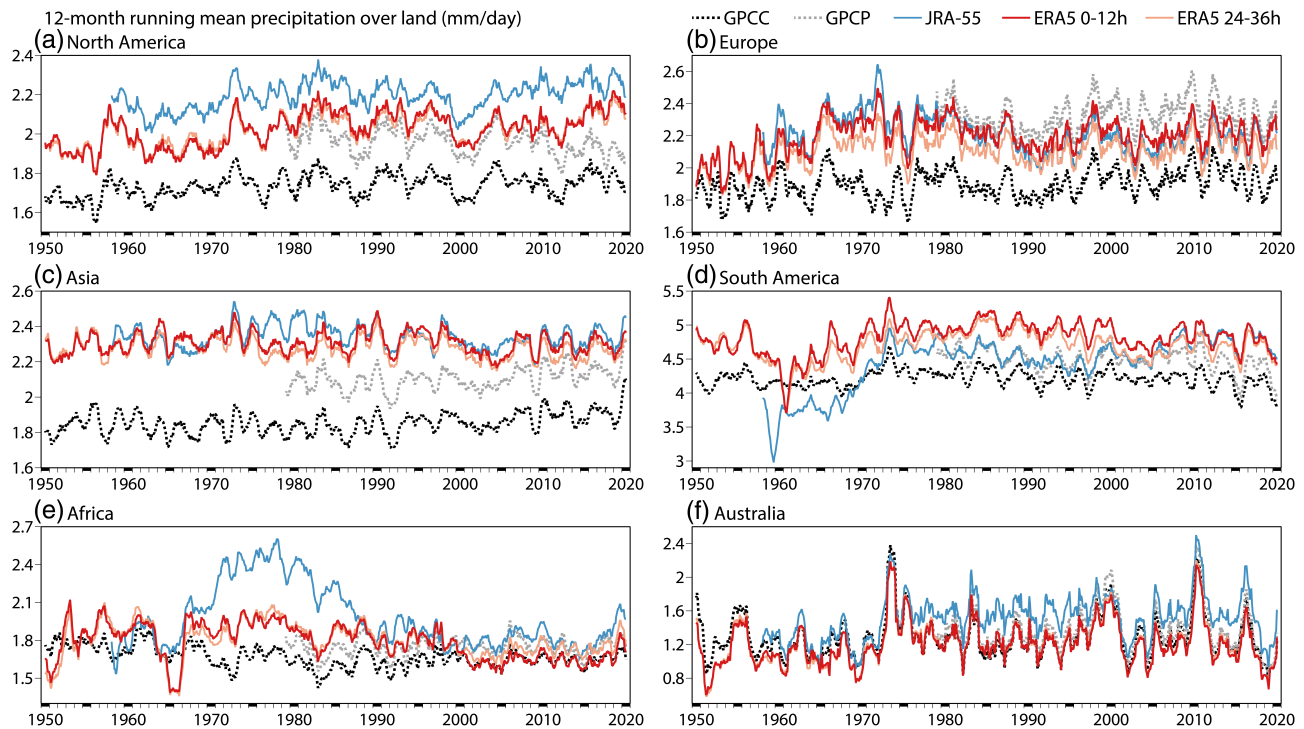


FIGURE 21 Twelve-month running means of monthly precipitation rates (mm/day) from 1950 to 2020 over land areas for (a) Europe (20° W to 40° E; 35° – 80° N), (b) North America (170° W to 50° W; 15° – 85° N), (c) Africa (25° W to 55° E; 40° S to 35° N), (d) South America (90° W to 25° W; 65° S to 15° N), (e) Asia (60° E to 180° E; 0° to 85° N) and (f) Australia (110° E to 160° E; 50° S to 10° S), for ERA5, JRA-55, GPCP and GPCP. ERA5 results are shown for both 0–12 hr and 24–36 hr forecasts

24 to 36 hrs ahead. It also uses newer, version 2020 GPCP products, the Full Data Monthly product for 1950–2019 and the Monitoring product for 2020, each at $1^{\circ} \times 1^{\circ}$ resolution. The standard ERA5 precipitation product is based on the precipitation from the first 12 hr of the forecast. The consistency between the 0–12 hr and 24–36 hr precipitation is an indication of the realism of the initial analysed structures, which depends on the amount and type of data assimilated, and of the realism of the assimilating model's representation of precipitation.

As noted by Hersbach *et al.* (2020), and earlier by Simmons *et al.* (2010) when assessing ERA-Interim, interpretation of mean differences between reanalyses and independent estimates of precipitation is complicated by differences between the independent estimates. This is particularly the case regarding long-term averages of precipitation, which in Figure 21 differ between GPCP and GPCP by amounts that can be as large in some regions as the differences between the reanalyses or between a particular reanalysis and either GPCP or GPCP. This is at least partly due in this case to the adjustments for gauge undercatch made in GPCP but not in GPCP. Aside from this, however, there is much that can be said about the variability over time of the differences between the various data sets.

In general, ERA5 provides overall precipitation amounts and inter-annual variability over land for the 1970s that are similar in quality to what it provides for the 1980s and 1990s. Behaviour further back in time varies from region to region:

1. Precipitation over North America from ERA5 varies quite similarly to that from GPCP back to 1950, both data sets exhibiting relatively low values from 1950 to 1957. Overall magnitudes differ, but there are differences of similar magnitude between GPCP and GPCP from 1979 onwards. ERA5 has slightly higher peak values. The largest discrepancy between ERA5 and the other data sets is in fact for the most recent years, when ERA5 shows an increase that is not seen in any of the other data sets. ERA5 also has relatively high values in the 1980s. There is little difference between the 0–12 hr and 24–36 hr ERA5 values over North America.
2. ERA5 performs more poorly over Europe. Its precipitation increases relative to GPCP's from 1950 to the late 1960s, remains quite substantially above GPCP's but below GPCP's until the 1990s, and then becomes closer to GPCP's. Inter-annual variability is higher for ERA5 than GPCP in the 1970s. Differences between ERA5's 0–12 hr and 24–36 hr rates are quite pronounced for Europe from the late 1960s onwards.

3. ERA5 produces quite uniform values over the large Asian region, and its inter-annual variability there is quite consistent with that of GPCC from the 1950s to the 1990s. It does not, however, show the increase in precipitation over the last 20 years or so indicated by GPCC and GPCP. In particular, it underestimates the high values for 2020 seen in GPCC and GPCP. The decrease in ERA5 precipitation from the 0–12 hr to 24–36 hr forecast range from the 1970s onwards is smaller than for Europe.
4. Precipitation over South America is more uniform over time for ERA5 than for JRA-55. ERA5 tracks GPCC quite closely for much of the period, but has relatively low values in the late 1950s and early 1960s, with especially low values in August and September 1961. Its 0–12 hr and 24–36 hr values are quite similar for parts of the period, but the 24–36 hr values are lower in the late 1960s and 1970s, and for around 20 years from the mid 1990s.
5. Hersbach *et al.* (2020) noted that precipitation over Africa from ERA5 declines around the turn of the century, becoming much closer to that from GPCC. This is seen here to be more so for the 0–12 hr than the 24–36 hr forecasts, indicating that a model bias for too strong rainfall is controlled by assimilating extra or different data that become available around the time the precipitation rate drops. The long-term level of African precipitation from ERA5 is quite steady prior to 1990, in contrast to that from JRA-55. It matches that from GPCC rather better in the 1950s and early 1960s, when values from GPCC but not ERA5 are higher than in later decades. ERA5 precipitation is particularly low from May to July in 1965 and 1966, and also low in 1951. Further discussion of this is given in Section 6.
6. The representation of precipitation is least problematic for Australia, in contrast to what has been seen for surface air temperature. Here, precipitation rates from GPCC and GPCP are closer than for the other regions considered, and ERA5 rates are quite close to GPCC rates from the 1960s onwards, though rather lower for the 1950s. ERA5 rates are insensitive to whether they come from the 0–12 hr or the 24–36 hr range. JRA-55 rates appear to be on the high side, more so from the late 1970s onwards. All data sets capture the heavy rainfall periods mentioned earlier and dry spells such as that experienced over the past 3 years.

Precipitation averaged over all sea (not shown) changes little from 1950 to the early 1990s, varying in the range from 3.0 to 3.2 mm/day, with hardly any net trend. The 0–12 hr precipitation subsequently increases, as illustrated by Hersbach *et al.* (2020), and reaches close

to 3.3 mm/day. The increase is distinctly smaller, to about 3.2 mm/day, in the 24–36 hr forecasts. This difference stems entirely from the tropics. Tropical 24–36 hr values are also lower than 0–12 hr values prior to the late 1970s. Precipitation over the extratropical oceans increases with increasing forecast range during this period, particularly in the Southern Hemisphere. Precipitation rises here by a few per cent between the 1950s and 1960s, and again after 1978. It is unclear how much of this is due to observing-system changes and how much is due to natural variability.

Hersbach *et al.* (2020) also showed that the imbalance between global-average precipitation and evaporation was about 0.11 mm/day for ERA5 in the early and mid 1980s, decreasing to reach much smaller values from the mid 1990s to the mid 2010s. Imbalance is also smaller in the 1950s and 1960s, when it is around 0.06 to 0.07 mm/day.

Maps indicating how well inter-monthly variability is represented are shown in Figure 22. The figure compares measures of the agreement between ERA5 and GPCC, and between JRA-55 and GPCC, for two periods: 1958–1978 and 1979–2020. Correlations are shown for both periods and standard deviations for 1979–2020. They were evaluated using the version 2020 GPCC products with 2.5° resolution in this case, to enable the 1.25° JRA-55 fields to be averaged onto the GPCC grid. Comparisons of ERA5 with the 1° GPCC product show similar geographical variations but somewhat poorer overall agreement. Although the GPCC values are viewed as generally more reliable than the values from reanalyses, this may not be the case at high northern latitudes where observations are sparse and frozen precipitation is difficult to measure. The GPCC products do not include values for Antarctica.

Geographical variations are similar for each of the periods, reanalyses and statistics shown in Figure 22. Agreement with GPCC is generally best over Europe, close over much of the United States and Australia and more moderate over mid-latitude Asia, northern and southern parts of Africa, central Chile and the east of South America southwards from the Nordeste Region of Brazil. It is poorest over much of tropical South America and Central Africa. The dry north-east of Africa has low standard deviations, as expected, but also low correlations.

Agreement with GPCC is poorer for the less well-observed 1958–1978 period than for 1979–2020, though not substantially so. It is better for the newer ERA5 reanalysis than for JRA-55, whose performance is more akin to that of ERA-Interim (not shown), though better in places. In broad terms, ERA5 is about as close to GPCC for 1958–1978 as JRA-55 is to GPCC for 1979–2020. Maps of standard deviations for 1958–1978 (not shown) confirm the conclusions drawn from the maps of correlations.

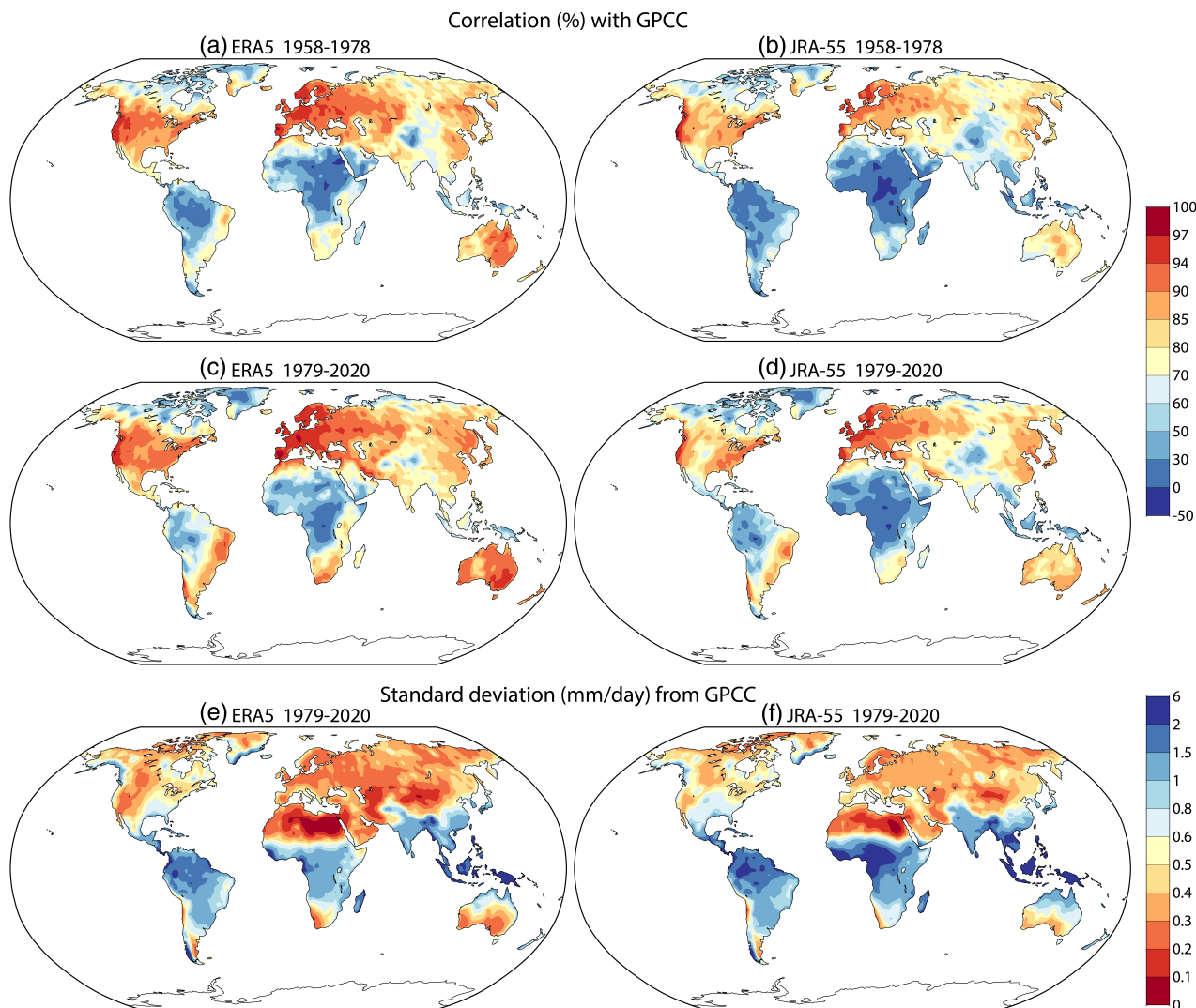


FIGURE 22 Spatial variation of correlations (%) and standard deviations (mm/day) between monthly-mean reanalysis and GPCP precipitation rates at 2.5° resolution. Correlations are shown for (a) ERA5 1958–1978, (b) JRA-55 1958–1978, (c) ERA5 1979–2020 and (d) JRA-55 1979–2020. Standard deviations are for (e) ERA5 1979–2020 and (f) JRA-55 1979–2020. The mean annual cycle for the period in question is removed from each data set prior to calculating the correlations

5.3 | Mass

Statistics on global mass provide clear-cut evidence of improvement over time in the quality of surface pressure and humidity analyses. The global mass of dry air is estimated from the global-mean surface pressure by subtracting the contribution from the water content of the atmosphere. It should be almost constant, varying only because of numerically small (though radiatively important) changes in atmospheric composition. Trenberth and Smith (2005) estimated a change of surface pressure of less than 1 Pa from the increase in carbon dioxide and related changes in oxygen content over the industrial period. Hersbach *et al.* (2020) showed in contrast changes over time and inter-reanalysis differences of a few tenths of an hPa in estimates of dry mass

from ERA5 and ERA-Interim for the period from 1979 onwards.

Trenberth and Smith (2005) had earlier examined how well ERA-40 conserved dry mass. ERA-40 was shown to have performed much more poorly prior to the early 1970s than it did subsequently. Month-to-month changes were at times higher than 1 hPa. There was also a net decadal-mean drop of 0.35 hPa from the 1960s to the 1980s, which was found by Uppala *et al.* (2005) to be associated with higher analysed surface pressure, particularly over the data-sparse oceans of the Southern Hemisphere, and with lower analysed water vapour prior to assimilation of IR soundings, which began in 1973 using VTPR data.

Figure 23 presents the monthly dry-mass estimates from ERA-40 along with estimates from the newer JRA-55 and ERA5 reanalyses, for the period from the 1950s to

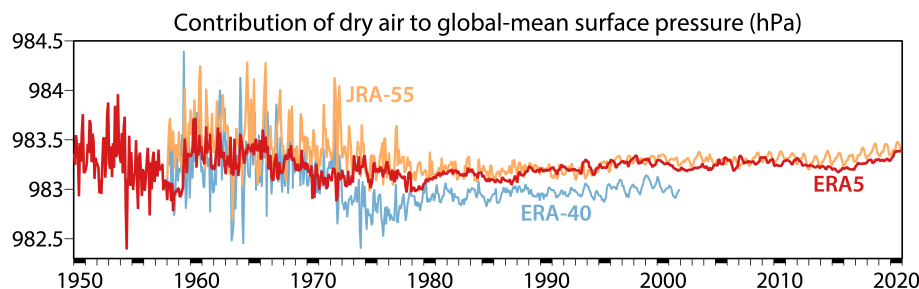


FIGURE 23 Monthly-mean estimates from 1950 to 2020 of the contribution of dry air to the global-mean surface pressure (hPa) from ERA5 (red). Values are also shown for ERA-40 (1958–2001; blue) and JRA-55 (from 1958; orange)

the present day. ERA5 clearly improves on the other two reanalyses prior to the 1980s, with generally smaller month-to-month variations and less of a long-term shift. The decadal-mean mass falls from the 1960s to the 1980s by 0.33 hPa for JRA-55 and 0.11 hPa for ERA5. The standard deviations of the monthly values for the 1960s are 0.31 hPa for ERA-40, 0.28 hPa for JRA-55 and 0.25 hPa for ERA5.

Changes in dry mass have also been examined for the hourly ERA5 analyses. These analyses are in fact the hourly outputs of 12-hr forecasts run twice per day from the initial states for 0900 and 2100 UTC, which are the times for which the 4D-Var analysis provides increments that are estimated to make the forecasts optimally fit the observations over the next 12 hr. Non-conservation of dry mass arises mainly from the changes that occur between hour twelve of one forecast and hour one of the subsequent forecast, that is, for 0900–1000 UTC and 2100–2200 UTC each day. Dry mass is also not formally conserved by the forecast model, but the change due to this is generally smaller. The mean absolute change due to non-conservation by the model for 1950–2020 is 0.005 hPa for the 1000–2100 UTC and 2200–0900 UTC differences. The mean absolute change for the 0900–1000 UTC and 2100–2200 UTC differences evaluated for each of the seven decades of ERA5 decreases monotonically over time, from 0.114 hPa for the 1950s and 0.084 hPa for the 1960s to 0.018 hPa for the 2000s and 2010s. The analysis scheme is thus seen to disturb dry-mass conservation least for the recent years for which plentiful observations are assimilated and background forecast errors are relatively low. The smaller numbers and larger errors of observations for the early decades cause greater disturbance, as they lead to large changes to relatively inaccurate background values.

Particular attention has been paid to the mass changes around the middle of 1959, in view of a suggestion that the sharp rise in mass for ERA5 at that time stems from the change in production stream at the beginning of July. This change is not seen to be the primary cause, however, as the period from late May to early July is characterized by several relatively large increments in mass. The monthly average ERA5 dry mass increases by 0.28 hPa between May

and June, and by 0.22 hPa between June and July. The monthly average ERA-40 dry mass increases by almost 0.93 hPa between May and June, and falls by 1.15 hPa from June to July.

5.4 | Upper air

Figure 24 shows the evolution of monthly and globally averaged anomalies in temperature, ozone partial pressure and specific humidity during the entire period covered by ERA5. Anomalies are calculated relative to the monthly climate of ERA5 during the period 1981–2010. Figure 24 allows us to compare the trends and anomalies evident in ERA5^{79→} with those observed in ERA5^{79→}.

For temperature, ERA5^{79→} shows a warming/cooling trend in the troposphere/mid-lower stratosphere, qualitatively consistent with that exhibited in ERA5^{79→}. The stratospheric cooling is punctuated by transient periods of warming associated with the eruptions of Agung in 1963, El Chichón in 1982 and Pinatubo in 1991. The transition from cold tropospheric anomalies to warm stratospheric anomalies occurs at lower levels in ERA5^{79→} (at around 150 hPa) than in ERA5^{79→} (warm tropospheric anomalies to cold stratospheric anomalies after 2000, around 100 hPa). Above 10 hPa, large anomalies are evident in ERA5^{79→}, although the form and magnitude of the anomalies during the period 1973–1978, when channel 1 of VTPR provides information on stratospheric temperatures in the layer from 2 to 20 hPa, are broadly similar to those prior to 1973. After January 1979, the observing system changes significantly following the introduction of observations from the first TOVS satellite, including observations from the Stratospheric Sounding Unit (SSU). Associated with this, the climatological component of the background error covariance also changes in January 1979 (see Section 3.6). Consequently, the form of the temperature anomalies changes at this time. The most prominent anomaly in temperature above 10 hPa around this time is the warm anomaly evident from 1979 to 1984, most probably associated with the assimilation of SSU channel 3 observations which are assimilated without bias correction to anchor the analysis and are known to suffer

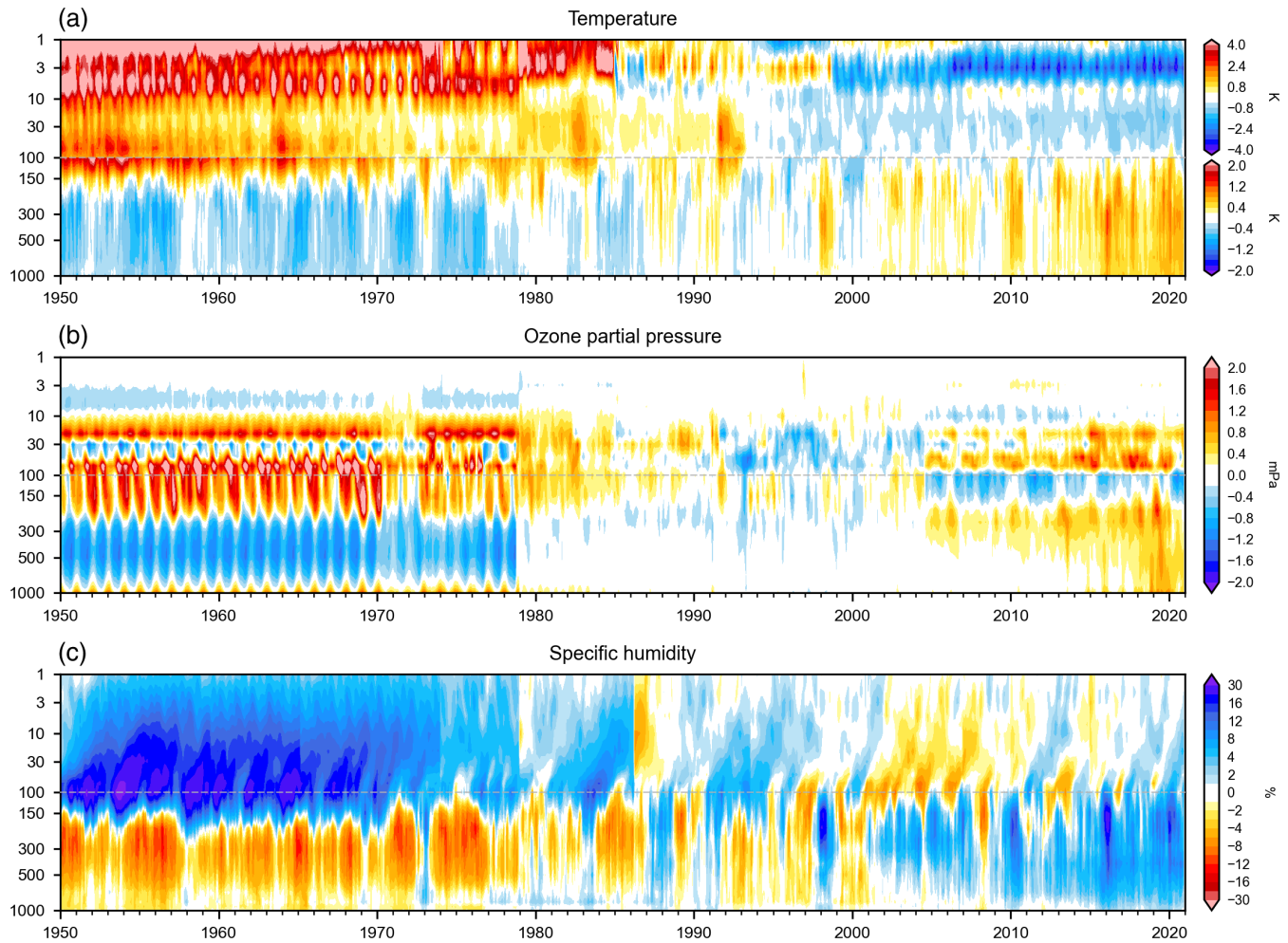


FIGURE 24 ERA5 monthly and globally averaged upper-air anomalies with respect to the 1981–2010 monthly climatology for (a) temperature, (b) ozone partial pressure and (c) specific humidity during the period 1950–2020. The period from January 2000 to December 2006 is based on ERA5.1. Anomalies for specific humidity are shown in per cent of the 1981–2010 monthly climatology. For temperature, note the different colour scales used above and below 100 hPa

from complex biases related to cell pressure leaks (see Hersbach *et al.* (2020)). Although improvements were made to the treatment of the cell pressure leak effects, through improved radiative transfer modelling, it is probable that residual biases remain which cause the anomalies observed. It is noteworthy that, in ERA5^{79–80}, the vertical structure and magnitude of the anomalies above 10 hPa remain very similar to those of ERA5⁷⁹ during 1973–1978 (not shown). This further highlights the prominent impact of the change in \mathbf{B}_{cli} in January 1979 on temperature anomalies and analysis increments at these levels in ERA5⁷⁹.

For specific humidity, the anomalies in ERA5⁷⁹ show a gradual moistening of the troposphere and drying of the stratosphere, related to the observed cooling. Due to the long spin-up timescales for stratospheric water vapour, often several years, seams were evident between the original production streams. Examples of this can

be seen between ERA5⁷⁹ and ERA5⁷⁹ in 1979 and in ERA5⁷⁹ in 1987. To reduce the magnitude of the associated steps in ERA5⁷⁹ time series, the final consolidated product was obtained by allowing some streams to run for longer than originally planned, to maximise spin-up times. The resulting selection of the production streams is described in Section 2. As a note, due to the longer spin-up of stratospheric water vapour in ERA5^{79–80} compared with ERA5⁷⁹, ERA5^{79–80} exhibits a seamless transition with ERA5⁷⁹ in January 1979 (not shown).

Prior to 1979, observations of ozone were limited to those from BUV. The impact of the assimilation of BUV observations (Section 3.5.2), available in large numbers from January 1970 to July 1972, is evident, as is the effect of the reduced coverage of BUV data after 1972, where the anomalies relax to the form of those for the period 1950–1970.

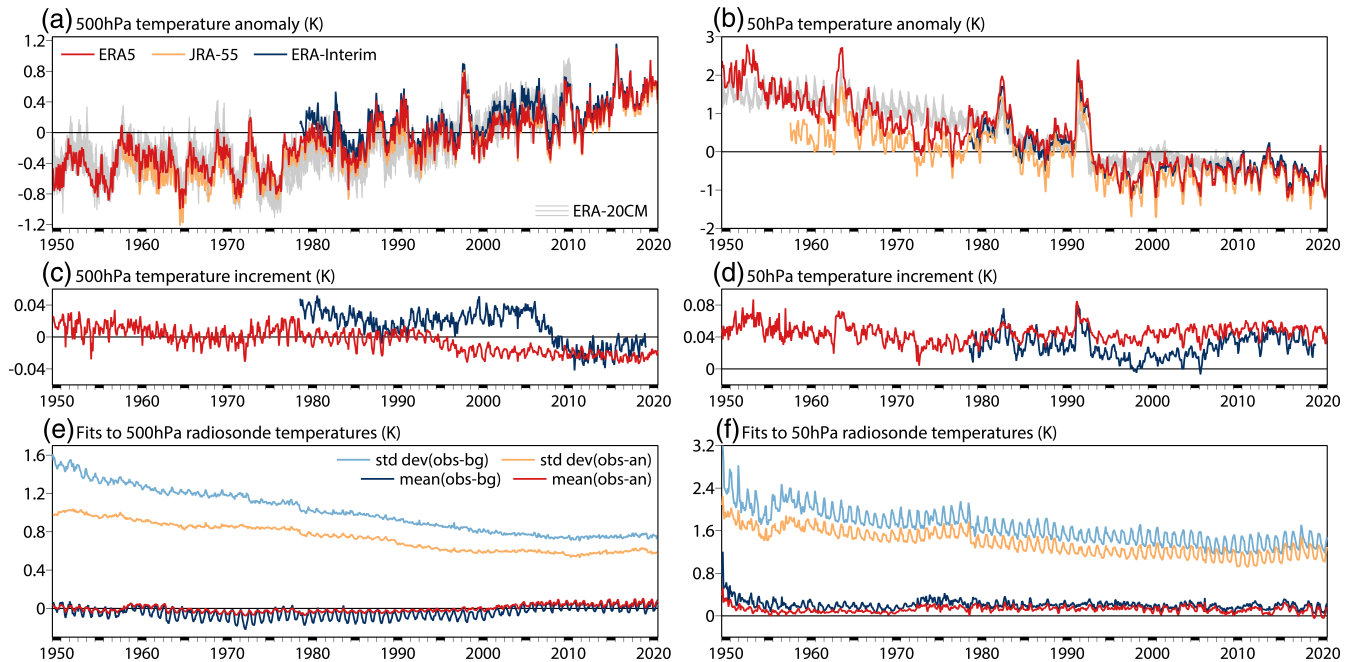


FIGURE 25 Time series from 1950 to 2020 of monthly-mean quantities related to global-mean temperature (K) at 500 hPa (left) and 50 hPa (right): (a, b) anomalies of ERA5, JRA-55 and ERA-Interim relative to the ERA5 climate for 1981–2010, and anomalies of the ERA-20CM ensemble members relative to the ERA-20CM ensemble-mean climate for 1981–2010; (c, d) analysis increments, for ERA5 and ERA-Interim; (e, f) standard deviations and means over all assimilated radiosonde observations of the ERA5 background and analysis departures from these data

Further detail for global-mean temperature at the 500 and 50 hPa levels is given in Figure 25. Panels a and b show anomalies of monthly values relative to the climate of the month for 1981–2010. Results for three reanalyses, viz. ERA5, JRA-55 and ERA-Interim, are shown relative to the ERA5 climatology in order to indicate the absolute differences in temperature between these reanalyses. These differences are generally small, at most a degree or so for the differences at 50 hPa between ERA5 and JRA-55 for the late 1950s and early 1960s. Panels a and b also show plots of the anomalies of the ten ensemble members of the ERA-20CM model simulations (Hersbach *et al.* (2015a)) carried out using similar (but not identical) versions of the ECMWF model and prescribed HadISST2 sea surface temperatures and sea ice concentrations. In this case, the climatological references are the monthly 1981–2010 averages of the ERA-20CM ensemble mean, as differences in climatological temperatures between the simulations and reanalyses are relatively large, at between 0.9 and 1.2 K depending on month for 500 hPa.

The other panels of Figure 25 show the monthly mean analysis increments (the analysis–background differences) for ERA5 and ERA-Interim and the means and standard deviations of the ERA5 background and analysis departures computed for all assimilated radiosonde observations at the 500 and 50 hPa levels.

ERA5 and JRA-55 temperatures are quite close for much of the period at 500 hPa, but JRA-55 has a least-squares-fit warming trend from 1981 to 2020 that is about 9% larger than that of ERA5, in contrast to its 5% smaller trend in surface air temperature (see Figure 19). This is equivalent to a 500 hPa temperature increase that is 0.06 K larger for JRA-55 than for ERA5 over the 40-year period. Trends at 500 hPa are in both cases smaller than trends in surface air temperature, by 97% for JRA-55 and 85% for ERA5. The two reanalyses give similar sharp peaks associated with El Niño events. Differences in 500 hPa temperature are larger in the more poorly observed 1950s and 1960s, typically ranging from 0.1 to 0.3 K from month to month, with ERA5 warmer than JRA-55. ERA5 generally lies within the range of the ERA-20CM ensemble. Together with the small mean analysis increments and close mean fit of the ERA5 analyses to the 500 hPa radiosonde data seen in panels c and e, this gives some confidence in the global-mean temperatures provided by the extension of ERA5 back to 1950. This is notwithstanding the larger standard deviations of the background and analysis departures, which point to some degradation of general analysis quality due to the poorer data coverage and quality of earlier years.

ERA5 and JRA-55 differ more from ERA-Interim than they do from each other at 500 hPa, in spells from 1979 to the late 1980s and in the 2000s. ERA-Interim is relatively

warm during both spells. This is consistent with a conclusion of Simmons *et al.* (2014) that ERA-Interim somewhat underestimates warming in the lower and middle troposphere.

Differences between ERA5 and JRA-55 are larger at 50 hPa. Here, temperatures decrease over time until the late 1990s, and are steady or slightly declining thereafter. The warm peaks associated with the 1962, 1982 and 1991 volcanic eruptions are prominent. The reanalyses are in close agreement from 2006 onwards, when plentiful radio occultation data from the COSMIC (and later other) receivers were assimilated, as has been discussed for a wider range of analyses and levels (Simmons *et al.* (2014); Ho *et al.* (2019)). JRA-55 is colder than ERA5 earlier in the 2000s, and more so back in time, especially in the late 1950s and early 1960s. The higher cooling rate from the 1950s to the 1990s in ERA5 is broadly consistent with the cooling rate in the ERA-20CM model runs, but temperature anomalies in the 1970s are lower for both ERA5 and JRA-55 than for ERA-20CM. This is especially so in late 1972 and much of 1973.

The 50 hPa ERA5 analysis increments are reasonably uniform over time at around 0.04 K, as the data assimilation adjusts for a cold lower-stratospheric bias of the assimilating model. They are larger at the times of the major volcanic eruptions, including Agung in the pre-satellite era, compensating for the model's underestimation of the effect of volcanic aerosol. They drop, however, to low values in late 1972 and early 1973, when the analysed temperature is lower than in neighbouring years. Radiosonde data are fitted well in the mean, with a small shift once radiance data begin to be assimilated at the end of 1972. The mean departures do not appear to be especially problematic in 1972 and 1973, but it has to be kept in mind that vast oceanic areas, particularly in the Southern Hemisphere, are not sampled by radiosondes. There thus remains a question mark over the performance of ERA5 for this period, as there is also for the early 1950s, when data numbers are low and mean departures are relatively large.

The standard deviations of the departures from radiosonde data decrease over time until 2010, with a distinct fall when VTPR begin to be assimilated at the end of 1972 and a larger fall due to the major observing-system changes between 1978 and 1979. The overlap analysis ERA5^{79–80} is very similar to ERA5^{79→} in this regard. After 2010, the fits of the ERA5 background forecasts and analyses to radiosonde data increase slightly, more so for the analysis than for the background. The standard deviations of the analysis departures for this period are similar to the prescribed observation errors for radiosonde temperatures used in the ERA5 data analysis, which are 0.61 K at 500 hPa and 1.28 K at 50 hPa. Although these values imply a limit to what may be inferred from such departure statistics,

the departures nevertheless still distinguish between the background forecasts and the analyses.

The behaviour shown may thus indicate that the information from radiosonde observations is not getting quite the weight in data assimilation that it merits in the presence of increasing amounts of satellite data. An alternative explanation is that the increase in the departure variances results from a change in correlations between background errors and observation errors. Further investigation is required to resolve this question.

5.5 | QBO

The establishment of routine radiosonde observations of wind in the tropical stratosphere in the 1950s led to the discovery by Ebdon (1960) and Reed *et al.* (1961) of the QBO, in which successive phases of easterly and westerly zonal winds propagate downwards in a cycle that has an average period of a little over 2 years. These observations have now been assimilated in ERA5^{→79}.

Figure 26 presents information related to the performance of ERA5 in representing the QBO at 30 hPa, based on monthly values averaged over the equatorial belt from 10° S to 10° N, back to 1950. Similar results are found for neighbouring standard pressure levels. Panel a shows the increase over time in the number of 30 hPa wind observations in the equatorial belt that were assimilated by ERA5. No such observations at all were assimilated for six of the months of 1950. Observations were used in every month from December 1950 onwards, and statistics related to them are included in Figure 26, even though there are fewer than ten observations for two months in 1951 and one in 1952. Observation numbers increase during the 1950s and 1960s, are relatively steady for most of the next three decades and increase again between 2000 and 2015. Spikes in numbers in 1974 and 1979 are consequences of special efforts made during the tropical-Atlantic and global observing experiments of the Global Atmospheric Research Programme.

Figure 26b shows the QBO as described by a simple averaging of all zonal-wind observations made in each month. The averages of corresponding co-located analysed winds from ERA5 are also shown. The amplitude of the wind oscillation at this level is about 40 m/s from peak westerly to peak easterly, whereas monthly-mean differences between observations and analyses, the analysis departures, vary from -2 to 2 m/s. The latter is shown explicitly in panel c, which also shows the differences between the observations and the ERA5 background forecasts, the background departures. The latter are distinctly larger, showing that the reanalysis is drawing well towards the observations.

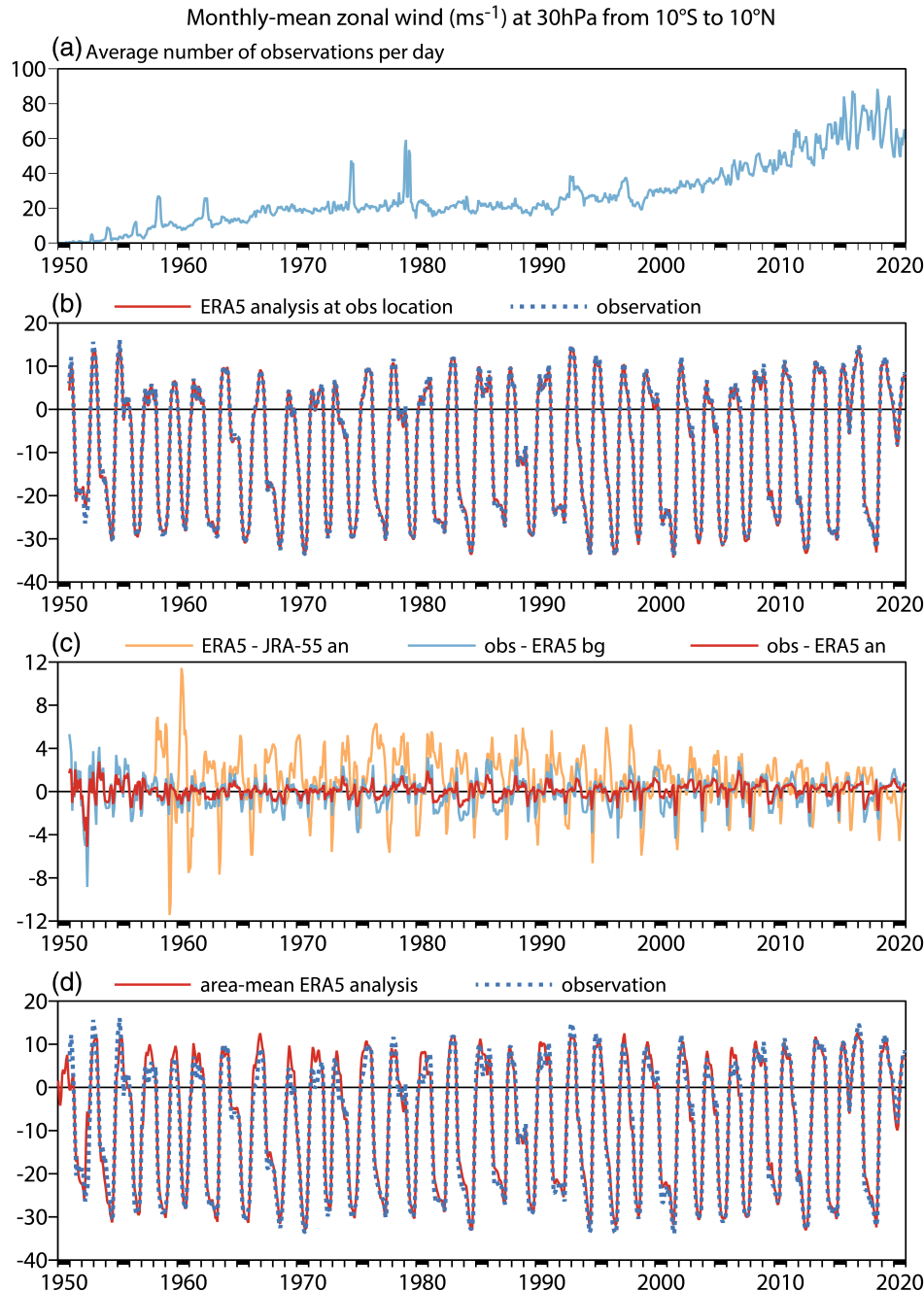


FIGURE 26 Averages over the tropical belt from 10°S to 10°N for each month from 1950 to 2020: (a) number of zonal-wind observations assimilated per day, (b) zonal-wind observations and co-located ERA5 analysis values, (c) corresponding ERA5 background and analysis departures, and the mean difference between JRA-55 and ERA5 zonal-wind analyses averaged over the area and (d) zonal-wind observations and area-mean ERA5 zonal-wind analyses. Observational averages and corresponding analysis values and departures are plotted only for the period of continuous monthly data coverage, from December 1950 onwards. Units: m/s

Both the background and the analysis departures are relatively large in the data-sparse early-to-mid 1950s, but relatively small from the late 1950s to the early 1970s, when only radiosonde data are assimilated in the stratosphere, aside from BUV ozone data from 1970. Departures then become larger, presumably because of the influence on winds of the multi-variate analysis of radiance data from the VTPR and TOVS satellites. Departures decrease in amplitude towards the end of the period, when they benefit from assimilation of temperature-sensitive data from GNSS radio occultation (Healy *et al.* (2020)), and perhaps also from improved radiance measurements and the increase in radiosonde numbers.

Panel c also shows monthly mean differences between the JRA-55 and ERA5 analyses of zonal wind, averaged over the equatorial belt. For much of the period, these differences are substantially larger than the average ERA5 departures. This is unlikely to be due simply to differences in sampling of the equatorial belt in forming averages, as differences between the ERA5 averages taken over the whole equatorial belt and only at observation locations (discussed in the next paragraph) are generally smaller than the differences shown between JRA-55 and ERA5. Consistent with what was found by Kawatani *et al.* (2016) in comparing JRA-55 with other reanalyses, the differences between JRA-55 and ERA5 decrease around the

year 2000, which is likely associated with the gradual introduction of data from the ATOVS suite of sounding instruments. Differences decrease further in later years, presumably due to the same changes in observing systems that lead to smaller background and analysis departures in ERA5.

Panel d is similar to panel b, but instead of showing averages of only those ERA5 winds that are co-located with observations, it shows average ERA5 winds for the whole equatorial belt. It is not surprising that agreement between analysis and observation is better when only co-located analysis values are used, but there is nevertheless reasonable agreement between the observational average for each month and the corresponding ERA5 average for the whole equatorial belt. ERA5 fits the observations quite closely, but maintains a high degree of zonal uniformity close to the Equator.

Discussion of Figure 26 would be incomplete without noting that panels b and d show that the QBO, for the second cycle in succession, has experienced disruption of its downward propagation, as discussed by Newman *et al.* (2016) for the 2015/16 event and Anstey *et al.* (2020) for the latest event. Nothing as extreme occurs in any of the other cycles analysed by ERA5. At 30 hPa, the disruption is characterised by unusually long spells of either westerly or atypically weak easterly flow. Figure 26 shows that 29 spells with monthly-mean observed zonal winds greater than -15 m/s have occurred since 1951. The latest of these spells had lasted 27 months by the end of 2020, as illustrated in the figure, and 32 months at the time of writing. The preceding one lasted 25 months. The other 27 spells varied in duration from 12 to 22 months; 18 of them lasted 15–17 months.

6 | SUB-OPTIMAL ASPECTS

As shown in Section 3.4, the configuration used for the assimilation of IBTrACS tropical cyclone bogus observations resulted in analyses of these events which were frequently sub-optimal. Specifically, the bypassing of quality control checks, based on first-guess departures, as well as a choice of observation error (0.78 hPa) which gave too much weight to these observations resulted in analysed tropical cyclones which were often too deep. Associated with this, wind speeds in the vicinity of such cyclones are erroneously large. Evidently, this has a knock-on effect on the statistics of ocean wave heights. Ocean waves essentially integrate the effect of wind on the ocean surface, and propagate over large distances, thus providing a good measure of how the impact of the anomalously intense tropical cyclones spreads over larger regions. The effect on ocean waves can be seen by inspecting the statistical distribution

of significant wave height (SWH, Supplementary Figures S11 and S12), particularly the upper tail of the frequency distribution. Higher 99th percentile values are evident in ERA5^{79→}, relative to ERA5^{79→}, in the ocean basins where tropical cyclones occur most frequently, namely the western North Atlantic, the western South Indian Ocean and the western North Pacific. Differences in the 90th and 95th percentile (not shown) values are much smaller. This suggests that the impact of the IBTrACS observations on ocean waves becomes apparent only for the very upper tail of the distribution of SWH (99th percentile and above).

Initial experiments in which quality control checks are reinstated, and the observation error for the IBTrACS observations is adjusted (to 2.0 hPa, from 0.78 hPa), results in a representation of tropical cyclones in much better agreement with that in ERA5^{79→}. This new configuration is used to re-run the entire ERA5^{79→} period. This updated product is currently being produced.

Several instances of relatively high temperatures and low precipitation that are not seen in independent data sets have been found in ERA5 analyses for the 1950s and 1960s. One occurs for the whole of the period in the averages over Australia shown for temperature in Figure 19(c) and precipitation in Figure 21(f). The other main instances are smaller scale and more intense: over and to the south of the Congo Basin in the early 1950s, over the Amazon Basin in 1961 and over a zone from Nigeria to Ethiopia in 1965 and 1966. Illustrations for these regions can be found in Simmons *et al.* (2021). Minima in continental-average precipitation for these cases have been noted in the earlier discussion of Figure 21d, e. Temperature anomalies during these periods average 2–4 °C over substantial parts of the regions concerned. Observational coverage is lacking in the 1965/66 case and over Brazil in 1961. Background temperatures are biased high compared with observations over the Congo Basin in the early 1950s, where relatively high analysed temperatures occur despite cooling analysis increments.

As discussed by Simmons *et al.* (2021), the ERA5^{79→} analyses of surface air temperature and humidity over Australia suffer because there was little enhancement of the small number of screen-level observations prior to 1977 processed for ERA-40. Moreover, when observations are more abundant, the ERA5 LDAS performs less well over Australia than elsewhere due to the preponderance of Australian observations made at non-standard synoptic hours. Although there are some quite straightforward steps that can be taken to address these issues in the future, their impact on long-term variations is relatively small after 1970 due to the quality of the background forecasts over the region.

Before 1970, the analysed surface air temperatures over Australia have a substantial warm bias, as judged

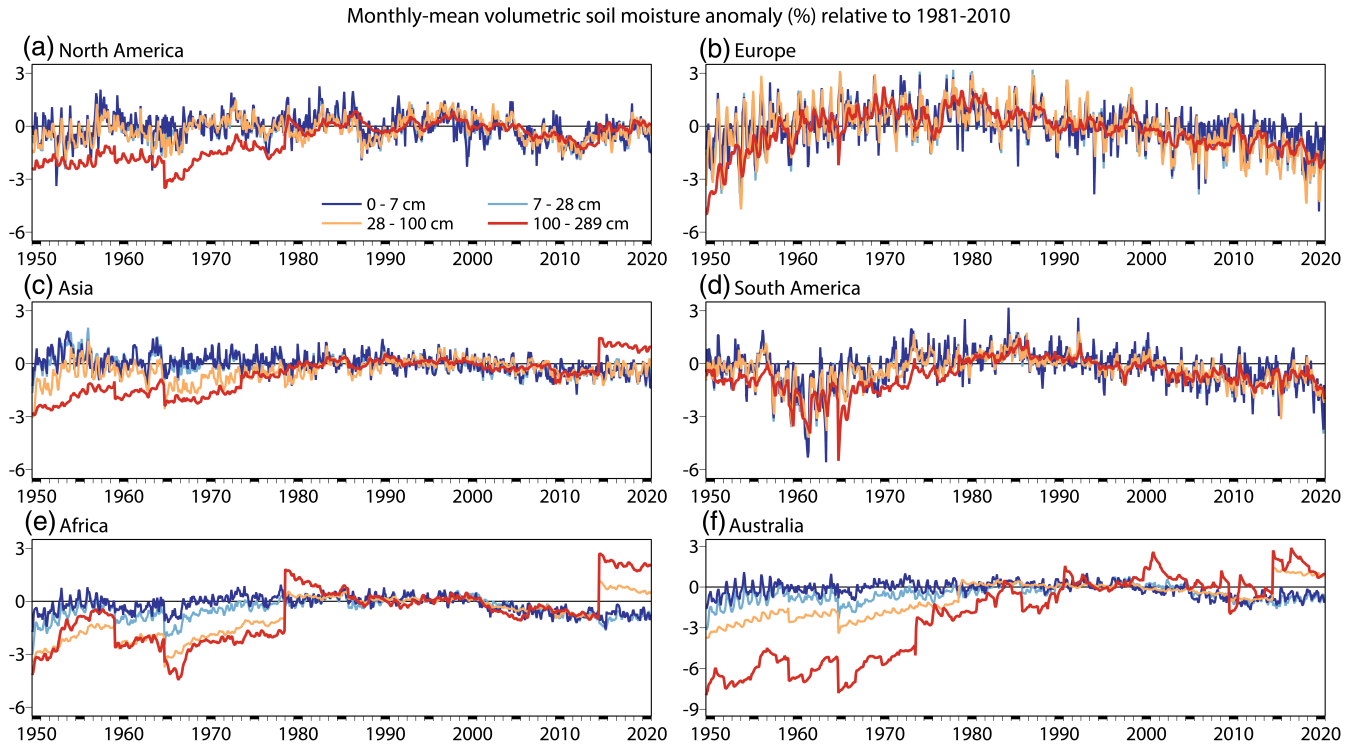


FIGURE 27 Monthly-mean volumetric soil moisture anomalies (%) relative to 1981–2020 for the four layers of the ERA5 land-surface model, averaged over the continental areas defined in the caption of Figure 21, from 1950 to 2020. The depths of the layers are shown in the legend

by comparison with conventional climatological data sets. The corresponding background temperatures are similarly biased, and may well have damaged the quality of the analyses even if a more comprehensive set of screen-level observations had been analysed. The reason for this behaviour remains to be fully understood, but several factors have been identified. The ERA5⁷⁹ 4D-Var data assimilation tend to cool and moisten the lower troposphere over Australia, but less so in the 1950s and 1960s than later. No radiosonde humidity data were assimilated before late August 1957, and the data assimilated for the next 10 years or so did not substantially reduce the dry bias of the background forecast. Cloud cover is also found to be lower in the 1950s and 1960s than in the following decades.

A further issue that relates to the periods and locations of excessive warmth and dryness seen in ERA5⁷⁹ concerns the initialization of soil moisture, particularly for the lower layers of the ERA5 land-surface model. Figure 27 presents the volumetric water content anomalies of each of the four modelled soil layers, averaged over continental regions. It shows that the ERA5⁷⁹ production streams were generally started with water contents that were much lower than those typical of ERA5⁷⁹. The response is a moistening (or spin-up) that is generally slower for the deeper layers, on a timescale that

varies from continent to continent. Sharp changes occur when the production streams change, something that also happened in ERA5⁷⁹ production at the beginning of 2015. The problem is least marked for Europe, which appears affected mainly in the early to mid 1950s. It is most marked for the deepest soil layer for Australia, and the deepest two layers for Africa. The uppermost layer shows little problem in general, but its soil moisture is relatively low for Africa in 1965 and 1966, when the start of a new production stream coincides with deficient observational cover. The near-surface soil moisture is also lower than the 1981–2010 average in the 1950s and 1960s over Australia and from 1950 to 1952 over Africa.

Although the too-warm periods over Africa and Australia might be due to or exacerbated by the dryness of the deep soil, the situation is different for South America. Here there are pronounced minima in the moisture of the deepest soil layer associated with the changes in production stream in 1959 and 1965, but they are short-lived, and the minimum in 1961 is larger for the topmost layer than the deep layer, suggesting that the behaviour of soil moisture is more a response than a cause in this case.

Soil moisture was initialised at the start of the ERA5⁷⁹ production streams using scaled values derived from earlier comprehensive reanalyses. The spin-up of soil moisture will be reduced in the rerun of

ERA5^{→79} by setting back the initial dates of the production streams so that the new streams can start from original ERA5^{→79} values that have been partly spun up. Use may also be made of a prototype (scout) ERA5 analysis for the 1940s to initialise the production stream for the early 1950s.

These issues, as well as any others which emerge following the release of ERA5^{→79}, are documented online in the Copernicus Knowledge Base (ECMWF, 2016a).

7 | CONCLUDING REMARKS AND DIRECTIONS FOR FUTURE WORK

The extension to 1950 makes ERA5 the longest full-input reanalysis produced to date at ECMWF. The extension offers several advantages over previous ECMWF reanalyses covering this period, principally higher resolution, hourly output, an uncertainty estimate based on a ten-member EDA as well as a forecast model and data assimilation system based on a 2016 version (41r2) of the ECMWF Integrated Forecasting System. The 70-year record offers a coherent and high-quality estimate of the atmospheric state to support the growing ERA5 user base. Nevertheless, as a result of the sub-optimal assimilation of tropical cyclone bogus observations which affects the representation of these events and has knock-on effects on the statistics of ocean wave heights, current plans foresee a re-run of the entire period from 1950 to 1978, to be undertaken during 2021–22. Following this, a further extension of ERA5 to 1940 is planned. Prior to 1940, the scarcity of upper-air observations means that a full-input reanalysis becomes similar in quality to that of previous centennial reanalyses which assimilate surface observations only.

The order of magnitude increase in the number of observations assimilated per day throughout the period 1950–1978 results in a steady improvement in analysis quality, as illustrated by the steadily reducing analysis ensemble spread, the reduction in first-guess departure variances, the coherence of analysis increments (at levels below 10 hPa) and the accuracy of re-forecasts initialised by ERA5. The most significant anomalies in this regard are the increases in first-guess departure variances for surface pressure and upper-air winds during 1965–66, associated with the absence of observations from China and several other countries during this period. Addressing this deficiency, if possible, will be a priority for the next ECMWF global reanalysis, ERA6, which is due to start in 2024. The additional sources of upper-air and surface observations that were ingested in ERA5^{→79} but not in ERA5^{79→} have a positive impact on the quality of the product. In particular, the significantly higher amounts of

surface pressure and (to a lesser extent) 10 m marine wind observations in the overlap period ERA5^{79→80} is noteworthy, and future reanalyses should ingest observations from these additional sources throughout.

A close inspection of the analysis increments for upper-air temperature, humidity and winds shows that, although the magnitudes are small, the vertical profile of increments is different for ERA5^{→79} and ERA5^{79→}, reflecting a shifting balance between model biases and observational constraints as the observing system evolves during the extension. For ozone, increments in ERA5^{→79} are generally small, other than for the period 1970–72 when BUV observations are assimilated in large numbers. During this period, the vertical profile of increments is similar to those during the period 1979 onwards, when ozone observations are assimilated in large numbers. Above 10 hPa, the behaviour of analysis increments for temperature, winds and ozone in ERA5^{→79} and ERA5^{79→} are quite different at times, reflecting the lack of observational information at these levels, compounded by several changes to \mathbf{B}_{cli} . This is also evident in the anomaly time series and is another area where improvements are required, for example, through implementing a more smoothly evolving \mathbf{B}_{cli} . The 2-year, non-public, overlap data set ERA5^{79→80}, which benefits from a longer spin-up and uses the 1978- \mathbf{B}_{cli} , has proved valuable to disentangle the origins of observed changes in behaviour in the upper stratosphere.

The depiction of the North Sea storm of 1953 and the events leading to the discovery of the phenomenon of sudden stratospheric warmings in 1952 serve to illustrate, by example, the quality and utility of ERA5^{→79}. Doubtless, the fidelity of ERA5 will be assessed for other events in the early period by other authors.

Global trends in surface temperature anomalies are in good agreement between ERA5, JRA-55 and conventional climatological data sets, however this article has highlighted significant regional differences, with trends over Europe in good agreement throughout the period but trends over Australia showing larger discrepancies, especially during the earliest periods covered. It is possible, as outlined in Section 6, that these differences are due to deficiencies in the initialisation of deep soil moisture. Addressing this issue will be a priority for ERA6. Regarding anomalies in upper-air temperatures, the evolution is coherent and consistent in ERA5, JRA-55 and observations. A detailed analysis of the evolution of the probability density functions (pdfs) of anomalies is beyond the scope of this article, but this type of analysis shows promise both for monitoring production quality as well as providing a new and useful diagnostic with which to test climate model predictions.

Priorities for future work are discussed in some detail in section 10.4 of Hersbach *et al.* (2020), but two key areas are listed here for their particular relevance to reanalysis of the pre-satellite era: the evaluation of the potential of weak constraint 4D-Var to reduce stratospheric temperature biases in this period, and the development of a scheme to allow the climatological component of **B** (B_{cli}) to evolve smoothly. In addition, there are several developments expected to be sufficiently mature to be incorporated into ERA6, including the assimilation of several early satellite data sets from the period prior to 1979, and allowing a dynamic evolution of the observation error covariances, to reflect the steadily improving quality of conventional observations in the period before 1979. Spin-up discontinuities in stratospheric humidity were partially mitigated by extending production streams, but this problem remains challenging and is an area where further development work is required.

AUTHOR CONTRIBUTIONS

Bill Bell: formal analysis; validation; writing - original draft; writing - review and editing. **Hans Hersbach:** conceptualization; formal analysis; project administration; supervision; writing - original draft; writing - review and editing. **Adrian Simmons:** formal analysis; validation; writing - original draft; writing - review and editing. **Paul Berrisford:** formal analysis; investigation; writing - review and editing. **Per Dahlgren:** investigation. **András Horányi, Joaquín Muñoz-Sabater, Julien Nicolas:** formal analysis; investigation; validation; writing - original draft; writing - review and editing. **Raluca Radu:** formal analysis; investigation; writing - review and editing. **Dinand Schepers:** formal analysis; investigation; writing - original draft; writing - review and editing. **Cornel Soci:** formal analysis; investigation; methodology; writing - original draft; writing - review and editing. **Sebastien Villaume:** data curation. **Jean-Raymond Bidlot:** investigation. **Leo Haimberger:** data curation; methodology; writing - review and editing. **Jack Woollen:** data curation; writing - review and editing. **Carlo Buontempo:** funding acquisition; project administration; writing - review and editing. **Jean-Noël Thépaut:** funding acquisition; project administration; writing - review and editing.

ACKNOWLEDGEMENTS

Reanalysis touches on a large number of activities at ECMWF, and its success relies on the efforts of many, many people across ECMWF and from many collaborations. This study has been partially funded by the Copernicus Climate Change Service. ECMWF implements this service and the

Copernicus Atmosphere Monitoring Service on behalf of the European Commission.

CONFLICT OF INTEREST

To our knowledge, there is no conflict of interest of the material presented in this article.

Glossary

Abbreviation	Description
ACARS	Aircraft Communications Addressing and Reporting System
ACORN-SAT	Australian Climate Observations Reference Network - Surface Air Temperature
AIREP	Air Report
AMDAR	Aircraft Meteorological Data Relay
ATOVS	Advanced TIROS Operational Vertical Sounder
BATHY	BATHYthermal
BUFR	Binary Universal Form for the Representation of meteorological data
BUV	Backscatter Ultra-violet Spectrometer
CDS	The C3S Climate Data Store
(C)ERA-20C	(Coupled) ECMWF Reanalysis of the 20th Century
CHUAN	Comprehensive Historical Upper-Air Network
CKB	Copernicus Knowledge Base
CMIP5	Coupled Model Intercomparison Project, Phase 5
C3S	Copernicus Climate Change Service
DRIBU	report from Drifting and moored Buoy
ECMWF	European Centre for Medium-Range Weather Forecasts
EDA	Ensemble of Data Assimilations
E-OBS	European daily high-resolution gridded data set
ERA	ECMWF reanalysis
ERA5	A 70-year ERA starting from January 1950 onwards with timely updates
ERA5 ^{→79}	Segment of ERA5 from 1950 to 1978
ERA5 ^{79→80}	Non-public extension of ERA5 ^{→79} for 1979 and 1980
ERA5 ^{79→}	Segment of ERA5 from 1979 onwards

Glossary (continued)

Abbreviation	Description
ERA-40	A 45-year ERA from September 1957 to August 2002
ERA-40 BUFR	Observational data stream as ingested in the ERA-40 reanalysis
ERA-Interim	A 40-year ERA from January 1979 to August 2019
ERA-CLIM	European Reanalysis of Global Climate Observations
ERA-CLIM2	European Reanalysis of Global Climate Observations 2
ERA-PreSAT	Non-public experimental ECMWF reanalysis from 1939 to 1967
GISS	Goddard Institute for Space Studies
GISTEMP	GISS surface temperature analysis
GNSS-RO	Global Navigation Satellite System
GPCC	Global Precipitation Climatology Centre
GPCP	Global Precipitation Climatology Project
HadCRUT5	Hadley Centre/Climatic Research Unit Temperature version 5
HadISSTx	Hadley Centre Sea Ice and Sea Surface Temperature data set version x
HRES	High-resolution component (of ERA5)
HIRS	High-Resolution Infrared Radiation Sounder
IBTrACKS	International Best Track Archive for Climate Stewardship
ICOADS	International Comprehensive Ocean and Atmosphere Data Set
IFS	ECMWF Integrated Forecasting System
ISPD	The International Surface Pressure Databank
JRA-55	Japanese 55-Year Reanalysis Project
LDAS	Land Data Assimilation System
MSU	Microwave Sounding Unit
NCAR	National Center for Atmospheric Research
NCEP	National Centers for Environmental Prediction (USA)
NOAA	National Oceanic and Atmospheric Administration
NOAAGlobalTemp	NOAA Merged Land Ocean Global Surface Temperature Analysis
NWP	Numerical Weather Prediction

Glossary (continued)

Abbreviation	Description
OI	Optimal interpolation
PILOT	Wind report from pilot balloon
Ps	Surface pressure
Q	Upper-air specific humidity
QBO	Quasi-Biennial Oscillation
Rh2m	2 m relative humidity
RICH	Radiosonde Innovation Composite Homogenization
RISE	Radiosonde adjustments with solar elevation dependence
Sd	Snow depth
SIC	Sea ice concentration
SST	Sea surface temperature
SSU	Stratospheric Sounding Unit
STDEV	Standard deviation
SWH	Significant wave height
SYNOP	Surface synoptic report
T	Upper-air temperature
TEMP	Report from radiosounding
TIROS	Television Infrared Observation Satellite
TOVS	TIROS Operational Vertical Sounder
T2m	2 m temperature
U	Upper-air zonal wind component
URDB-2	NCAR Upper-Air Database version 2
U.S.	United States
U10	Zonal wind component at 10 m height
V	Upper-air meridional wind component
VarBC	Variational bias correction
VTPR	Vertical Temperature Profiling Radiometer
V10	Meridional wind component at 10 m height
20CRv3	Twentieth Century Reanalysis version 3
4D-Var	4-Dimensional Variational data assimilation

ORCID

Bill Bell  <https://orcid.org/0000-0002-8151-5449>

Hans Hersbach  <https://orcid.org/0000-0001-5330-7071>

Joaquín Muñoz-Sabater  <https://orcid.org/0000-0002-5997-290X>

REFERENCES

- Adler, R.F., Huffman, G.J., Chang, A., Ferraro, R., Xie, P.-P., Janowiak, J., Rudolf, B., Schneider, U., Curtis, S., Bolvin, D., Gruber, A., Susskind, J., Arkin, P. and Nelkin, E. (2003) The version-2 Global Precipitation Climatology Project (GPCP) monthly precipitation analysis (1979-present). *Journal of Hydrometeorology*, 4, 1147–1167.
- Anstey, J.A., Banyard, T.P., Butchart, N., Coy, L., Newman, P.A., Osprey, S. and Wright, C. (2020) Quasi-biennial oscillation disrupted by abnormal southern hemisphere stratosphere. *Earth and Space Science Open Archive*, 16.
- Ayarzagüena, B., Palmeiro, F.M., Barriopedro, D., Calvo, N., Lange-matz, U. and Shibata, K. (2019) On the representation of major stratospheric warmings in reanalyses. *Atmospheric Chemistry and Physics*, 19, 9469–9484.
- Becker, A., Finger, P., Meyer-Christoffer, A., Rudolf, B., Schamm, K., Schneider, U. and Ziese, M. (2013) A description of the global land-surface precipitation data products of the Global Precipitation Climatology Centre with sample applications including centennial (trend) analysis from 1901-present. *Earth System Science Data*, 5, 71–99.
- Bonavita, M., Hólm, E., Isaksen, L. and Fisher, M. (2016) The evolution of the ECMWF hybrid data assimilation system. *Quarterly Journal of the Royal Meteorological Society*, 142, 287–303.
- Brönnimann, S., Allan, R., Atkinson, C., Buizza, R., Bulygina, O., Dahlgren, P., Dee, D., Dunn, R., Gomes, P., John, V.O., Jourdain, S., Haimberger, L., Hersbach, H., Kennedy, J., Poli, P., Pulliainen, J., Rayner, N., Saunders, R., Schulz, J., Sterin, A., Stickler, A., Titchner, H., Valente, M.A., Ventura, C. and Wilkinson, C. (2018a) Observations for reanalyses. *Bulletin of the American Meteorological Society*, 99, 1851–1866.
- Brönnimann, S., Brugnara, Y., Allan, R.J., Brunet, M., Compo, G.P., Crouthamel, R.I., Jones, P.D., Jourdain, S., Luterbacher, J., Siegmund, P., Valente, M.A. and Wilkinson, C.W. (2018b) A roadmap to climate data rescue services. *Geoscience Data Journal*, 5, 28–39. <https://doi.org/10.1002/gdj3.56>.
- Butler, A.H., Sjöberg, J.P., Seidel, D.J. and Rosenlof, K.H. (2017) A sudden stratospheric warming compendium. *Earth System Science Data*, 9, 63–76.
- Charlton, A.J. and Polvani, L.M. (2007) A new look at stratospheric sudden warmings. Part I: climatology and modeling benchmarks. *Journal of Climate*, 20, 449–469.
- Compo, G.P., Whitaker, J.S., Sardeshmukh, P.D., Matsui, N., Allan, R.J., Yin, X., Gleason, B.E., Vose, R.S., Rutledge, G., Bessemoulin, P., Brönnimann, S., Brunet, M., Crouthamel, R.I., Grant, A.N., Groisman, P.Y., Jones, P.D., Kruk, M.C., Kruger, A.C., Marshall, G.J., Maugeri, M., Mok, H.Y., Nordli, R.o.s.s., Trigo, R.M., Wang, X.L., Woodruff, S.D. and Worley, S.J. (2011) The twentieth century reanalysis project. *Quarterly Journal of the Royal Meteorological Society*, 137, 1–28.
- Cornes, R.C., van der Schrier, G., van den Besselaar, E.J.M. and Jones, P.D. (2018) An ensemble version of the E-OBS temperature and precipitation data sets. *Journal of Geophysical Research: Atmospheres*, 123, 9391–9409.
- Cowan, K., Hausfather, Z., Hawkins, E., Jacobs, P., Mann, M., Miller, S., Steinman, B., Stolpe, M. and Way, R. (2015) Robust comparison of climate models with observations using blended land air and ocean sea surface temperatures. *Geophysical Research Letters*, 42, 6526–6534.
- Cram, T.A., Compo, G.P., Yin, X., Allan, R.J., McColl, C., Vose, R.S., Whitaker, J.S., Matsui, N., Ashcroft, L., Auchmann, R., Bessemoulin, P., Brandsma, T., Brohan, P., Brunet, M., Comeaux, J., Crouthamel, R., Gleason, J.R., Groisman, P.Y., Hersbach, H., Jones, P.D., Jónsson, T., Jourdain, S., Kelly, G., Knapp, K.R., Kruger, A., Kubota, H., Lentini, G., Lorrey, A., Lott, N., Lubker, S.J., Luterbacher, J., Marshall, G.J., Maugeri, M., Mock, C.J., Mok, H.Y., Nordli, Ø., Rodwell, M.J., Ross, T.F., Schuster, D., Srncic, L., Valente, M.A., Vizi, Z., Wang, X.L., Westcott, N., Woollen, J.S. and Worley, S.J. (2015) The International Surface Pressure Databank version 2. *Geoscience Data Journal*, 2, 31–46.
- Desroziers, G., Berre, L., Chapnik, B. and Poli, P. (2005) Diagnosis of observation, background and analysis-error statistics in observation space. *Quarterly Journal of the Royal Meteorological Society*, 131, 3385–3396.
- Ebdon, R.A. (1960) Notes on the wind flow at 50 mb in tropical and sub-tropical regions in January 1957 and January 1958. *Quarterly Journal of the Royal Meteorological Society*, 86, 540–542.
- ECMWF, C.D. (2016a). Copernicus Knowledge Base. Available at: <https://confluence.ecmwf.int/display/CKB>.
- ECMWF, R.-D. (2016b). IFS documentation cy41r2. Available at: <https://www.ecmwf.int/en/forecasts/documentation-and-support/changes-ecmwf-model/ifs-documentation>.
- Grant, A.N., Brönnimann, S., Ewen, T. and Nagurny, A. (2009) A new look at radiosonde data prior to 1958. *Journal of climate*, 22, 3232–3247.
- Haimberger, L., Tavolato, C. and Sperka, S. (2012) Homogenization of the global radiosonde temperature dataset through combined comparison with reanalysis background series and neighboring stations. *Journal of Climate*, 25, 8108–8131.
- Healy, S.B., Polichtchouk, I. and Horányi, A. (2020) Monthly and zonally averaged zonal wind information in the equatorial stratosphere provided by gnss radio occultation. *Quarterly Journal of the Royal Meteorological Society*, 146, 3612–3621. <https://doi.org/10.1002/qj.3870>.
- Hersbach, H., Bell, B., Berrisford, P., Hirahara, S., Horányi, A., Muñoz-Sabater, J., Nicolas, J., Peubey, C., Radu, R., Schepers, D., Simmons, A., Soci, C., Abdalla, S., Abellan, X., Balsamo, G., Bechtold, P., Biavati, G., Bidlot, J., Bonavita, M., De Chiara, G., Dahlgren, P., Dee, D., Diamantakis, M., Dragani, R., Flemming, J., Forbes, R., Fuentes, M., Geer, A., Haimberger, L., Healy, S., Hogan, R.J., Hólm, E., Janisková, M., Keeley, S., Laloyaux, P., Lopez, P., Lupu, C., Radnoti, G., de Rosnay, P., Rozum, I., Vamborg, F., Villaume, S. and Thépaut, J.-N. (2020) The ERA5 global reanalysis. *Quarterly Journal of the Royal Meteorological Society*, 146, 1999–2049. <https://doi.org/10.1002/qj.3803>.
- Hersbach, H., Brönnimann, S., Haimberger, L., Mayer, M., Villiger, L., Comeaux, J., Simmons, A., Dee, D., Jourdain, S., Peubey, C., Poli, P., Rayner, N., Sterin, A.M., Stickler, A., Valente, M.A. and Worley, S.J. (2017) The potential value of early (1939–1967) upper-air data in atmospheric climate reanalysis. *Quarterly Journal of the Royal Meteorological Society*, 143, 1197–1210.
- Hersbach, H., Peubey, C., Simmons, A., Berrisford, P., Poli, P. and Dee, D. (2015a) ERA-20CM: a twentieth-century atmospheric model ensemble. *Quarterly Journal of the Royal Meteorological Society*, 141, 2350–2375.
- Hersbach, H., Poli, P. and Dee, D. (2015b) *The Observation Feedback Archive for the ICOADS and ISPD Data Sets*, (p. 29). ECMWF ERA Report Series 27.

- Hirahara, S., Balmaseda, M.A., de Boisseson, E. and Hersbach, H. (2016) *Sea Surface Temperature and Sea Ice Concentration for ERA5*, (p. 25). ECMWF ERA Report Series 26.
- Ho, S.-P., Anthes, R.A., Ao, C.O., Healy, S., Horanyi, A., Hunt, D., Mannucci, A.J., Pedatella, N., Randel, W.J., Simmons, A., Steiner, A., Xie, F., Yue, X. and Zeng, Z. (2019) The COSMIC/FORMOSAT-3 Radio Occultation Mission after 12 years: accomplishments, remaining challenges, and potential impacts of COSMIC-2. *Bulletin of the American Meteorological Society*.
- Hólm, E., Andersson, E., Beljaars, A., Lopez, P., Mahfouf, J., Simmons, A. and Thépaut, J. (2002) *Assimilation and Modelling of the Hydrological Cycle: ECMWF's Status and Plans*. Reading: ECMWF.
- Johnson, J.E., DeLand, M. and McPeters, R. (2012) *Document for the Creating a Long Term Multi-Sensor Ozone Data Record Project*. Greenbelt, MD: NASA Goddard Space Flight Center. Technical Report.
- Kawatani, Y., Hamilton, K., Miyazaki, K., Fujiwara, M. and Anstey, J.A. (2016) Representation of the tropical stratospheric zonal wind in global atmospheric reanalyses. *Atmospheric Chemistry and Physics*, 16, 6681–6699.
- Kennedy, J.J., Rayner, N.A., Atkinson, C.P. and Killick, R.E. (2019) An ensemble data set of sea-surface temperature change from 1850: the Met Office Hadley Centre HadSST.4.0.0.0 data set. *Journal of Geophysical Research*, 124, 7719–7763.
- Knapp, K.R., Kruk, M.C., Levinson, D.H., Diamond, H.J. and Neumann, C.J. (2010) The international best track archive for climate stewardship (IBTrACS) unifying tropical cyclone data. *Bulletin of the American Meteorological Society*, 91, 363–376.
- Kobayashi, S., Ota, Y., Harada, Y., Ebata, A., Moriya, M., Onoda, H., Onogi, K., Kamahori, H., Kobayashi, C., Endo, H., Miyaoka, K. and Takahashi, K. (2015) The JRA-55 reanalysis: general specifications and basic characteristics. *Journal of the Meteorological Society of Japan. Series II*, 93, 5–48.
- Kosaka, Y. (2018) *Assimilation of tropical cyclone best track reports in CERA-20C*. Reading: ECMWF. Research Department Memorandum, available upon request, RD18-115.
- Krzeminski, B., Bormann, N., Kelly, G., McNally, T. and Bauer, P. (2009) *Revision of the HIRS Cloud Detection at ECMWF*. Reading: ECMWF. EUMETSAT/ECMWF Fellowship Programme, Research Report No. 19.
- Laloyaux, P., de Boisseson, E., Balmaseda, M., Bidlot, J.-R., Broennimann, S., Buizza, R., Dalhgren, P., Dee, D., Haimberger, L., Hersbach, H., Kosaka, Y., Martin, M., Poli, P., Rayner, N., Rustemeier, E. and Schepers, D. (2018) CERA-20C: a coupled reanalysis of the twentieth century. *Journal of Advances in Modeling Earth Systems*.
- Lenssen, N., Schmidt, G., Hansen, J., Menne, M., Persin, A., Ruedy, R. and Zyss, D. (2019) Improvements in the GISTEMP uncertainty model. *Journal of Geophysical Research: Atmospheres*, 124, 6307–6326.
- Li, X., Kelly, G., Uppala, S., Saunders, R. and Gibson, J.K. (2005) *ECMWF ERA-40 Project Report Series No. 21: The use of VTPR raw radiances in ERA-40*. Reading: ECMWF.
- Lupu, C. and Geer, A. (2015) *Operational Implementation of RTTOV-11 in the IFS*. Reading: ECMWF. ECMWF Technical Memorandum No. 636.
- McMillin, L.M., Wark, D.Q., Siomkajlo, J.M., Abel, P.G., Werbowetzi, A., Lauritson, L.A., Pritchard, J.A., Crosby, D.S., Woolf, H.M., Luebbe, R.C., Weinreb, M.P., Fleming, H.E., Bittner, F.E. and Hayden, C.M. (1973) *Satellite Infrared Soundings from NOAA Spacecraft*. Washington, D.C.: NOAA. NOAA Technical Report NES 65.
- McPeters, R.D., Bhartia, P., Haffner, D., Labow, G. and Flynn, L. (2013) The version 8.6 SBUV ozone data record: an overview. *Journal of Geophysical Research: Atmospheres*, 118, 8032–8039.
- MetOffice (1954) *The Monthly Weather Report for the Year 1953*. Exeter: Met Office. Met Office Digital Library and Archive.
- Morice, C.P., Kennedy, J.J., Rayner, N.A., Winn, J.P., Hogan, E., Killick, R.E., Dunn, R.J.H., Osborn, T.J., Jones, P.D. and Simpson, I.R. (2020) An updated assessment of near-surface temperature change from 1850: the HadCRUT5 dataset. *Journal of Geophysical Research: Atmospheres*, n/a, e2019JD032361.
- NCAR (2014). Research Data Archive/Computational and Information Systems Laboratory/National Center for Atmospheric Research/University Corporation for Atmospheric Research, NCAR Upper Air Database, 1920-ongoing. Research Data Archive at the National Center for Atmospheric Research, Computational and Information Systems Laboratory, Boulder, CO. [Available online at <https://rda.ucar.edu/datasets/ds370.1/>] Accessed 01 Jun 201
- Newman, P.A., Coy, L., Pawson, S. and Lait, L.R. (2016) The anomalous change in the QBO in 2015-2016. *Geophysical Research Letters*, 43, 8791–8797.
- Poli, P., Hersbach, H., Dee, D.P., Berrisford, P., Simmons, A.J., Vitart, F., Laloyaux, P., Tan, D.G., Peubey, C., Thépaut, J.-N., Trémolet, Y., Hólm, E.V., Bonavita, M., Isaksen, I. and Fisher, M. (2016) ERA-20C: an atmospheric reanalysis of the twentieth century. *Journal of Climate*, 29, 4083–4097.
- Prichard, B. (2013) The north sea surge and east coast floods of 1953. *Weather*, 68, 31–36. <https://doi.org/10.1002/wea.2044>.
- Raoult, B., Bergeron, C., Alós, A.L., Thépaut, J. and Dee, D. (2017) Climate Service Develops User-friendly Data Store. *ECMWF Newsletter*, 151, 22–27.
- Rayner, N.A., Parker, D.E., Horton, E.B., Folland, C.K., Alexander, L.V., Rowell, D.P., Kent, E.C. and Kaplan, A. (2003) Global analyses of sea surface temperature, sea ice, and night marine air temperature since the late nineteenth century. *Journal of Geophysical Research: Atmospheres*, 108.
- Reed, R.J., Campbell, W.J., Rasmussen, L.A. and Rogers, D.G. (1961) Evidence of a downward-propagating, annual wind reversal in the equatorial stratosphere. *Journal of Geophysical Research*, 66, 813–818.
- Rohde, R. and Hausfather, Z. (2020) The Berkeley earth land/ocean temperature record. *Earth System Science Data*, 12, 3469–3479.
- Scherhag, R. (1952) Die explosionsartige Stratosphärenenerwärmung des Spätwinters 1951-1952. *Berichte des Deutschen Wetterdienstes*, 6, 51–63.
- Simmons, A., Berrisford, P., Dee, D., Hersbach, H., Hirahara, S. and Thépaut, J.-N. (2017) A reassessment of temperature variations and trends from global reanalyses and monthly surface climatological datasets. *Quarterly Journal of the Royal Meteorological Society*, 143, 101–119.
- Simmons, A., Hersbach, H., Muñoz-Sabater, J., Nicolas, J., Vamborg, F., Berrisford, P., de Rosnay, P., Willett, K. and Woollen, J. (2021) *Low Frequency Variability and Trends in Surface Air Temperature and Humidity from ERA5 and Other Datasets*. Reading: ECMWF. ECMWF Technical Memorandum 881.

- Simmons, A., Soci, C., Nicolas, J., Bell, B., Berrisford, P., Dragani, R., Flemming, J., Haimberger, L., Healy, S., Hersbach, H., Horányi, A., Inness, A., Muñoz-Sabater, J., Radu, R. and Schepers, D. (2020) *Global Stratospheric Temperature Bias and Other Stratospheric Aspects of ERA5 and ERA5.1*. Reading: ECMWF. ECMWF Technical Memorandum 859.
- Simmons, A.J., Poli, P., Dee, D.P., Berrisford, P., Hersbach, H., Kobayashi, H. and Peubey, C. (2014) Estimating low-frequency variability and trends in atmospheric temperature from the ERA-Interim reanalysis. *Quarterly Journal of the Royal Meteorological Society*, 140, 329–353.
- Simmons, A.J., Willett, K.M., Jones, P.D., Thorne, P.W. and Dee, D.P. (2010) Low-frequency variations in surface atmospheric humidity, temperature and precipitation: inferences from reanalyses and monthly gridded observational datasets. *Journal of Geophysical Research*, 115, 22987–22994.
- Slivinski, L.C., Compo, G.P., Whitaker, J.S., Sardeshmukh, P.D., Giese, B.S., McColl, C., Allan, R., Yin, X., Vose, R., Titchner, H., Kennedy, J., Spencer, L.J., Ashcroft, L., Brönnimann, S., Brunet, M., Camuffo, D., Cornes, R., Cram, T.A., Crouthamel, R., Domínguez-Castro, F., Eric Freeman, J., Gergis, J., Hawkins, E., Jones, P.D., Jourdain, S., Kaplan, A., Kubota, H., Le Blancq, F., Lee, T.C., Lorrey, A., Luterbacher, J., Maugeri, M., Mock, C.J., Kent Moore, G.W., Przybylak, R., Pudmenzky, C., Reason, C., Slonosky, V.C., Smith, C.A., Tinz, B., Trewin, B., Valente, M.A., Wang, X.L., Wilkinson, C., Wood, K. and Wyszynski, P. (2019) Towards a more reliable historical reanalysis: improvements for version 3 of the twentieth century reanalysis system. *Quarterly Journal of the Royal Meteorological Society*, 145, 2876–2908.
- Stickler, A., Brönnimann, S., Valente, M., Bethke, J., Sterin, A., Jourdain, S., Roucaute, E., Vasquez, M., Reyes, D., Allan, R. and Dee, D. (2014) ERA-CLIM: historical surface and upper-air data for future reanalyses. *Bulletin of the American Meteorological Society*, 95, 1419–1430.
- Stickler, A., Grant, A.N., Ewen, T., Ross, T.F., Vose, R., Comeaux, J., Bessemoulin, P., Jylhä, K., Adam, W., Jeannet, P., Nagurny, A., Sterin, A., Allan, R., Compo, G., Griesser, T. and Brönnimann, S. (2010) The comprehensive historical upper air network (CHUAN). *Bulletin of the American Meteorological Society*, 91, 741–751.
- Stocker, T.F., Qin, D., Plattner, G.-K., Tignor, M., Allen, S., Boschung, J., Nauels, A., Xia, Y., Bex, V. and Idgley(eds.), P. (2013) *Climate Change 2013: The Physical Science Basis. Contribution of Working Group I to the Fifth Assessment Report of the Intergovernmental Panel on Climate Change*. Cambridge: Cambridge University Press. IPCC Report. 119–158. <https://doi.org/10.1017/CBO9781107415324.007>.
- Tavolato, C. and Isaksen, L. (2015) On the use of a Huber norm for observation quality control in the ECMWF 4D-Var. *Quarterly Journal of the Royal Meteorological Society*, 141, 1514–1527.
- Teweles, S. (1958) Anomalous warming of the stratosphere over North America in early 1957. *Monthly Weather Review*, 86, 377–396.
- Thépaut, J., Dee, D., Engelen, R. and Pinty, B. (2018). The Copernicus Programme and its Climate Change Service, *IGARSS 2018 - 2018 IEEE International Geoscience and Remote Sensing Symposium*, pp. 1591–1593. <https://doi.org/10.1109/IGARSS.2018.8518067>
- Titchner, H.A. and Rayner, N.A. (2014) The Met Office Hadley Centre sea ice and sea surface temperature data set, version 2: 1. Sea ice concentrations. *Journal of Geophysical Research: Atmospheres*, 119, 2864–2889.
- Trenberth, K.E. and Smith, L. (2005) The mass of the atmosphere: a constraint on global analyses. *Journal of Climate*, 18, 864–875.
- Trewin, B. (2013) A daily homogenized temperature data set for Australia. *International Journal of Climatology*, 33, 1510–1529.
- Uppala, S.M., Kållberg, P.W., Simmons, A.J., Andrae, U., da Costa Bechtold, V., Fiorino, M., Gibson, J.K., Haseler, J., Hernandez, A., Kelly, G.A., Li, X., Onogi, K., Saarinen, S., Sokka, N., Allan, R.P., Andersson, E., Arpe, K., Balmaseda, A.M., Beljaars, A.C.M., van de Berg, L., Bidlot, J., Bormann, N., Caires, S., Chevallier, F., Dethof, A., Dragosavac, M., Fisher, M., Fuentes, M., Hagemann, S., Hólm, E., Hoskins, B.J., Isaksen, L., Janssen, P.A.E.M., Jenne, R., McNally, A.P., Mahfouf, J.-F., Morcrette, J.-J., Rayner, N.A., Saunders, R.W., Simon, P., Sterl, A., Trenberth, K.E., Untch, A., Vasiljevic, D., Viterbo, P. and Woollen, J. (2005) The ERA-40 re-analysis. *Quarterly Journal of the Royal Meteorological Society*, 131, 2961–3012.
- Woodruff, S.D., Worley, S.J., Lubker, S.J., Ji, Z., Freeman, J.E., Berry, D.I., Brohan, P., Kent, E.C., Reynolds, R.W., Smith, S.R. and Wilkinson, C. (2011) ICOADS release 2.5: extensions and enhancements to the surface marine meteorological archive. *International Journal of Climatology*, 31, 951–967.
- Zhang, H.-M., Lawrimore, J.H., Huang, B., Menne, M.J., Yin, X., Sánchez-Lugo, A., Gleason, B.E., Vose, R., Arndt, D., Rennie, J.J. and Williams, C.N. (2019) Updated temperature data give a sharper view of climate trends. *Eos*, 100.

SUPPORTING INFORMATION

Additional supporting information may be found online in the Supporting Information section at the end of this article.

How to cite this article: Bell, B., Hersbach, H., Simmons, A., Berrisford, P., Dahlgren, P., Horányi, A. *et al.* (2021) The ERA5 global reanalysis: Preliminary extension to 1950. *Quarterly Journal of the Royal Meteorological Society*, 1–42. Available from: <https://doi.org/10.1002/qj.4174>